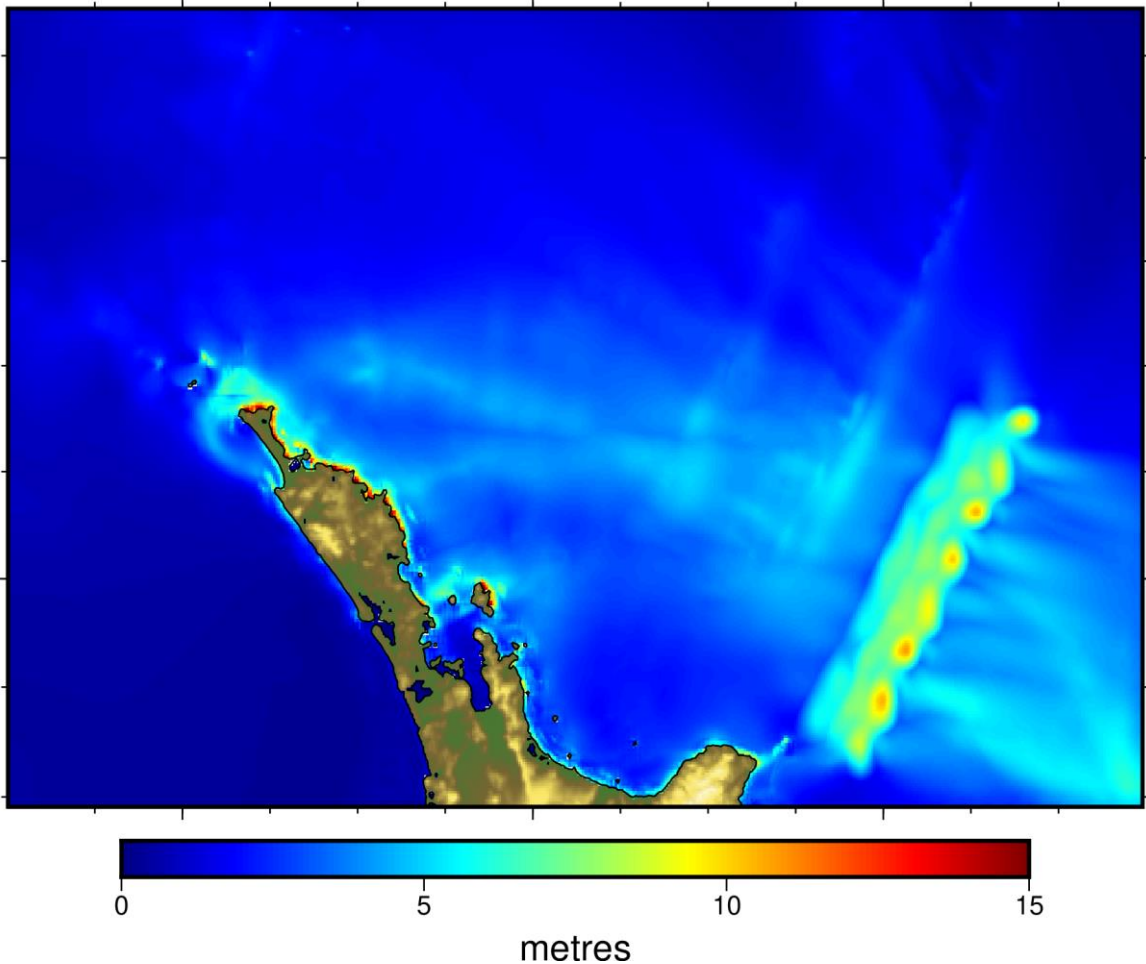


Tsunami Inundation Modelling for Evacuation Planning in Northland



Report Status

Version	Date	Status	Approved By:
V1	30 May 2024	Progress	JCB
V2	9 Sep 2024	First Final	JCB

Jose C. Borrero Ph.D.
Sam O'Neill M.Sc.
Dianne Zucchetto M.Sc.



Cover Picture: Tsunami propagation for a large magnitude rupture on the southern segment of the Tonga Kermadec Trench.

EXECUTIVE SUMMARY

The objective of this study was to produce tsunami inundation and evacuation zones for the Northland region that are compliant with guidelines set forth in the document 'Tsunami Evacuation Zones: Director's Guidelines for Civil Defence Emergency Management Groups' (MCDEM, 2016). This document defines three tsunami evacuation zones: Red, Orange, and Yellow. The Red Zone is the area closest to the coast which would be evacuated in most tsunami warning situations. The Orange Zone is an intermediate zone that considers tsunami hazard from either large tsunami sources located far away or moderate tsunami sources close by (but more than 1 hr travel time away). The Yellow Zone represents the area to be evacuated in the most extreme scenarios of a very large near-source earthquake.

To define these zones, we conducted a numerical modelling study focussed on determining the extents of the tsunami inundation zones for the Northland Region. The study used a Level 3/Level 4 modelling approach (as defined in MCDEM 2016) whereby a physics based numerical model was used to model the evolution of the tsunami from source through to inundation. We used multiple source scenarios based on output from probabilistic tsunami hazard models. Aspects of a Level 4 methodology were also incorporated in that we considered a wide variety of sources, both local and distant, and that the inundation lines were determined based on aggregating the results from multiple sources.

We used the ComMIT tsunami modelling software to simulate the tsunami hydrodynamics from tsunami generation through to inundation on land. The ComMIT model was validated for tsunami effects in the Northland region for several distant and near-source events including the recent Raoul Island earthquake of March 5, 2021. Numerical modelling grids were derived from the best available bathymetry and LiDAR topography. Sixty (60) nearshore modelling grids at 10 m resolution were developed for the simulations and the models were run a mean high-water spring (MHWS) water level with a final model run resolution of 20 m. Twenty-seven (27) source models were run over sixty (60) grids for a total of 1,620 model simulations. Models were batch run on 12 and 16 core desktop modelling computers and were conducted from mid-March to mid-May 2024.

Model output was compared to existing probabilistic tsunami hazard analyses. This includes the work of Power et al. (2021) which provides probabilistic estimates of tsunami heights at the shoreline along 50 km segments of the New Zealand coast. However, these estimates are based on an empirical relationship between earthquake magnitude and tsunami height and do not consider the effects of detailed hydrodynamics, coastal or bathymetric irregularities. Model output was also compared to the probabilistic model of Davies and Griffen (2018). In this model they provided tsunami amplitudes at a range of recurrence intervals (RIs) at deep-water, offshore locations derived from 10's of thousands of hydrodynamic simulations initialised with a wide variety of earthquake sources.

Based on our investigation we determined that the most extreme hazard, the one which governs the Yellow Zone for the east coast, is represented by a large rupture of the southern segments of the Tonga Kermadec Trench. For this scenario we modelled rupture over a 400x100 km fault plane with average slip amount of 30 m. As a matter of comparison, we note that this source is slightly larger in terms of areal extent and average slip than the 2010 Tohoku Japan earthquake and tsunami.

For the Orange Zone, we determined that the hazard was best represented by aggregating the inundation results from a suite of large magnitude, distant and regional source earthquakes. In this case, simulations that produced anomalously large tsunami heights either at the shoreline or at the offshore location were not used in the aggregation. All in all, the final inundation zones correspond best to a tsunami threat level of 3-5 m as defined in the DGL.

Raster files of tsunami inundation flow depth and inundated area were compiled for each of the 60 high resolution model grid regions for the Yellow and Orange Zones. This data was transferred to the GIS Specialist for processing into the continuous inundation zones. As expected, the inundation zones derived from the hydrodynamic model output model were significantly smaller than those produced using GIS-based attenuation rules and an assume uniform value for tsunami height at the shoreline.

CONTENTS

EXECUTIVE SUMMARY	I
TABLE OF FIGURES	III
TABLE OF TABLES.....	V
1 INTRODUCTION.....	6
1.1 PREVIOUS STUDIES ON TSUNAMI HAZARDS IN NORTHLAND	6
1.1.1 <i>THE NIWA STUDIES (2006-2010)</i>	6
1.1.2 <i>OTHER REPORTS AND STUDIES</i>	7
1.1.3 <i>THE EXISTING TSUNAMI INUNDATION AND EVACUATION MAPS</i>	8
2 HISTORY OF TSUNAMIS AFFECTING NORTHLAND	10
2.1 PREHISTORIC TSUNAMI RECORDS.....	10
2.2 HISTORIC TSUNAMI RECORDS	11
3 MODELLING APPROACH.....	14
3.1 A NOTE ON TERMINOLOGY	15
3.2 NUMERICAL MODELLING GRIDS	16
4 TSUNAMI SOURCE CHARACTERISATION	18
4.1 YELLOW ZONE SOURCES	21
4.2 ORANGE ZONE SOURCES.....	28
4.3 DISCUSSION	32
4.3.1 <i>YELLOW ZONE</i>	32
4.3.2 <i>ORANGE ZONE</i>	33
4.4 AGGREGATING THE MODEL OUTPUT	33
4.5 TSUNAMI TRAVEL TIMES.....	35
5 DEVELOPMENT OF DRAFT INUNDATION ZONES FROM MODEL OUTPUT.....	36
5.1 DIFFERENCES BETWEEN THE OLD AND NEW INUNDATION ZONES	36
5.1.1 <i>OTAIPANGO (HENDERSON BAY) AND PUKENUI</i>	38
6 SUMMARY AND CONCLUSION	40
7 REFERENCES.....	41
8 APPENDIX 1: VALIDATION OF THE COMMIT MODEL TSUNAMIS AFFECTING NORTHLAND.....	44
8.1 CASE 1: THE FEBRUARY 27, 2010, MAULE, CHILE EARTHQUAKE AND TSUNAMI	44
8.2 CASE 2: THE MARCH 11, 2011, TOHOKU EARTHQUAKE AND TSUNAMI.....	45
8.3 CASE 3: THE SEPTEMBER 2 ND , 2016, EAST CAPE EARTHQUAKE AND TSUNAMI.....	46
8.4 MODELLING THE 1976 EVENT IN TUTUKAKA	50
8.4.1 <i>1976 SOURCE SENSITIVITY ASSESSMENT</i>	53
8.5 USING COMMIT TO MODEL TSUNAMI CURRENTS	56
9 APPENDIX 2: GRID REGIONS.....	59
10 APPENDIX 3: TRANS-PACIFIC PROPAGATION PLOTS	64

TABLE OF FIGURES

Figure 1.1 Tsunami hazard and risk levels for Northland proposed by Chagué-Goff <i>et al.</i> , 2006.	7
Figure 1.2 Modelled tsunami current speeds at Tutukaka for a large magnitude tsunami from South America representative of the 1868 Arica event. (top) NIWA modelling results. (bottom) results from Borrero and O’Neill (2019). Note: 1 knot = ~2 m/s.....	9
Figure 2.1 Locations of prehistoric tsunami deposits or evidence in Northland.	10
Figure 2.2 The locations of evidence related to three separate prehistoric tsunami events believed to have affected Northland (from Goff <i>et al.</i> , 2010a).....	11
Figure 3.1 The ComMIT propagation model database for tsunamis in the world’s oceans. Insets show the details of the source zone discretization into rectangular sub-faults.....	14
Figure 3.2 Definition sketch for tsunami height, flow depth, runup and inundation distance.	15
Figure 3.3 Extents of the B level (red) and C level (yellow) grids. Areas with low population density along the coast were not modelled in detail. This was more evident along the open west coast	17
Figure 4.1 The Northland region coastline as discretized in Power (2013/2012). Pink shaded regions are the west coast and green shaded regions on the east coast.	19
Figure 4.2 Tsunami heights at different recurrence intervals from the GNS/Power (2013) probabilistic hazard model for coastal zones on Northland’s west coast (top) and east coast (bottom).	20
Figure 4.3 Model output locations (left) and maximum tsunami amplitudes at each point for three different recurrence intervals from the Davies and Griffing (2018) probabilistic tsunami hazard model.....	21
Figure 4.4 Maximum modelled tsunami amplitudes across the A-Grid for the TK4 Source. Red dots are the locations of the Davies and Griffing (2018) output nodes. Black boxes are the B-grid extents. Insets shows the six ‘TK tsunami sources positioned on the southern 800 km of the Tonga-Kermadec Subduction Zone. Each source was 400x100 km and separated by 200 km. One set used a slip amount of 35 m while the other used 30 m.	22
Figure 4.5 Maximum computed tsunami heights around the North Island and in the vicinity of Keri Keri for three identical tsunami sources (400x100 km, 30 m slip) positioned successively northward along the Tonga-Kermadec Subduction Zone.	23
Figure 4.6 Overland flow depth at Otaipango (Henderson Bay) from Sources TK4,5 and 6 depicted in Figure 4.5.....	24
Figure 4.7 (left) Maximum modelled tsunami amplitude for the TK 4 source in the C07 grid. (top right) Histogram of modelled tsunami amplitudes at the shoreline. (bottom right) Table of values.....	25
Figure 4.8 West Pacific (WP) Source regions. Note the WP6 and WP 7 overlap.	29
Figure 4.9 Example of aggregating model output for the Orange Zone extents. The maximum tsunami height from each model run at each output node is selected to create the overall maximum value which is contained in the plot with the red outline. This process was repeated for each C grid and each source region.	34
Figure 4.10 Tsunami travel times to Northland (red star). The 72 source locations are shown with black dots while the tsunami travel times are shown as white contours.....	35
Figure 5.1 Comparison of inundation zones from the GIS attenuation rule (left) vs. hydrodynamic modelling (right) for the entrance to Whangarei Harbour (top) and Whangarei Town area (bottom).....	37
Figure 5.2 Modelled maximum tsunami heights from the TK 4 Source in the Otaipango/Henderson Bay grid (left) and Pukenui grid (right).	38
Figure 5.3 Inundation extents for Otaipango/Henderson Bay for the GIS attenuation model (left) and the hydrodynamic modelling (right).	39
Figure 8.1 Tsunami source model (left) and the trans-pacific propagation pattern (right) for the 2010 Maule, Chile tsunami. Slip amounts (in meters) for the individual fault segments are indicated in white.....	44
Figure 8.2 Modelled water level time series compared to measured data at the Marsden Point tide gauge for the 2010 Maule, Chile tsunami.	44
Figure 8.3 Tsunami source model (left) and the trans-pacific propagation pattern (right) for the 2011 Tohoku, Japan tsunami. Slip amounts (in meters) for the individual fault segments are indicated in white.....	45
Figure 8.4 Modelled water level time series compared to measured data at Marsden Point for the 2011 Tohoku, Japan tsunami.	45
Figure 8.5 Source location of the September 2 nd East Cape Earthquake (USGS, 2017).....	47
Figure 8.6 (following page) Top panel: Earthquake source model for the September 2 nd , 2016, East Cape earthquake (reproduced from USGS, 2016). The top panel shows the location of the fault plane (white region). Epicentre of the	

mains shock is indicated by a star with aftershocks indicated by black circles. Coloured patches indicate coseismic slip amounts according to the colour scale. The thin red line is the top of the fault plane. The white line is the axis of the Tonga-Kermadec Trench. The purple rectangle shows the location of a 100x50 km fault plane source available in the ComMIT tsunami modelling database. Bottom panel: A detail of the slip distribution along the fault plane with the amount of slip indicated by the colour scale. The location of the earthquake hypocentre is indicated by the star with the arrows indicating the direction of the rupture displacement. The contour lines are the timing (in seconds) of the rupture. The red arrow at the top of the fault plane corresponds to the red arrow in the upper panel. The purple box shows the dimensions of a 100x50 km fault plane..... 47

Figure 8.7 Modelled (blue and black traces) versus measured (red trace) water levels at Lottin Point (top) and Tauranga (bottom) for the 2nd September 2016 tsunami. 49

Figure 8.8 Photos from a newspaper account of the 1976 tsunami in Tutukaka. The caption reads “[Left]: A yacht heads out to sea at Tutukaka to escape the tidal wave. In the foreground men steady a pile loosened by surging water. [Right]: Mr D. Cutfield, owner of the launch Willie O inspects a pile snapped off at the base. 50

Figure 8.9 The source segments (left) and the trans-Pacific propagation pattern. 51

Figure 8.10 Time series of modelled tsunami water level inside Tutukaka Harbour. 51

Figure 8.11 Modelled Maximum tsunami amplitude (top) and current speed (bottom). 52

Figure 8.12 Source segments and slip amounts for the January 1976 Kermadec earthquake and tsunami. 54

Figure 8.13 Comparison of modelled time series outputs at Tutukaka for the 13 different source scenarios. The black line is Source 5, the one used in the initial modelling shown in Figure 8.9 through Figure 8.11 55

Figure 8.14 Validation and comparison of numerical simulation tools for water surface elevation and currents in Crescent City, CA; (a) comparison of MOST (blue solid), Boussinesq (green dashed), and tide station data (red solid + dots) for the 2011 Tohoku tsunami; (b) comparison of MOST (blue solid) and tide station data (red solid + dots) for 60 h post-EQ; (c) comparison of fluid speed (m/s) at inner boat basin entrance between Boussinesq (yellow) and digitized video data (red solid + dots); (d) comparison of fluid speed (m/s) at inner boat basin entrance between MOST (yellow) and digitized video data (red solid + dots); (e) maximum speed predicted by COULWAVE across a range of different tsunami sources; and (f) maximum speed predicted by MOST across a range of different tsunami sources. (reproduced from Lynett *et al.*, 2014). 57

Figure 8.15 Modelled maximum tsunami current speeds at the Port of Salalah during the 2004 Indian Ocean tsunami. Black trace represents the estimated path of the Maersk Mandraki container ship as it drifted through port after it was torn from its mooring by the tsunami currents (see Okal *et al.*, 2006b). Figure reproduced from Borrero, 2017. 58

Figure 8.16 Modelled vs. measured tsunami heights (top) and current speeds (bottom) from the 2011 Japan tsunami at the entrance to Tauranga Harbour using the MOST/ComMIT model. Figure reproduced from Borrero *et al.*, 2015. 58

TABLE OF TABLES

Table 2.1 Summary of some historical tsunami events and effects in Northland.	12
Table 3.1 Some details of the computational grids.	16
Table 4.1 Tsunami heights at different recurrence intervals from Power (2021) for each of the coastal zones depicted in Figure 4.1. These data are plotted in Figure 4.2 below.	19
Table 4.2 Maximum modelled tsunami amplitudes from the suite of TK tsunami sources. The 'GNS Zone' numbers are indicated in Figure 4.1 while the locations of the output points are indicated in Figure 4.3 and Figure 4.4.	22
Table 4.3 Comparison between modelled 95 th percentile maximum tsunami heights at the shoreline for each source in each grid against the 2500-year RI, 50 th and 84 th %-ile values from the Power et al (2021) probabilistic model for east coast locations.	26
Table 4.4 Comparison between modelled 95 th percentile maximum tsunami heights at the shoreline for each source in each grid against the 2500-year RI, 50 th and 84 th %-ile values from the Power et al (2021) probabilistic model for west coast locations.	27
Table 4.5 Tsunami sources trialled for the Orange Zone analysis. The largest known historical events are indicated for some of the source regions are indicated as well.	28
Table 4.6 Comparison between modelled tsunami heights at the offshore locations for each source against the 500-year RI value from the Davies and Griffen (2018) probabilistic model. The corresponding 'GNS Zone' numbers are indicated in Figure 4.1 while the Point locations are indicated in Figure 4.3.	30
Table 4.7 Comparison between modelled tsunami heights at the offshore locations for each source against the 500-year RI value from the Power et al (2021) probabilistic model. East coast locations. The output from sources with the values stricken out in the table below was not used as part of the aggregation step used to determine the overall inundation zone.	31
Table 4.8 Comparison between modelled tsunami heights at the offshore locations for each source against the 500-year RI value from the Power et al. (2021) probabilistic model. West coast locations. The output from sources with the values stricken out in the table below was not used as part of the aggregation step used to determine the overall inundation zone.	32
Table 4.9 Comparison of maximum modelled tsunami amplitudes for the WP sources against the offshore values from PTHA18.	33

1 INTRODUCTION

This study focuses on the tsunami hazard for the Northland Region of New Zealand – Te Tai Tokerau o Aotearoa. As with the rest of New Zealand, Northland has a relatively high tsunami hazard owing to its exposure to the Tonga Kermadec Subduction zone, as well as exposure to tsunami generated in the subduction zones of the SW Pacific.

1.1 Previous Studies on Tsunami Hazards in Northland

There have been numerous reports prepared that focus on tsunami effects in Northland. However, these reports have focussed primarily on overland tsunami inundation resulting from very large or 'maximum credible event' (MCE) type sources.

Written in 2004, the Beetham (2004) report gives a broad-brush overview of tsunami hazards in Northland. Possibly because this report was written in the era before the 2004 Sumatra-Andaman tsunami and the 2011 Tohoku Japan tsunami, the report fails to identify the Tonga-Kermadec (TK) Trench as an important potential tsunami source. Instead, the authors focus on potential volcanic sources associated with the TK Trench as the largest near-source hazard. Indeed, the authors state:

"The locally most damaging tsunamis for the Northland region are likely to be generated by volcanic eruptions along the Tonga-Kermadec Trench – at for example the recently discovered Healy Caldera, only 275 km from Northland. There have been no large eruptions in this area in the last 160 years."

This is an odd conclusion given the fact that a damaging tectonically generated tsunami from the TK Trench affected Northland in 1976.

1.1.1 The NIWA Studies (2006-2010)

From 2006 through 2010 a series of five tsunami hazard studies were commissioned by the Northland Regional Council and conducted by NIWA. The first study in this series (Chagué-Goff and Goff, 2006) undertook a comprehensive literature review of tsunami hazards for Northland. This included a review of palaeotsunami evidence, historical information as well as contemporaneous archaeological studies and a sediment stratigraphy analysis for the identification of palaeotsunami deposits.

The study noted that four moderate tsunamis (heights of 1-5 m) had affected the Northland region in the past 150 years while palaeotsunami evidence suggested that at least one large event had occurred in the preceding 600 years. They identified the South American Subduction Zone as a frequent source of moderate to large distant source tsunami. They noted that other source regions such as Indonesia and the Southwest Pacific (Solomon Islands, New Hebrides) are poorly represented in the historical record if at all. They also noted that while a large regional event (such as from the TK Trench) had not occurred in historical times, there was evidence to suggest such an event had occurred in the past 600 years. Ultimately, they proposed that a moderate hazard and risk level be assigned to Northland's east coast with a high hazard and moderate risk for the north and low hazard and risk for the west.

Shortly after this report, Goff et al. (2006) completed their report on tsunami sources relevant to the Northland, Auckland, Waikato and Bay of Plenty regions. This report identified the four most significant tsunami sources relevant to these regions which included sources from South America, the Solomon/New Hebrides region, the TK Trench and selected local sources. This study was pioneering in that they proposed that a large subduction zone earthquake along the TK Trench represented the most significant tsunami source for the region. The modelling presented in this report was done over relatively coarse modelling grids and only produced offshore maximum amplitudes highlighting areas of tsunami amplification. Furthermore, the distant source modelling did not directly model the trans-Pacific propagation, but rather uses a synthetic, ad-hoc time series applied to the eastern boundary of the model domain. As such, the modelling results are quite limited in their applicability.



Figure 1.1 Tsunami hazard and risk levels for Northland proposed by Chagué-Goff *et al.*, 2006.

More detailed modelling was presented in the next report prepared by Lane *et al.*, (2007). This study focused on tsunamis from South America and from the TK Trench and used the same hydrodynamic model as in Goff *et al.*, (2006) but over more detailed bathymetric and topographic grids. As with the previous work, this study has the serious flaw of using an assumed time series imposed along the eastern boundary of the model domain rather than considering the full propagation of the tsunami waves across the Pacific basin. Ultimately this study produced inundation and flow speed maps for several sites in Northland.

This work was carried on in subsequent reports by Gillebrand *et al.*, (2008), Arnold *et al.*, (2009) and Arnold *et al.*, (2011). Each of these studies used the same modelling methodology and tsunami sources as the original Goff *et al.* (2006) and Lane *et al.* (2007) reports. As a result, they all suffer from the same flaw of not properly accounting for the trans-Pacific propagation or inherent variability in tsunamis emanating from distant sources.

1.1.2 Other Reports and Studies

Although not specifically focussing on the Northland region, there have been several reports and papers published dealing with the assessment of the New Zealand tsunami hazard from a variety of far-field sources or studies that focus on the northern and eastern coasts of the North Island.

Firstly, Power *et al.* (2007) proposed a methodology for the probabilistic assessment of tsunami runup around New Zealand focussing on tsunamis emanating from South America. This was followed by the work of Power and Gale (2010) who proposed a methodology for the rapid assessment of a tsunami's potential impact based on earthquake magnitude and location. This methodology is to some extent replicated in this study whereby a set of scenario events is used to precompute the tsunami impact at a site of interest. A look up table (or more specifically, an interactive pdf document) is then produced that allows a user to select a scenario and instantly access information describing the tsunami effects. In the Power and Gale (2010) study this was done for a suite of magnitude (M_w) 8.7, 9.0 and 9.3 earthquakes situated around the Pacific Rim with broad-brush hazard levels determined for the entirety of the New Zealand and the Chatham Islands. In this the analysis is carried out to a higher level of detail for several specific sites in the Northland region. Following this, Power *et al.* (2011) investigated the effect of large magnitude earthquake generated tsunamis from the Tonga-Kermadec, Solomon Islands, and New Hebrides Subduction Zones. As with the other studies mentioned above, the tsunami sources featured uniform slip

distributions and provided only rough scale projections of offshore tsunami wave heights rather than any detailed assessments of tsunami effects at specific sites.

New Zealand's National Tsunami Hazard Model (referred to as either NTHM 2013 or NTHM 2021) has been developed since 2013. The original incarnation described in Power (2013) provided the first probabilistic estimates of coastal tsunami heights for the entirety of New Zealand with detailed information provided in Power (2014). These reports were updated in the studies Power *et al.*, (2022) and Power *et al.* (2023) with the latter providing the site specific, probabilistically derived coastal tsunami heights that are to be used for defining inundation and evacuation zones as per the DGL (2016).

In the period from 2012 through 2019, Borrero conducted a series of probabilistically informed inundation studies for the Waikato and Bay of Plenty regions. In these studies, he considered the recently released New Zealand probabilistic model while also using tsunami sources based on historical large-magnitude events. This included distant source events based on large South American earthquakes as well as regional and near-source events on the TK Trench which were based on the tsunami source models used to replicate the near-field effects of the 2011 Tohoku tsunami in Japan. What sets this work apart from the studies of Power *et al.* described above, is the effort to replicate historical events, the use of heterogeneous slip distributions for the tsunami source models and the detailed analysis of tsunami wave heights and current speeds on fine-scale grids.

Borrero and O'Neill (2019) conducted a detailed assessment of tsunami effects at maritime facilities in the Northland region. Their work developed a series of tsunami response playbooks based on a suite of 216 near, regional and distant source earthquake sources with magnitudes of 8.7, 9.0 and 9.3. The sources covered the entirety of the Pacific Rim, the SW Pacific, as well as the Tonga-Kermadec Trench and Puysegur Subduction zones. One of the key results from their study was showing that previous modelling conducted for Northland suffered from a distinct underprediction and lack of detail in the assessments of the tsunami current speeds (see Figure 1.2).

1.1.3 The Existing Tsunami Inundation and Evacuation Maps

The tsunami evacuation zones currently in use for the Northland Region were developed by Lukovic and Heron (2016). For their study they used an assumed offshore tsunami height, then doubled it to account for tsunami runup on land. The inundation extents were then determined by applying a GIS-calculated attenuation rules developed for use in open coast, shallow harbour, and river situations.

The assumed offshore tsunami heights were derived from two sources. For the Orange Zone, they used a 3-5 m tsunami height based on the tsunami hazard threat levels defined by NEMA. For the Yellow zone, they used the shoreline tsunami height estimates from Power (2013,2014) – the precursor to the Power (2022, 2023) values used in this study.

In the case of the Orange Zone, the assumed runup was 10 m (5 m times 2) plus the height of the water level at high tide which ranged from 1.0 to 1.5 m. For the orange zone, the Power (2013, 2014) shoreline heights ranged from ~5 to 23 m, when doubled this yields tsunami runup of ~11 to 46 m. However, the upper end was truncated to a maximum of 35 m and it was this value that was added to high tide to create the value used to define the inundation zone.

These water levels were then projected inland over their topographic DEM model using different attenuation relationships for the tsunami height depending on whether the coastal zone being analysed was an open coast, shallow harbour or river environment. The specifics of the attenuation relationships can be found in the Lukovic and Heron (2016) report. The end result was a very conservative estimate of the inundation extents.

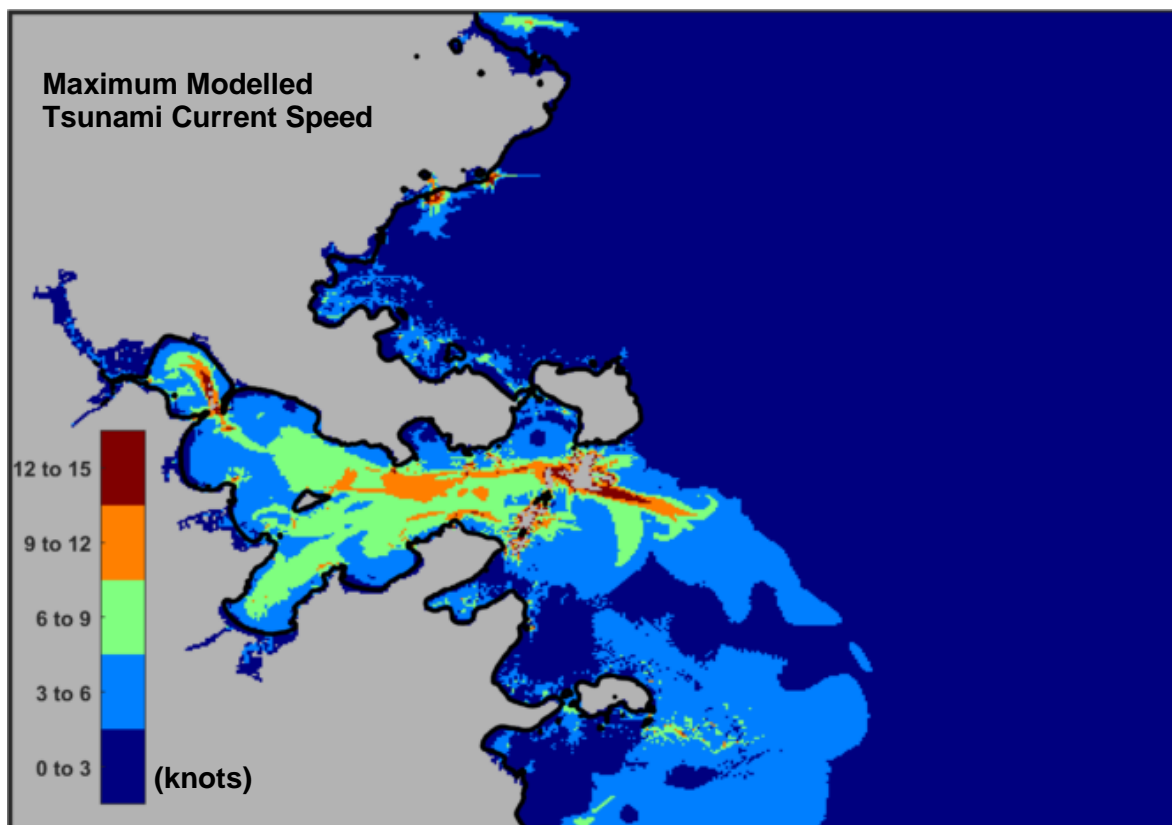
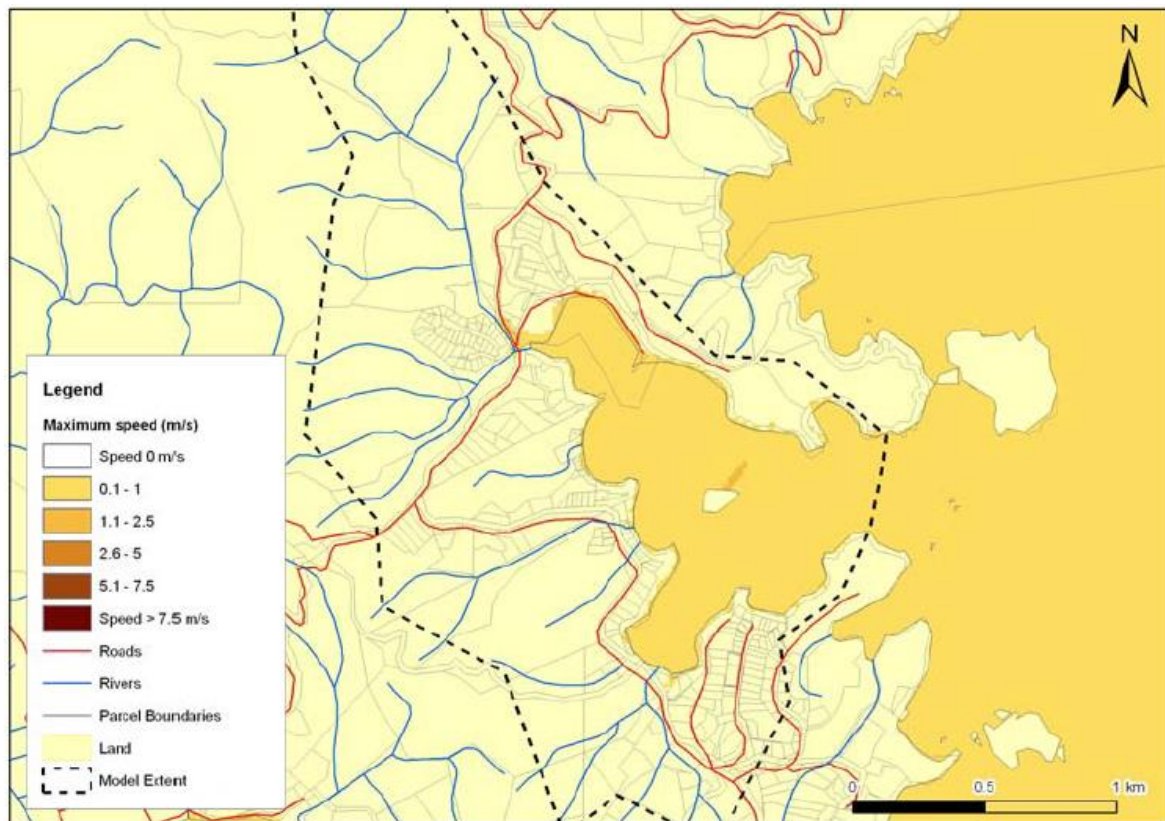


Figure 1.2 Modelled tsunami current speeds at Tutukaka for a large magnitude tsunami from South America representative of the 1868 Arica event. (top) NIWA modelling results. (bottom) results from Borrero and O'Neill (2019). Note: 1 knot = ~2 m/s.

2 HISTORY OF TSUNAMIS AFFECTING NORTHLAND

Northland has been affected by numerous tsunamis in historical times and there is evidence of tsunami affecting the area in prehistoric times.

2.1 Prehistoric Tsunami Records

The New Zealand Palaeotsunami Database. (NZPTB, 2017) contains numerous records of evidence pointing to the occurrence of a palaeotsunami affecting the coast of Northland. Some of this data was originally reported in the work of Chagué-Goff and Goff (2006) and Goff *et al.* (2010a, b) among others. In Figure 2.1 we reproduce an image from the NZPTB website showing the location of palaeotsunami evidence. This figure suggests that substantial evidence exists for the occurrence of significant palaeotsunamis having affected the Northland coastline.

Goff *et al.* (2010a) describe the available data in more detail and ascribe the data points to three separate events. The oldest of these events are believed to have occurred approximately ~6500, ~2800 years before present (BP) and are associated with possible large magnitude earthquakes on the TK Trench. The most recent of the three events was dated to 1450 AD (569 years BP), however no clear source for this event has been determined. Goff *et al.* (2010a) tentatively associate it with the eruption of the Kuwae Caldera in 1452/1453 AD.

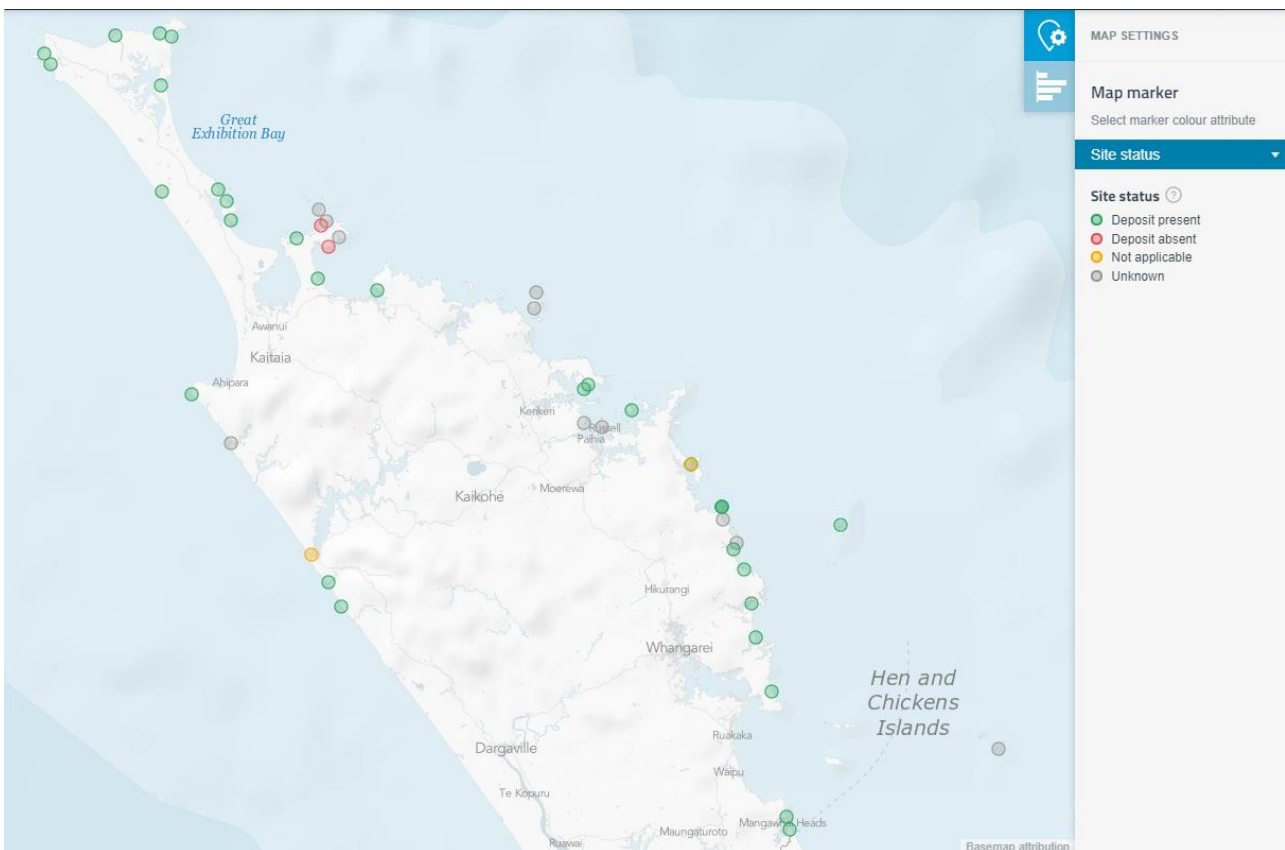


Figure 2.1 Locations of prehistoric tsunami deposits or evidence in Northland.

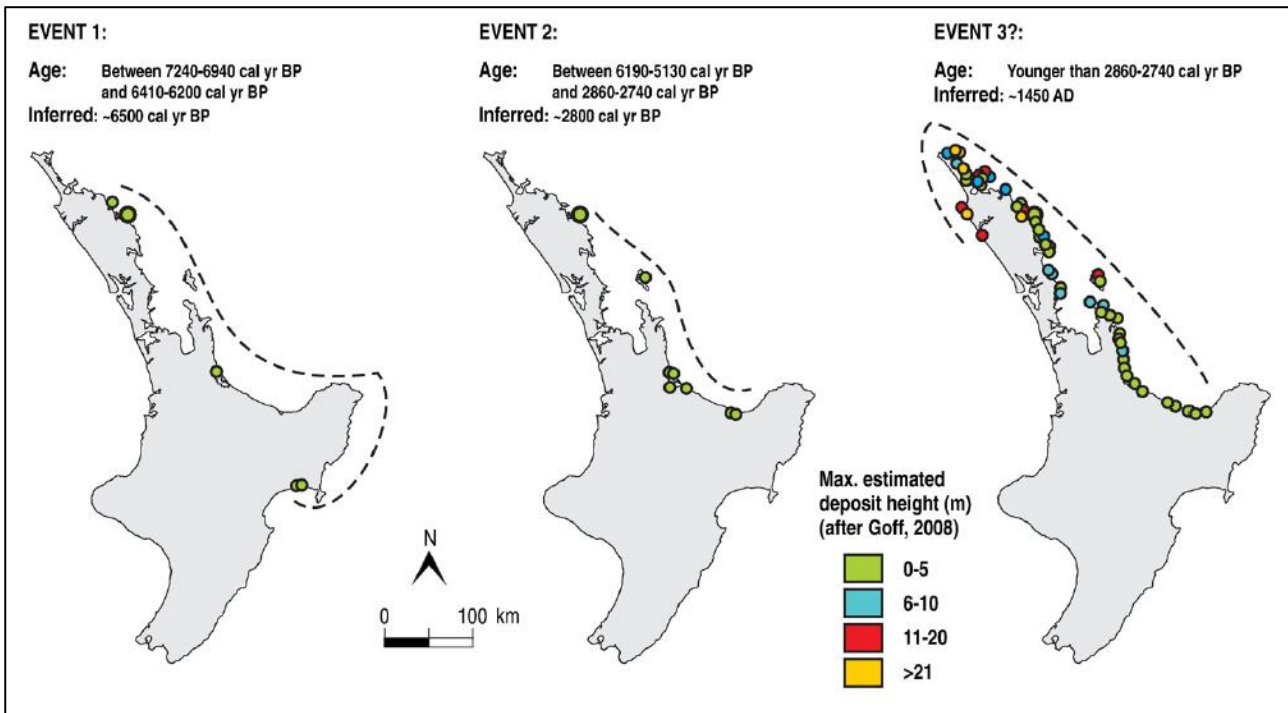


Figure 2.2 The locations of evidence related to three separate prehistoric tsunami events believed to have affected Northland (from Goff *et al.*, 2010a)

2.2 Historic Tsunami Records

There are numerous accounts of tsunamis affecting Northland in the historical record. In Table 2.1 we summarise these accounts collected from De Lange and Healy (1986) and from GNS’s on-line historical tsunami database (Downes *et al.*, 2017, GNS, 2018). Of these, all are distant source events other than the 1976 Kermadec Island event which was a regional event.

Besides the events listed below, the Northland Region was also affected by the February 2010 Maule Chile tsunami and the 11 March 2011 Tohoku, Japan tsunami (GNS Database, Borrero and Greer, 2012, Borrero *et al.*, 2012). The available complete and detailed descriptions of the effects of the different tsunami events at locations in the Northland Region are reproduced in Appendix 2.

Of the events listed below, the 1877 and 1960 events from northern and southern Chile respectively are the most thoroughly described with strong effects observed and or recorded in Tutukaka and the Bay of Islands area. It is interesting to note that the 1877 event seems to have been larger – or at least more widely noticed - than the 1868 event although the 1868 event is generally regarded to have been a ‘bigger’ tsunami. However, we note that given the relatively sparse population of New Zealand in the mid 1800’s and inconsistencies in data collection and reporting, all of the tsunami data recorded prior to the 1970’s should be treated with caution.

Table 2.1 Summary of some historical tsunami events and effects in Northland.

Site Name	Tsunami Height (m)	Inundation depth (m)	Note
1835 Central Chile			
Waitangi			reported
1868 Southern Peru, 13 August, 21:30 UTC			
Doves Bay	1.2	0.6	
Mangonui	1.2-1.5		
Russel	n/a		above spring high tide.
1877 Northern Chile, 10 May, 00:59 UTC			
Waitangi	1.8, 3.0		Large tidal wave into the bay, 3.0 m reported by Laing (1954), tender from 'Iona' swept above the high tide mark
Tutukaka		1.6	Several waves came in each succeeding wave decreasing in size/force
Russel	1.8		The tide ebbed and flowed seven times on May 11. Max. fluctuation of 1.8 m
Paihia	3.1, 3.6(?)		Mid-day May 11th, water dropped 1.2 m then rose 1.9 m by 12:25 pm. 'Gazelle' grounded in water depth of 3.6 m
Wairoa Bay	n/a		4 pm, May 11th, wave rushed in and flooded 9 m (laterally) above high-water mark. Two boats washed ashore and left high and dry in a paddock
Bay of Islands (various)	2.5		Reports from islands within the bay of sudden rise of 2.5 m around 5 pm on May 11th, followed by ebbing and flowing every 20 min.
1946 Aleutian Islands 1 April, 12:28 UTC			
Tutukaka	0.6	1.2	waves in rapid succession occurring for several days
Tutukaka	0.3-0.5		0.3 m bore observed on the river at 7:30 pm on the 5th of November followed by 'tidal fluctuations' of about 0.5 m
1952 Kamchatka, 4 November, 16:58 UTC			
Tutukaka	0.75		
1960 Chile, 22 May, 19:11 UTC			
Mangonui	1.2		1.2 m rise and fall was recorded within 10 minutes. A submarine telephone cable was broken on the 24th.
Whangaroa			Boat left "high and dry"
Waitangi	n/a		Strong flood and ebb flows at 20-40 min intervals starting late on 23rd May. Whirlpools observed, one boat damaged following a collision with the Waitangi Bridge.
Opuā	1-1.5	1.5	water level changed 3-4ft in minutes, formation of whirlpools
Opuā	3.0		Reports are similar to those from Waitangi, flashing channel marker beacon was damaged when strong flows broke a supporting pile. Boats moored in 3 m of water were grounded.
Tutukaka	2.8	1.5	water receded then returned, rising 2.8 m within minutes. Surges continued at 15-30-minute intervals. Coast road flooded and a bridge abutment damaged.
Whangarei	1		A series of 1 m swells were reported from the Town Basin.
Marsden Point		2	no damage

Table 2.1 (continued)

1964 Alaska March 28, 03:36 UTC			
Whangaroa	1		Boat left "high and dry"
Waitangi		0.6	10 knot tides
Opuā			10 knot tides
Marsden Point	0.3	0.3	1ft variation in tide
1976 Kermadec Islands, 15 January, 07:10 UTC			
Tutukaka	0.2	0.75	0.2m rise lasting 5-6 minutes came in as a "big whirlpool"
Tutukaka	0.75		Sudden surge of 0.75 m. Several yachts damaged when one broke its moorings and was swept in to the others in the harbour. Wave arrived about 3 hours after the earthquake.
1977 Tonga, 22 June, 22:09 UTC			
Opuā	0.15	0.15	
1994 Kuril Islands, 4 October, 13:23 UTC			
Marsden Point	0.1		
2001 Southern Peru 23 June, 20:34 UTC			
Marsden Point	0.18		
2006 Tonga 3 May, 15:27 UTC			
Marsden Point	0.15		
2010 Maule, Chile, 27 February, 18:34 UTC			
Numerous accounts throughout Northland, +/- 0.2 m on Marsden Point tide gauge (see Section 4.1 of this report), also see GNS database and Borrero and Greer (2012) for more details.			
2011 Tohoku, Japan, 11 March, 05:46 UTC			
Numerous accounts throughout Northland, +/- 0.3 m on Marsden Point tide gauge (see Section 4.2 of this report), also see GNS database, Borrero <i>et al.</i> , (2012) and Borrero and Greer (2012) for more details.			

3 MODELLING APPROACH

The numerical modelling presented in this study was carried out using the Community Model Interface for Tsunamis (ComMIT) numerical modelling tool. The ComMIT model interface was developed by the United States Government National Oceanic and Atmospheric Administration’s (NOAA) Centre for Tsunami Research (NCTR) at the Pacific Marine Environmental Laboratory (PMEL) following the December 26, 2004, Indian Ocean tsunami as a way to efficiently distribute assessment capabilities amongst tsunami prone countries.

The backbone of the ComMIT system is a database of pre-computed deep-water propagation results for tsunamis generated by unit displacements on fault plane segments (100 x 50 km) positioned along the world’s subduction zones. Currently, there are 1,691 pre-computed unit source propagation model runs covering the world’s oceans included in the propagation database. Using linear superposition, the deep ocean tsunami propagation results from more complex faulting scenarios can be created by scaling and/or combining the pre-computed propagation results from a number of unit sources (Titov *et al.*, 2011). The resulting trans-oceanic tsunami propagation results are then used as boundary inputs for a series of nested near shore grids covering a coastline of interest. The nested model propagates the tsunami to shore computing wave height, velocity and overland inundation. The hydrodynamic calculations contained within ComMIT are based on the MOST (Method Of Splitting Tsunami) algorithm described in Titov and Synolakis (1995, 1997) and Titov and Gonzalez (1997). The ComMIT tool can also be used in conjunction with real time recordings of tsunami waveforms on one or more of the deep ocean tsunameter (DART) stations deployed throughout the oceans to fine tune details of an earthquake source mechanism in real time. An iterative algorithm that selects and scales the unit source segments is used until an acceptable fit to the observed DART data is met (Percival *et al.*, 2010).

Validation of the ComMIT modelling methodology for historical tsunami affecting Northland and other parts of New Zealand is presented in Appendix 1.

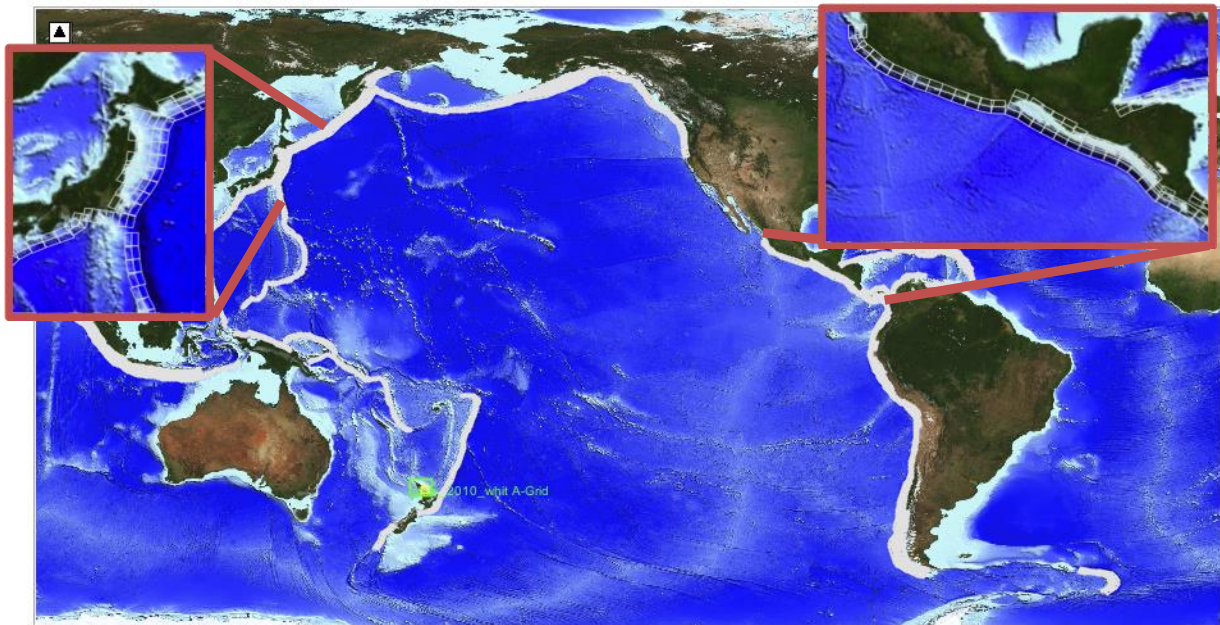


Figure 3.1 The ComMIT propagation model database for tsunamis in the world’s oceans. Insets show the details of the source zone discretization into rectangular sub-faults.

3.1 A Note on Terminology

There is often some ambiguity in the terminology used to describe the size of a tsunami. Generally, the term 'height' is used as defined in Figure 3.2 below, i.e. the measure of a distance above a particular datum. However, since tsunamis are waves, it is also common to use the term 'amplitude' which is the distance (height?) above or below a particular datum. For a perfectly symmetrical sine wave, the 'height' is twice the 'amplitude'.

In Power (2013) he writes:

“TSUNAMI HEIGHT (m) is the vertical height of waves above the tide level at the time of the tsunami (offshore it is approximately the same as the AMPLITUDE). It is far from constant, and increases substantially as the wave approaches the shoreline, and as the tsunami travels onshore. The term “WAVE HEIGHT” is also often used, but there is a potential ambiguity as many scientists define WAVE HEIGHT as the peak-to-trough height of a wave (approximately twice the amplitude). Note that this is a change in terminology from the 2005 Tsunami Hazard and Risk Review, intended to bring greater consistency with international usage of these terms.

And with regards to runup he says:

“TSUNAMI RUN-UP (m), a measure much used in tsunami-hazard assessment, is the elevation of inundation above the instantaneous sea level at the time of impact at the farthest inland limit of inundation. This measure has a drawback in that its relationship with the amplitude of the waves at the shore depends markedly on the characteristics of waves and on the local slopes, vegetation, and buildings on the beach and foreshore areas, so it is highly site-specific.”

And finally, with regards to the hazard curves for the National Tsunami Hazard Model he writes:

“in the curves shown here the ‘maximum amplitude’ should be interpreted as the tsunami height measured at the location within the section where it is highest”

Hence there is a degree of interchangeability in the use of 'height' and 'amplitude'. In this report we use 'height' for the elevation of the water surface above the sea level datum at the start of a model run. When discussing the hazard curves, we use the term 'amplitude' in line with Power (2013), which, as we see above, is used interchangeably with 'height'.

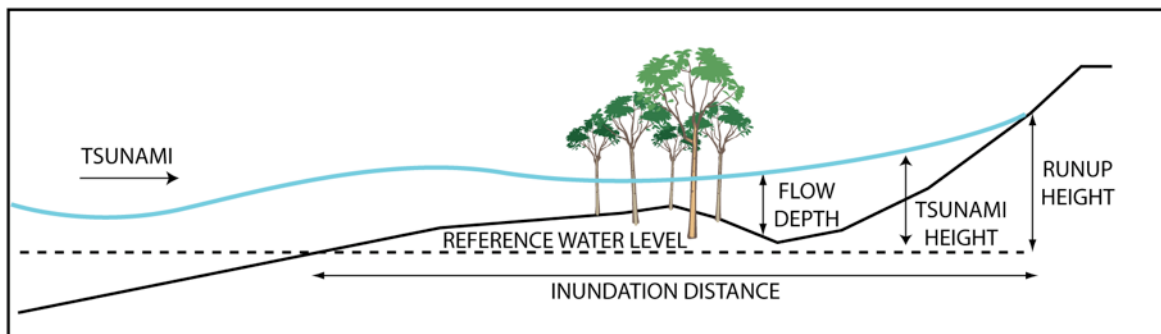


Figure 3.2 Definition sketch for tsunami height, flow depth, runup and inundation distance.

3.2 Numerical Modelling Grids

The Northland Regional Council provided LiDAR topography data for construction of the numerical modelling grids. This data was combined with additional data sets covering the regional offshore bathymetry and on land topography. This included the Shuttle Radar Topography Mission (SRTM) 90 m resolution topography, 200 m resolution bathymetry from NIWA, as well as hydrographic chart data from Land Information New Zealand (LINZ). The data were combined into a master set of (x,y,z) triplets and then gridded into different resolutions and coverage areas using the Kriging algorithm from the Surfer software package. Model grids were set up for mean sea level (MSL). Each model run utilized the same A grid, but the areas studied were divided into 9 separate B grids for modelling. Details for each of the model grids used in this study are presented in Table 3.1. The orientation and location of the A, B and C-level grids is shown in Figure 3.3. Close up views of each B and C-grid region with numbering are presented in Appendix 2.

Table 3.1 Some details of the computational grids.

I.D.	Name	W	E	S	N	I.D.	Name	W	E	S	N
B1	Far North B	172.55	173.15	-34.7	-34.3	B7	Whangaroa B	173.6	174.025	-35.1	-34.9
C1	Cape Reinga	172.61	172.75	-34.5	-34.4	C28	Motuhakahaka	173.615	173.68	-34.97	-34.94
C2	North Cape	172.75	172.87	-34.46	-34.4	C29	Taupo Bay	173.7	173.76	-35	-34.97
C3	Piwhane Bay	172.93	172.995	-34.44	-34.39	C30	Whangaroa	173.7	173.78	-35.06	-35
C4	Takapakura	172.99	173.03	-34.49	-34.42	C31	Tauranga Bay	173.77	173.84	-35.02	-34.98
C5	Te Hapua	172.9	173.02	-34.55	-34.49	C32	Te Ngare Bay	173.84	173.89	-35.025	-34.97
B2	Kari Kari B	173.025	173.6	-35.025	-34.675	C33	Matauri Bay	173.895	173.93	-35.045	-35.015
C6	Rarawa	173.04	173.1	-34.73	-34.69	C34	Motukawanui	173.925	173.98	-35.04	-34.965
C7	Hendersons	173.11	173.17	-34.79	-34.73	B8	Bay of Islands B	173.92	174.46	-35.47	-35.06
C8	Pukenui	173.11	173.19	-34.85	-34.8	C35	Takou Bay	173.93	174	-35.13	-35.08
C9	Rangiputa	173.25	173.33	-34.925	-34.85	C36	Te Puna Inlet	173.98	174.065	-35.19	-35.14
C10	Maitai Bay	173.37	173.46	-34.85	-34.77	C37	Purerua	174.065	174.15	-35.19	-35.14
C11	Tokerau	173.36	173.4	-34.91	-34.87	C38	Keri Keri	173.96	174.075	-35.24	-35.18
C12	Coopers Beach	173.44	173.57	-35.01	-34.96	C39	Moturoa	174.07	174.12	-35.22	-35.195
B3	Ahipara B	173	173.22	-35.33	-35	C40	Rawhiti	174.15	174.27	-35.29	-35.19
C13	Waipapakauri	173.15	173.18	-35.06	-35.02	C41	Waitangi-Russel	174.05	174.15	-35.33	-35.24
C14	Ahipara	173.11	173.165	-35.185	-35.145	C42	Elliot Bay	174.28	174.34	-35.31	-35.24
C15	Tauroa	173.04	173.11	-35.24	-35.15	C43	Whangaruru	174.3	174.39	-35.4	-35.33
C16	Herekino	173.14	173.21	-35.31	-35.26	C44	Helena Bay	174.34	174.425	-35.45	-35.4
B4	Hokianga B	173.25	173.55	-35.6	-35.35	B9	Tutukaka B	174.4	174.62	-35.77	-35.41
C17	Omapere	173.35	173.405	-35.55	-35.5	C45	Mimiwhangata	174.425	174.46	-35.47	-35.43
C18	Opononi	173.395	173.415	-35.485	-35.465	C48	Whananaki	174.445	174.49	-35.54	-35.47
C19	Rawene	173.495	173.51	-35.41	-35.39	C49	Matapouri	174.465	174.53	-35.575	-35.54
B5	West Coast B	173.55	173.95	-36.15	-35.75	C50	Tutukaka	174.525	174.55	-35.625	-35.605
C20	Omamari	173.63	173.69	-35.885	-35.84	C51	Ngunguru	174.48	174.535	-35.66	-35.62
C21	Baylys	173.71	173.77	-35.98	-35.93	C52	Patua	174.505	174.55	-35.725	-35.69
C22	Glinks Gully	173.84	173.875	-36.1	-36.07	C53	McGregors Bay	174.525	174.58	-35.75	-35.71
B6	Kaipara B	173.95	174.35	-36.5	-36.1	B10	Whangarei B	174.31	174.8	-36.15	-35.7
C23	Ruawai	174	174.04	-36.15	-36.12	C54	Whangarei	174.32	174.39	-35.78	-35.72
C24	Kellys Bay	174.09	174.14	-36.27	-36.24	C55	Marsden Point	174.43	174.54	-35.87	-35.765
C25	Pouto	174.17	174.195	-36.37	-36.35	C56	Ocean Beach	174.54	174.59	-35.85	-35.78
C26	Tinopai	174.24	174.28	-36.26	-36.23	C57	Ruakaka	174.445	174.48	-35.95	-35.87
C27	Birds Beach	174.25	174.28	-36.33	-36.3	C58	Waipu	174.45	174.5	-36.01	-35.95
						C59	Langs Beach	174.49	174.6	-36.06	-36.01
						C60	Mangawhai	174.57	174.63	-36.13	-36.07

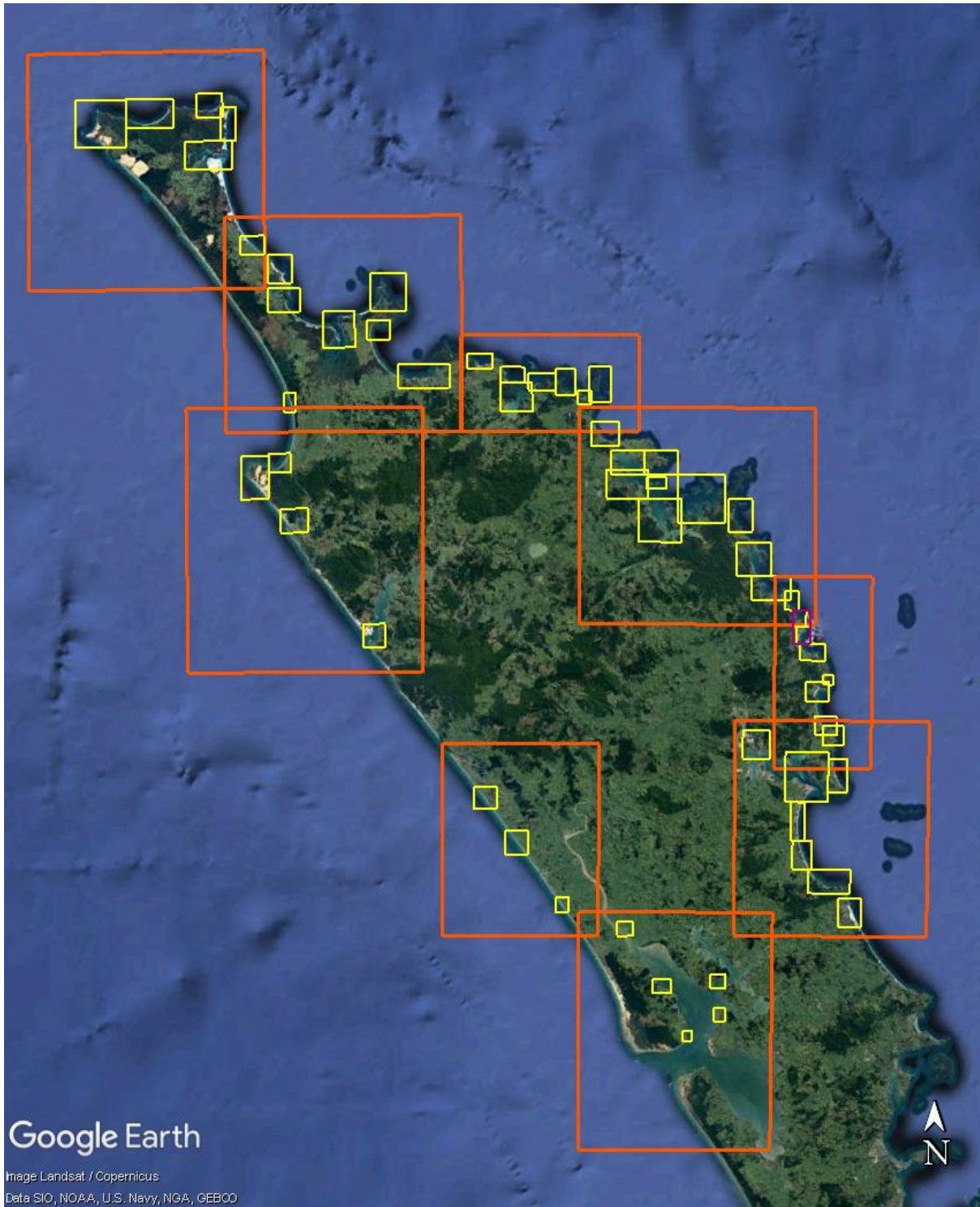


Figure 3.3 Extents of the B level (red) and C level (yellow) grids. Areas with low population density along the coast were note modelled in detail. This was more evident along the open west coast

4 TSUNAMI SOURCE CHARACTERISATION

Sources for the inundation modelling are defined according to guidance from the DGL. For the yellow zone we focussed on defining a source that would produce tsunami height consistent with a 'maximum credible event' (MCE) which according to the DGL this should correspond to the 84th percentile tsunami heights at a 2500-year recurrence interval as defined in the New Zealand National Tsunami Hazard Model (NTHM 2021 - Power et al., 2022). For the orange zone, the tsunami heights at the shoreline should be consistent with a 500-year RI event.

The Power et al. (2022) study is an update to Power (2013) and as with the earlier study, the coast of New Zealand is broken into ~50 km segments with tsunami hazard curves (tsunami height vs. recurrence interval) and source disaggregation pie charts provided for each segment. The relevant coastal zones for this study are reproduced in Figure 4.1 while the probabilistically defined tsunami heights at various recurrence intervals are listed in Table 4.1 and plotted in Figure 4.2.

The main takeaway from these plots are as follows:

- The hazard on Northland's east coast is substantially higher than on the west coast.
- The east coast sites show greater variability from zone to zone as compared to the west coast.

We also point out that the tsunami height values presented in the GNS/Power et al. (2021) hazard curves are not modelled output, but rather are values derived from empirical relationships between earthquake magnitude and tsunami runup and as such, they should be treated with caution and used only as a guideline. Furthermore, the GNS PTHA 2021 data is a single value for a large section of coastline. In reality, tsunami heights are highly variable along stretches of coast as a result of irregularities in the offshore bathymetry. This results in large difference in the tsunami height at the shoreline and the corresponding runup and inundation.

For this study, we provide additional comparison between the output from the tsunami source models and the probabilistic tsunami modelling prepared by Geoscience Australia (PTHA 18: Davies and Griffen, 2018). In their study, hydrodynamic modelling of thousands of tsunami sources was used to generate probabilistic hazard curves for points located in relatively deep water offshore of the New Zealand coastline. A plot of their model output locations and the relevant tsunami amplitudes at these locations is presented in Figure 4.3.

The comparison between our modelling and the output from both of these probabilistic models is presented in the sections below.

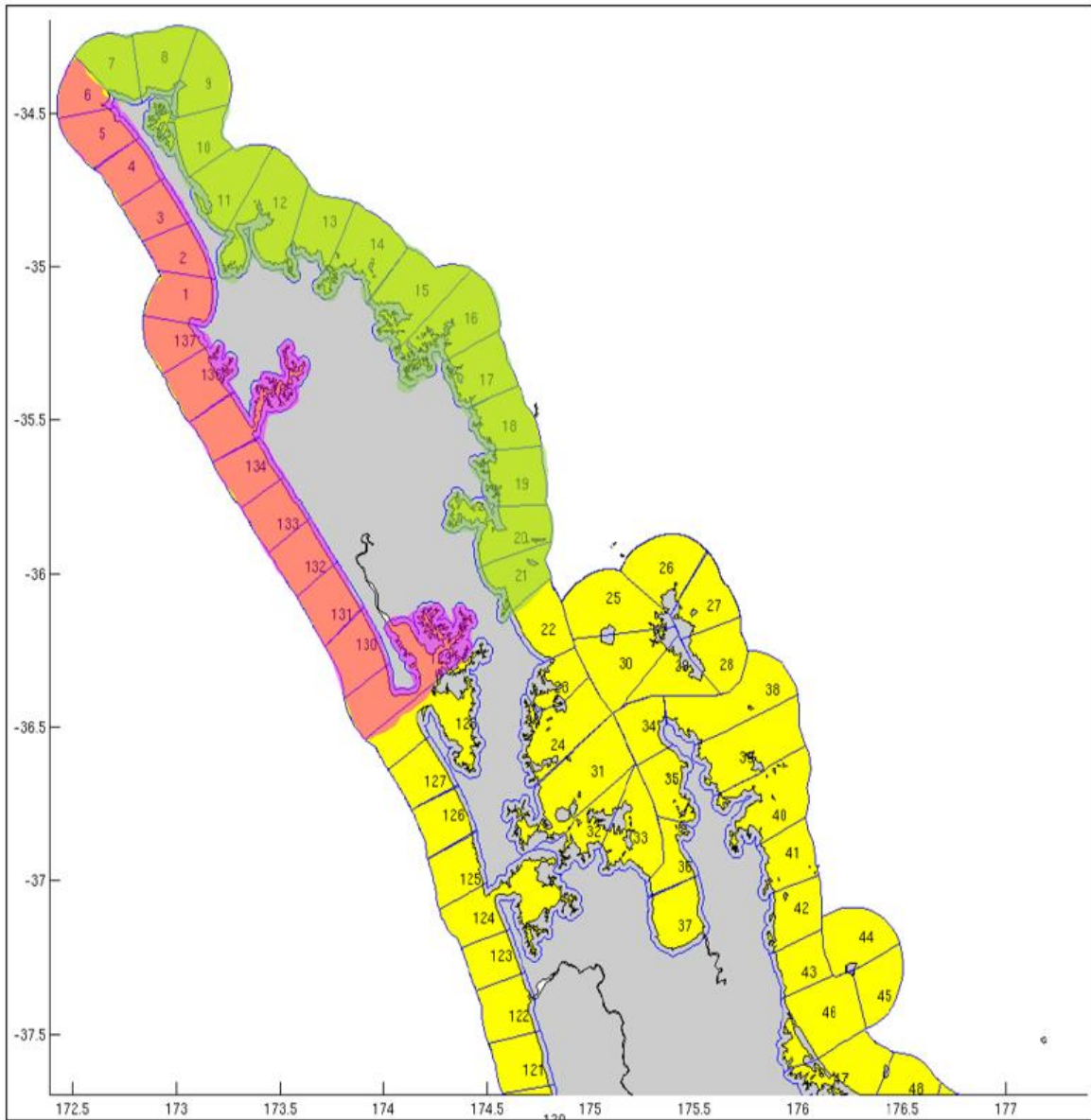


Figure 4.1 The Northland region coastline as discretized in Power (2013/2012). Pink shaded regions are the west coast and green shaded regions on the east coast.

Table 4.1 Tsunami heights at different recurrence intervals from Power (2021) for each of the coastal zones depicted in Figure 4.1. These data are plotted in Figure 4.2 below.

WEST COAST

EAST COAST

Zone # and Name	100-yr 50%-ile	500-yr 50%-ile	1000-yr 50%-ile	2500-yr 50%-ile	2500-yr 84%-ile	Zone # and Name	100-yr 50%-ile	500-yr 50%-ile	1000-yr 50%-ile	2500-yr 50%-ile	2500-yr 84%-ile
(129) Kaipara Entrance North	1.8	3.3	4.1	5.4	7.1	(7) Cape Reinga	3.2	7.4	10.8	16.6	24.8
(130) Lake Wairere	2.1	3.4	4.2	5.4	7.1	(8) Hooper Point	2.8	6.3	9.5	15.6	24.6
(131) Mahuta	1.2	2.3	3.0	4.1	5.8	(9) North Cape	2.1	4.7	6.9	11.4	20.3
(132) Baylys Beach	1.4	2.6	3.4	4.8	6.4	(10) Great Exhibition Bay - Kokota	2.0	4.1	5.6	8.8	14.4
(133) Aranga Beach	1.7	3.4	4.4	6.1	9.6	(11) Granville Point	2.4	4.8	6.5	10.0	17.1
(134) Kaikai Beach	1.8	3.6	4.8	6.9	10.3	(12) Karikari Peninsula	2.5	4.8	6.3	9.1	15.2
(135) Omapere	2.0	3.8	5.2	7.6	10.8	(13) Motukahakaha Bay	2.8	5.8	7.9	12.1	19.2
(136) Owata	2.0	4.4	6.0	8.8	12.7	(14) Cavalli Islands	2.6	5.8	8.5	14.4	25.8
(137) Waitaha Stream	1.8	3.9	5.6	8.3	13.2	(15) Pureua Peninsula	2.3	5.1	7.5	12.4	20.2
(1) Ahipara	3.0	6.0	7.9	10.6	14.8	(16) Cape Brett	2.9	6.2	8.9	14.4	22.6
(2) Hukatere	2.4	4.6	6.0	8.5	13.5	(17) Whangaruru Bay	2.9	6.3	8.9	14.2	23.6
(3) Ninety Mile Beach	2.1	4.0	5.2	7.4	12.2	(18) Sandy Bay	3.1	6.2	8.4	12.5	19.2
(4) Te Wakatehaua Island	2.3	4.3	5.4	7.2	10.1	(19) Ngunguru Bay	2.7	5.0	6.5	9.0	13.8
(5) Tiriparepa Point	2.1	3.9	5.0	6.8	9.2	(20) Whangarei	1.8	3.5	4.7	6.8	11.7
(6) Cape Maria van Diemen	2.8	4.8	6.0	8.0	11.3	(21) Mangawhai Heads	1.8	3.3	4.3	6.0	9.1

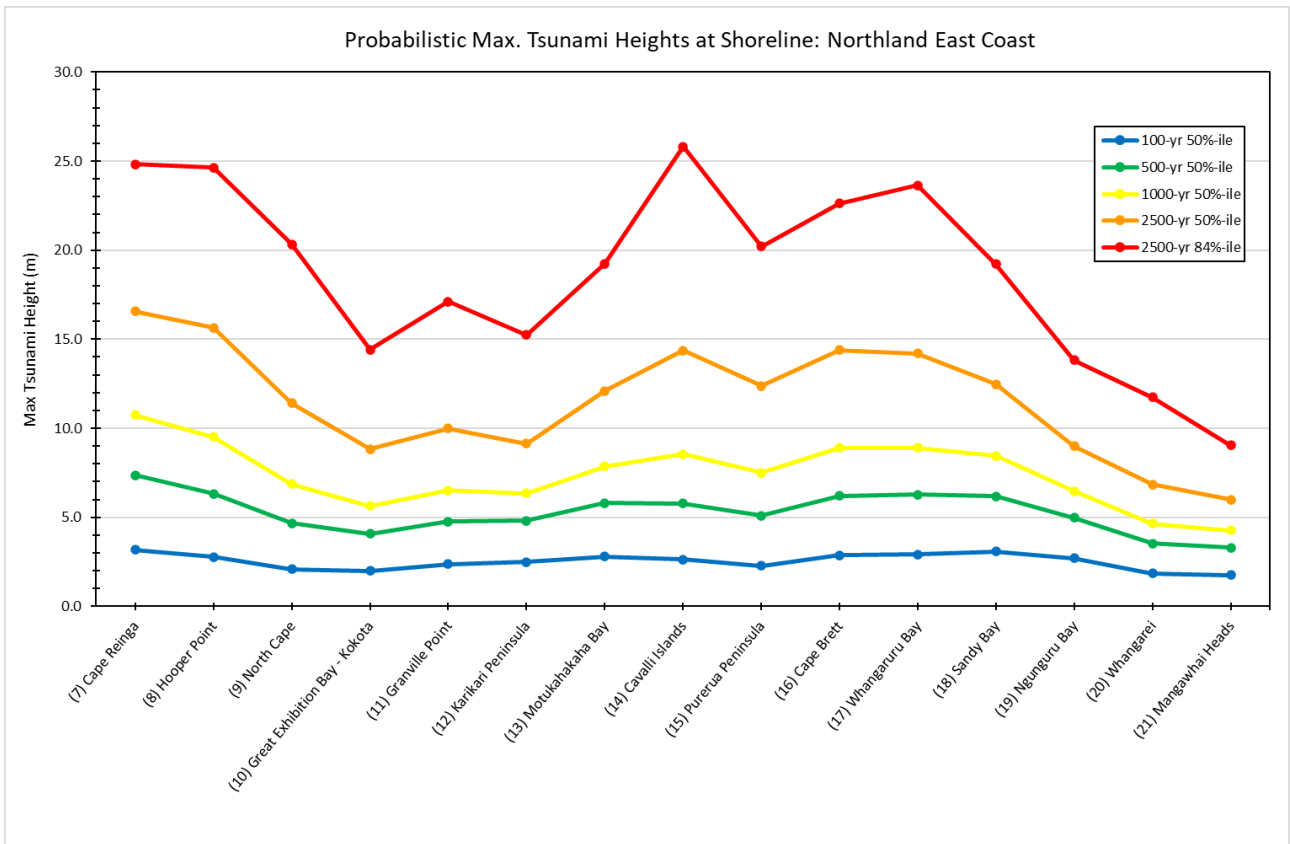
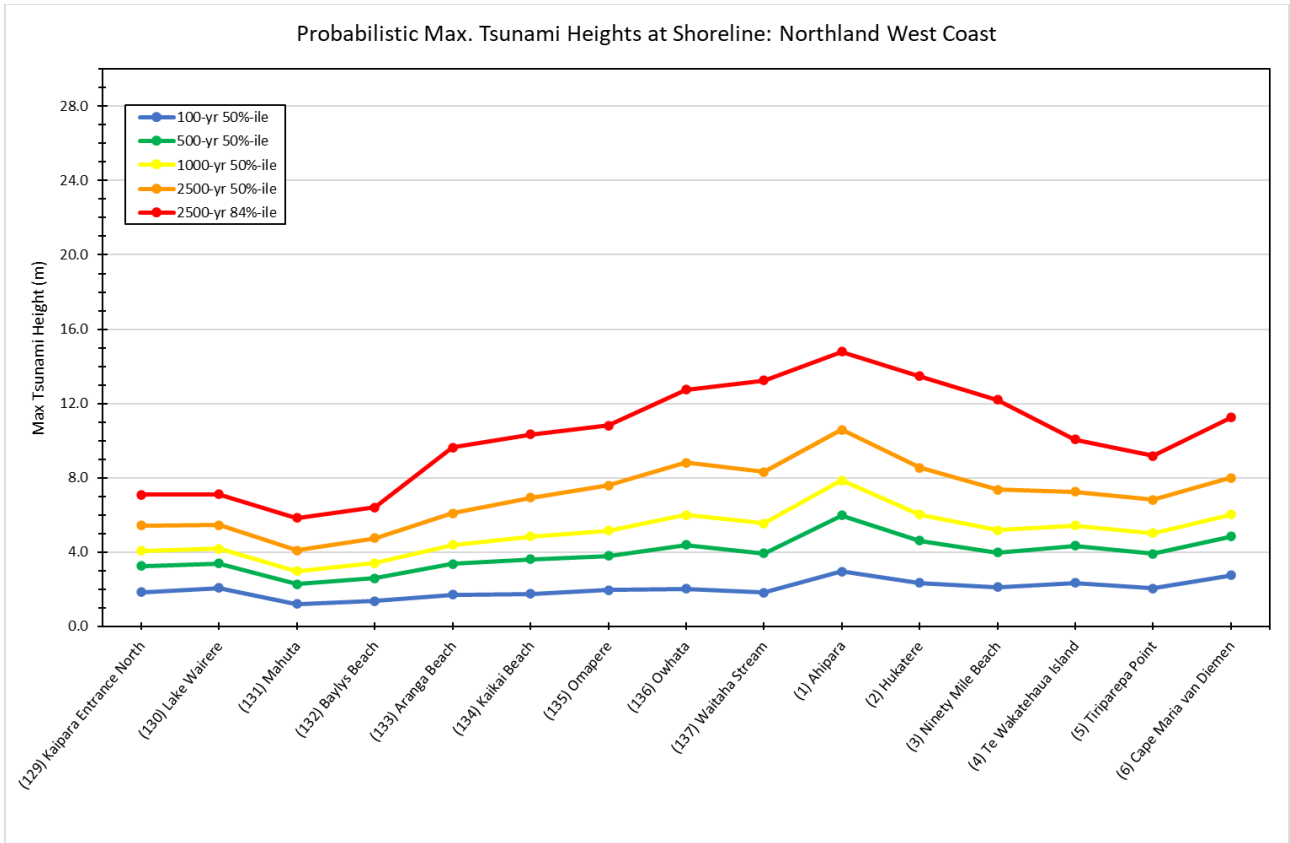
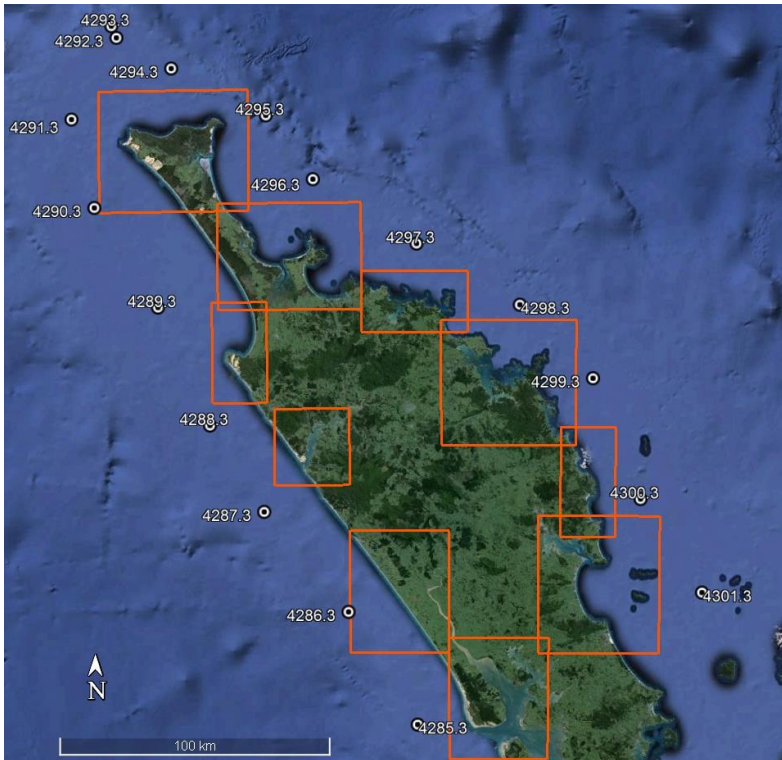


Figure 4.2 Tsunami heights at different recurrence intervals from the GNS/Power (2013) probabilistic hazard model for coastal zones on Northland’s west coast (top) and east coast (bottom).



	POINT	2500-yr 84th %-ile	2500-yr mean	500-yr mean
WEST COAST	4285.3	1.7	1.5	0.8
	4286.3	1.5	1.3	0.7
	4287.3	1.8	1.6	0.9
	4288.3	2.0	1.7	0.9
	4289.3	3.6	2.9	1.4
	4290.3	3.6	2.9	1.4
	4291.3	5.6	4.0	1.7
EAST COAST	4292.3	4.8	3.6	1.4
	4293.3	4.9	3.6	1.4
	4294.3	5.3	3.7	1.4
	4295.3	4.0	2.8	1.1
	4296.3	4.2	3.0	1.3
	4297.3	4.1	3.2	1.5
	4298.3	4.3	3.2	1.5
	4299.3	4.7	3.5	1.7
	4300.3	3.8	3.2	1.8
	4301.3	3.9	3.2	1.8

Figure 4.3 Model output locations (left) and maximum tsunami amplitudes at each point for three different recurrence intervals from the Davies and Griffing (2018) probabilistic tsunami hazard model.

4.1 Yellow Zone Sources

Recall from the DGL that:

“The Yellow Zone should cover all maximum credible tsunami events including the highest impact events. The intention is that the Yellow Zone provides for local-source maximum credible events, based on locally determined risk. People should evacuate this zone in natural or informal warnings from a local source event, and when instructed via formal warnings.

The Yellow Zone Should be defined in such a way that it encompasses the area expected to be inundated by the 2500-year tsunami at the 84% confidence level. This timeframe includes large subduction interface earthquakes, including events comparable to the earthquake that caused the 2011 Great East Japan tsunami, in those areas where they are considered possible. It is not an absolute ‘worst case’, as this is not well defined. It is a compromise between the very low probability of even larger events and the issues and risks involved in a mass-evacuation in the aftermath of strong earthquake shaking.”

Based on modelling conducted for the Auckland Council (Borrero and O’Neill, 2020) it was shown that the Yellow Zone inundation extents were governed by large scale ruptures on the southern segments of the Tonga-Kermadec subduction zone. Thus, for this study we used a suite of six scenarios positioned along the southern 800-km of the TK trench (Figure 4.4). Our source model uses a compact, 400 x 100 km rupture with relatively large values of co-seismic slip. The source is positioned at three different locations, each 200 km further north. We trialled cases with 35 m and 30 m co-seismic slip and then compared the results to the probabilistic models described above.

Model output presented in Figure 4.5 shows that as the source region is moved northward along the trench, the tsunami heights along the east coast of New Zealand’s north island fall off rapidly. The effect on inundation at Otaipango (Henderson Bay) is shown in Figure 4.6. The model output from the points indicated in Figure 4.3 are compared to the probabilistic model results from Davies and Griffen (2018) in Table 4.2. Here we see that the TK1 source generally overpredicts the values from the probabilistic model with the TK2 and TK4 sources providing a better match to the target offshore amplitude.

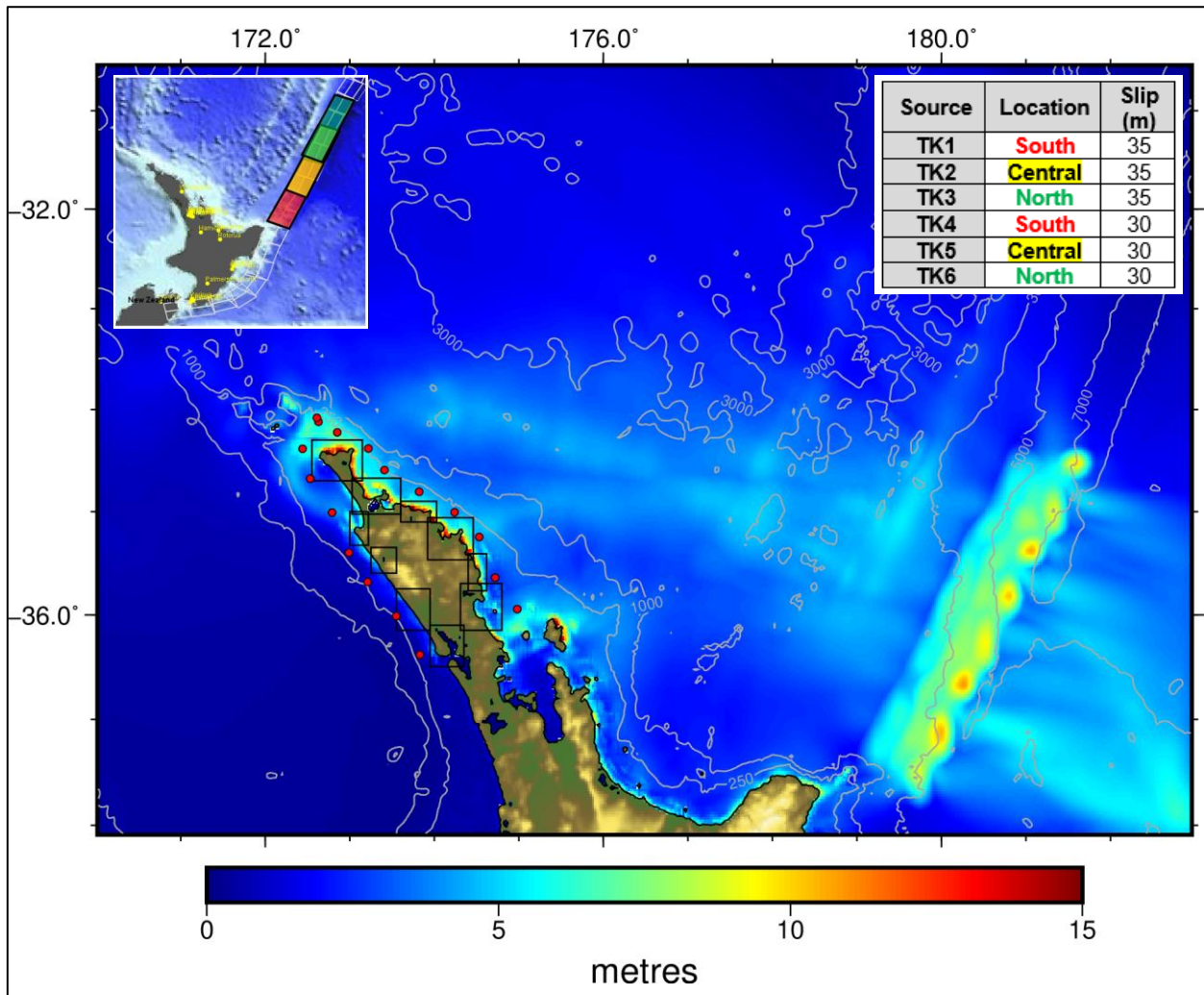


Figure 4.4 Maximum modelled tsunami amplitudes across the A-Grid for the TK4 Source. Red dots are the locations of the Davies and Griffen (2018) output nodes. Black boxes are the B-grid extents. Inset shows the six 'TK' tsunami sources positioned on the southern 800 km of the Tonga-Kermadec Subduction Zone. Each source was 400x100 km and separated by 200 km. One set used a slip amount of 35 m while the other used 30 m.

Table 4.2 Maximum modelled tsunami amplitudes from the suite of TK tsunami sources. The 'GNS Zone' numbers are indicated in Figure 4.1 while the locations of the output points are indicated in Figure 4.3 and Figure 4.4.

	B Zones	GNS ZONES	POINT	TK1	TK2	TK3	TK4	TK5	TK6	Target 2500-yr 84th	Target 2500-yr mean
WEST COAST	B6	129,130	4285.3	0.9	1.0	0.9	0.8	0.8	0.7	1.7	1.5
	B5	131,132,133	4286.3	0.9	1.0	0.8	0.8	0.9	0.7	1.5	1.3
	B4	134,135	4287.3	1.1	1.2	0.8	1.0	1.1	0.7	1.8	1.6
	B3	136,137	4288.3	1.5	1.3	1.0	1.3	1.1	0.8	2.0	1.7
	B3	1,2,3	4289.3	4.4	4.2	2.3	3.7	3.5	2.0	3.6	2.9
	n/a	4,5	4290.3	3.1	3.0	2.1	2.7	2.6	1.8	3.6	2.9
EAST COAST	B1	6	4291.3	6.9	6.1	2.9	5.9	5.2	2.5	5.6	4.0
	B1	7	4292.3	7.0	5.9	2.6	6.0	5.1	2.2	4.8	3.6
	B1	7	4293.3	7.3	6.2	2.7	6.3	5.3	2.4	4.9	3.6
	B1	7,8	4294.3	7.8	6.2	2.6	6.7	5.3	2.2	5.3	3.7
	B1	9	4295.3	5.8	4.4	2.2	4.9	3.8	1.9	4.0	2.8
	B2	10,11,12	4296.3	5.9	4.5	2.4	5.0	3.9	2.1	4.2	3.0
	B7	13,14	4297.3	5.5	3.8	2.5	4.7	3.3	2.2	4.1	3.2
	B8	15	4298.3	5.1	3.3	2.4	4.4	2.8	2.1	4.3	3.2
	B8	16,17	4299.3	5.0	3.6	3.2	4.3	3.1	2.7	4.7	3.5
	B9	18,19	4300.3	3.0	2.0	2.3	2.6	1.7	2.0	3.8	3.2
B10	20,21	4301.3	5.0	2.1	2.4	4.3	1.8	2.0	3.9	3.2	

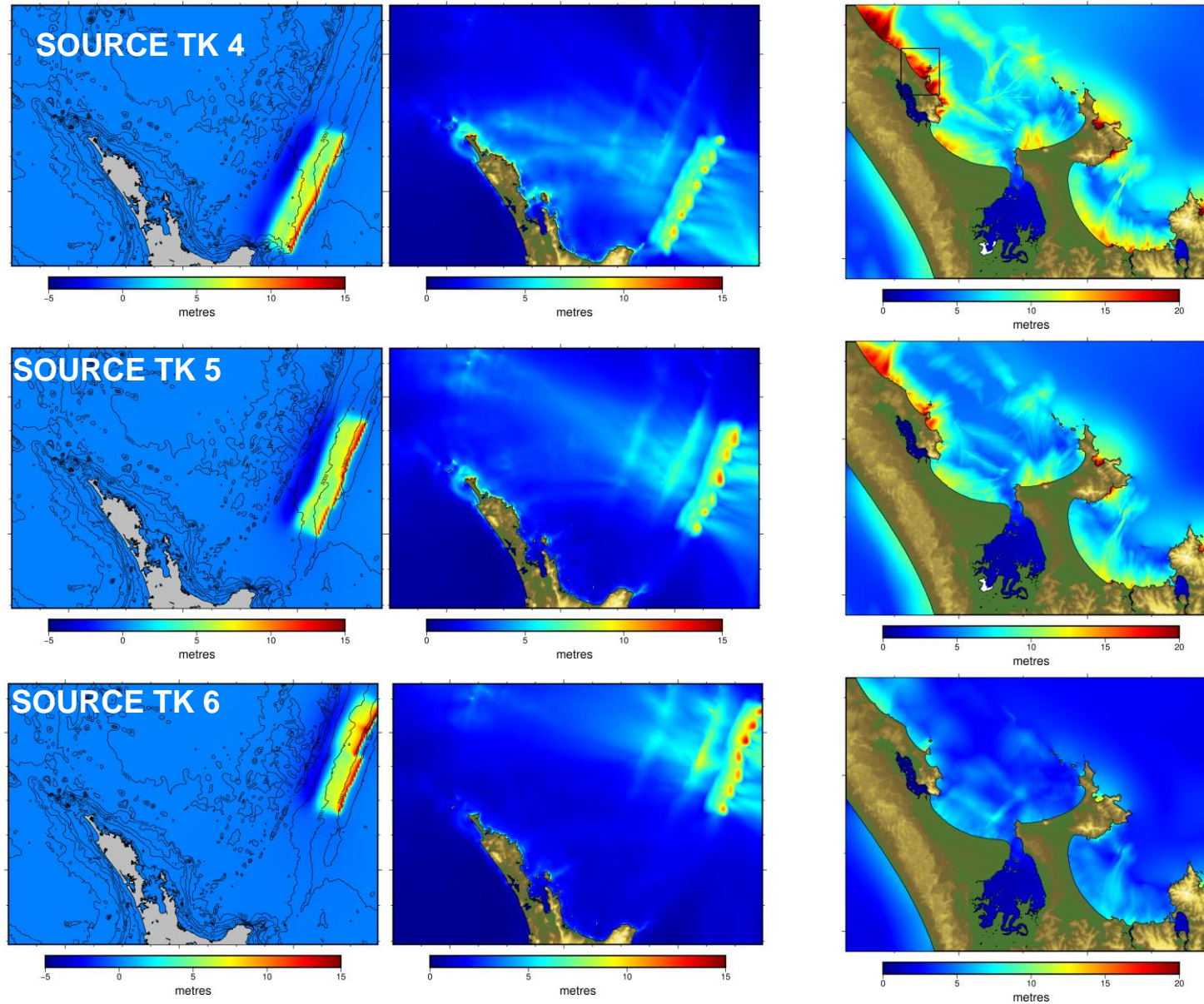


Figure 4.5 Maximum computed tsunami heights around the North Island and in the vicinity of Keri Keri for three identical tsunami sources (400x100 km, 30 m slip) positioned successively northward along the Tonga-Kermadec Subduction Zone.

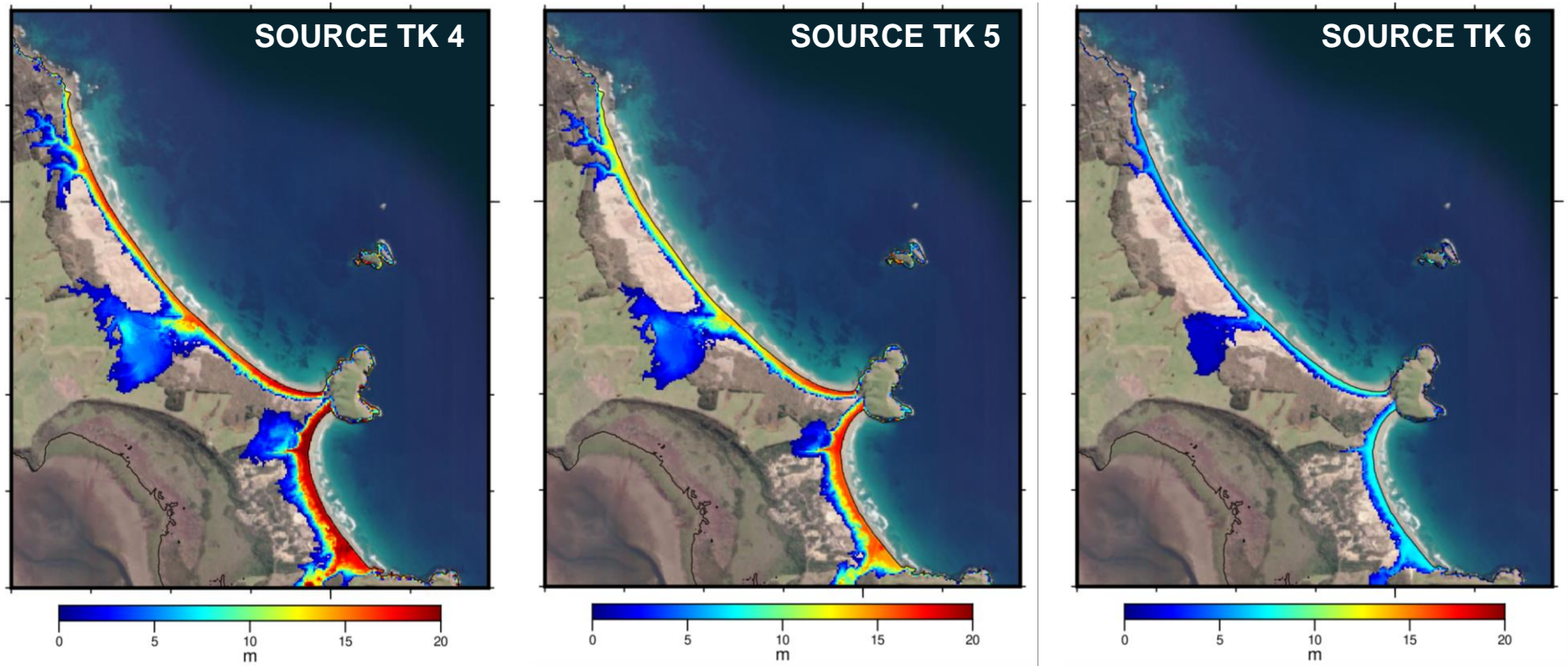


Figure 4.6 Overland flow depth at Otaipango (Henderson Bay) from Sources TK4,5 and 6 depicted in Figure 4.5.

While comparison to the Davies and Griffin (2018) model is relatively simple because the output location is clearly defined as a positive tsunami amplitude at a specific location offshore, comparison to the NTHM 2022 is not as straightforward. This is because the NTHM 2022 output is a single value for maximum tsunami height at the shoreline over a relatively large coastal extent. Also, as we noted above, the NTHM 2022 values are not output from a hydrodynamic model, rather they are values derived from an empirically derived relationship between tsunami runup height and earthquake magnitude with coefficients tuned by a limited number of coarse grid hydrodynamic model simulations.

Thus, our approach for comparing our model results to the NTHM 2022 model is as follows:

- 1) For each simulation we used the model output from the innermost, high resolution C grid.
- 2) The maximum computed tsunami height at the shoreline was extracted
- 3) We determined the mean, median, 95th and 99th percentile values along the shoreline
- 4) We used the 95th percentile as the value to compare against the NTHM 2022

This process is illustrated in Figure 4.7 below and the tabulated values for sources TK1 through TK6 over the sixty model grids are presented in Table 4.3 and Table 4.4.

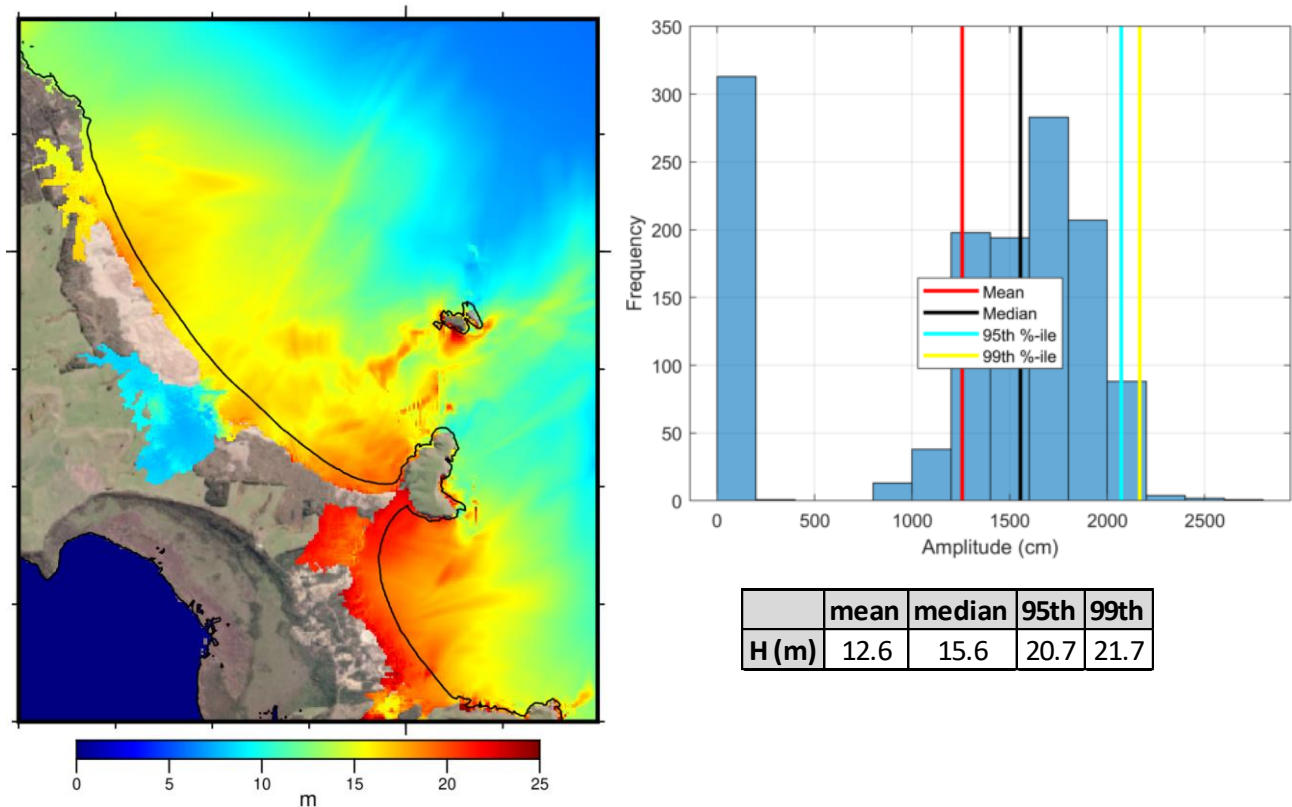


Figure 4.7 (left) Maximum modelled tsunami amplitude for the TK 4 source in the C07 grid. (top right) Histogram of modelled tsunami amplitudes at the shoreline. (bottom right) Table of values.

Table 4.3 Comparison between modelled 95th percentile maximum tsunami heights at the shoreline for each source in each grid against the 2500-year RI, 50th and 84th %-ile values from the Power et al (2021) probabilistic model for east coast locations.

	EAST COAST	GNS ZONE	2500-yr 84th %ile Target H	2500-yr 50th %ile Target H	TK1	TK2	TK3	TK4	TK5	TK6
B1	Far North B									
C1	Cape Reinga	6,7	24.8	16.6	27.4	23.8	8.8	24.2	19.8	7.5
C2	North Cape	9	20.3	11.4	21.4	17.9	8.6	18.7	15.8	7.5
C3	Piwhane Bay	7,8	24.8	16.6	26.5	21.9	11.2	22.7	18.8	9.5
C4	Takapakura	8	24.6	15.6	30.7	26.2	11.5	26.8	22.7	9.8
C5	Te Hapua	9	20.3	11.4	15.5	13.5	7.4	14.1	12.0	6.4
B2	Kari Kari B									
C6	Rarawa	10	14.4	8.8	23.9	20.4	11.0	20.8	18.0	9.5
C7	Hendersons	11	17.1	10.0	23.7	19.9	10.3	20.7	17.2	9.0
C8	Pukenui	11	17.1	10.0	20.6	16.6	7.8	18.0	13.7	6.8
C9	Rangiputa	12	15.2	9.1	14.2	13.1	7.4	13.2	11.7	6.6
C10	Maitai Bay	12	15.2	9.1	19.4	16.5	11.5	17.4	14.9	10.3
C11	Tokerau	12	15.2	9.1	9.2	7.9	6.1	8.4	7.0	5.4
C12	Coopers Beach	12	15.2	9.1	14.0	12.0	7.9	12.5	10.6	6.8
B7	Whangaroa B (100 m)									
C28	Motuhakahaka	13	19.2	12.1	25.9	20.5	13.7	22.7	17.9	11.8
C29	Taupo Bay	13	19.2	12.1	25.4	18.5	11.4	21.3	15.8	9.8
C30	Whangaroa	14	25.8	14.4	17.4	13.6	9.8	15.2	11.9	8.6
C31	Tauranga Bay	14	25.8	14.4	22.4	15.5	9.5	19.1	13.1	8.1
C32	Te Ngare Bay	14	25.8	14.4	18.7	14.0	9.8	16.1	12.4	8.7
C33	Matauri Bay	14	25.8	14.4	20.1	15.3	10.3	18.1	13.3	8.9
C34	Motukawanui	14	25.8	14.4	18.5	13.3	10.1	16.4	11.5	8.6
B8	Bay of Islands B									
C35	Takou Bay	14,15	25.8	14.4	26.3	18.5	11.9	22.5	16.1	10.3
C36	Te Puna Inlet	15	20.2	12.4	6.8	5.2	4.1	6.2	4.8	3.7
C37	Purerua	15	20.2	12.4	19.9	13.0	8.9	18.4	11.0	8.1
C38	Keri Keri	15	20.2	12.4	13.4	9.8	7.5	12.4	9.1	6.2
C39	Moturoa	15	20.2	12.4	11.6	8.7	6.6	10.7	7.7	5.6
C40	Rawhiti	16	22.6	14.4	13.8	9.4	6.9	12.0	8.1	6.1
C41	Waitangi-Russel	16	22.6	14.4	11.1	7.4	5.4	9.6	6.3	4.8
C42	Elliot Bay	16	22.6	14.4	23.3	15.4	12.2	20.1	13.2	10.5
C43	Whangaruru	17	23.6	14.2	12.6	8.7	8.9	11.6	7.8	7.6
C44	Helena Bay	17	23.6	14.2	19.3	14.0	12.0	17.1	12.2	10.2
B9	Tutukaka B									
C45	Mimiwhangata	18	19.2	12.5	17.8	13.0	11.1	15.7	11.5	9.8
C46	Whananaki North	18	19.2	12.5	16.9	12.4	12.1	14.9	10.8	10.8
C47	Whananaki South	18	19.2	12.5	21.0	13.6	11.8	17.7	11.8	10.3
C48	Whananaki All	18	19.2	12.5	19.1	13.4	11.8	16.9	11.6	10.2
C49	Matapouri	18	19.2	12.5	19.8	13.2	12.6	17.2	11.5	10.8
C50	Tutukaka Harbour	18,19	19.2	12.5	12.2	7.0	11.0	10.1	6.0	9.4
C51	Ngunguru	19	13.8	9.0	11.0	7.5	6.6	9.6	6.7	5.9
C52	Patua	19	13.8	9.0	14.2	8.7	8.0	12.4	7.5	6.9
C53	McGregors Bay	19	13.8	9.0	12.2	7.4	6.6	10.4	6.8	5.7
B10	Whangarei B									
C54	Whangarei Town	20	11.7	6.8	0.9	0.8	0.7	0.8	0.7	0.6
C55	Marsden Point	20	11.7	6.8	7.0	5.2	4.6	6.3	4.8	4.1
C56	Ocean Beach	20	11.7	6.8	11.7	7.0	7.3	10.1	6.0	6.4
C57	Ruakaka	20	11.7	6.8	6.7	5.3	5.6	6.1	4.5	5.0
C58	Waipu	20	11.7	6.8	10.4	6.1	6.3	9.2	5.2	5.5
C59	Langs Beach	20	11.7	6.8	15.5	6.8	7.8	13.2	5.9	6.6
C60	Mangawhai	20	11.7	6.8	9.1	4.8	4.7	8.0	4.2	4.1

Table 4.4 Comparison between modelled 95th percentile maximum tsunami heights at the shoreline for each source in each grid against the 2500-year RI, 50th and 84th %-ile values from the Power et al (2021) probabilistic model for west coast locations.

#	WEST COAST	GNS ZONE	2500-yr 84th %ile Target H	2500-yr 50th %ile Target H	TK1	TK2	TK3	TK4	TK5	TK6
B3	Ahipara B									
C13	Waipapakauri	1,2	14.8	10.6	11.3	10.9	6.5	9.7	9.3	5.5
C14	Ahipara	1	14.8	10.6	10.0	9.7	7.9	9.0	8.3	6.9
C15	Tauroa	137,1	14.8	10.6	17.9	17.1	7.5	15.7	14.8	6.3
C16	Herekino	137	13.2	8.3	8.9	9.1	4.9	8.4	8.5	4.5
B4	Hokianga B									
C17	Omapere	135	10.8	7.6	6.8	7.6	5.4	5.9	6.5	4.8
C18	Opononi	135	10.8	7.6	6.8	7.2	5.5	6.2	6.5	5.0
C19	Rawene	135	10.8	7.6	1.8	1.8	1.5	1.6	1.7	1.4
B5	Northland West Coast B									
C20	Omamari	132	6.4	4.8	5.3	5.4	3.5	4.8	4.9	3.1
C21	Baylys	131	5.8	4.1	4.6	5.3	3.9	4.1	4.7	3.4
C22	Glinks Gully	131, 130	7.1	5.4	4.1	4.6	3.9	3.6	4.0	3.5
B6	Kaipara B									
C23	Ruawai	129	7.1	5.4	0.2	0.2	0.1	0.1	0.1	0.1
C24	Kellys Bay	129	7.1	5.4	0.3	0.3	0.3	0.3	0.3	0.3
C25	Pouto	129	7.1	5.4	0.7	0.7	0.7	0.6	0.6	0.6
C26	Tinopai	129	7.1	5.4	0.4	0.4	0.4	0.3	0.4	0.4
C27	Birds Beach	129	7.1	5.4	0.3	0.4	0.4	0.3	0.3	0.3

4.2 Orange Zone Sources

As noted in the DGL:

*The Orange Zone is intended to be the area evacuated in most if not all **distant and regional-source official warnings** (i.e., warnings that extend beyond the Red Zone, for tsunami from sources more than one hour of travel time away from the mapped location). The intent is to provide for a middle-zone to avoid over-evacuation in most official warnings; however larger regional/distant-source events may occur in which case the Yellow Zone will apply. Local differentiation of this zone can be achieved using terms that are familiar to the community such as street names and key landmarks.*

*The Orange Zone is intended to be used for official warnings of distant or regional source tsunami. It should be **linked to a particular threat level** and encompass the range of tsunami that can result in a warning being issued at that threat-level. It is generally anticipated that the choice of threat level should at least encompass the largest tsunami **with travel time >1 hour that is to be expected on a 500-year time frame**; though this is not a rigid requirement on the basis that the Yellow Zone will also be evacuated if a warning of a tsunami belonging to a higher threat level is made.*

Careful reading of these guidelines reveals multiple criteria that should be met for defining the Orange Zone. As will be shown below, linking of the tsunami heights to a particular threat level AND to the 500-year time frame for probability of occurrence is difficult to reconcile.

As with the Auckland study (Borrero and O'Neill, 2020), we modelled 21 large magnitude (M_w 9.3-9.6) earthquake tsunami sources from around the Pacific Rim (see Table 4.5) through to inundation over each of the 60 fine resolution C grids. The source locations for the regional/SW Pacific sources are shown in Figure 4.8 and the trans-Pacific propagation pattern of the tsunami energy from each of these sources is presented in Appendix 3. In

Table 4.5 Tsunami sources trialled for the Orange Zone analysis. The largest known historical events are indicated for some of the source regions are indicated as well.

South America		M_w	L (km)	W (km)	Slip (m)
SA-1	Patagonia	9.6	1000	150-200	35.2
SA-2	South-Central Chile (1960, M_w 9.4)	9.6	1000	100-150	47.0
SA-3	Chile-Peru (1868, M_w 9.4?)	9.6	1200	100-200	47.0
SA-4	Central Peru	9.6	1100	150	42.7
SA-5	Central America	9.6	1000	150	47.0
SA-6	Mexico	9.6	1200	100	46.9
North Pacific		M_w	L	W	Slip
NP-1	Cascadia (1700, M_w 9.0)	9.4	900	150	35.0
NP-2	Gulf of Alaska	9.5	1500	100	33.2
NP-3	Gulf of Alaska/Shumagin (1964, M_w 9.2)	9.6	1000	150	47.0
NP-4	Central Aleutians	9.6	1000	150	47.0
NP-5	Kamchatka (1952, M_w 9.0)	9.6	1200	150	33.0
NP-6	Hokkaido (2011, M_w 9.0)	9.5	800	200	35.8
NP-7	Nankai Trough	9.5	800	200	35.8
Western Pacific		M_w	L	W	Slip
WP-1	Eastern Solomon	9.3	800	100	35.0
WP-2	Western Solomon	9.3	800	100	35.0
WP-3	Vanuatu	9.3	800	100	35.0
WP-4	Vanuatu-New Hebrides	9.3	800	100	35.0
WP-5	Samoa-Tonga (2009, M_w 8.1)	9.3	800	100	35.0
WP-6	Tonga-Raoul	9.3	800	100	35.0
WP-7	Raoul (M_w 8.1)	9.3	800	100	35.0
WP-8	Puysegur (2009, M_w 7.8)	9.3	700	100	35.0

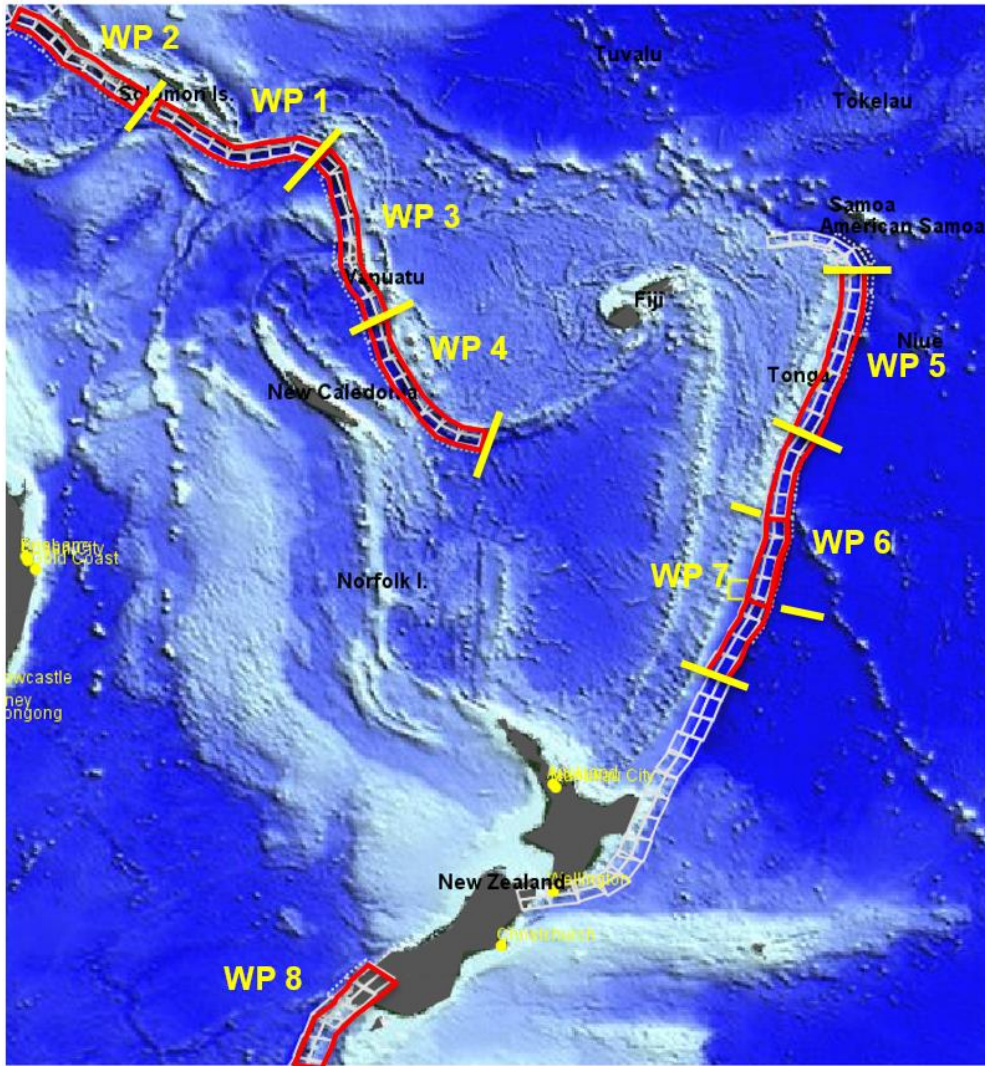


Figure 4.8 West Pacific (WP) Source regions. Note the WP6 and WP 7 overlap.

As with the Yellow Zone (TK) source discussed above, we compared the model output to both the New Zealand NTHM 2021 and Australia's PTHA 18. For the latter, we extracted the maximum modelled tsunami amplitude at each of the offshore locations (Figure 4.3) and compared them to the mean 500-year RI tsunami amplitudes (Table 4.6). For the most part, these sources correspond well to the mean 500-year RI tsunami amplitudes, with the WP4, WP7 and WP8 sources somewhat over predicting.

We then determined the 95th percentile shoreline tsunami height in each of the C-grids (as described above) and compared these values to the 500-year RI 50th percentile tsunami heights from NTHM 2021 (Table 4.7 for east coast sites and Table 4.8 for west coast sites). As with the PTHA 18, the modelled shoreline tsunami heights for the most part cover the range of tsunami heights present in the NTHM 2021 with some over prediction from the WP4, WP7 and WP8 sources.

Table 4.6 Comparison between modelled tsunami heights at the offshore locations for each source against the 500-year RI value from the Davies and Griffen (2018) probabilistic model. The corresponding 'GNS Zone' numbers are indicated in Figure 4.1 while the Point locations are indicated in Figure 4.3.

	B Zones	GNS ZONES	POINT	NP1	NP2	NP3	NP4	NP5	NP6	NP7	SA1	SA2	SA3	SA4	SA5	SA6	WP1	WP2	WP3	WP4	WP5	WP6	WP7	WP8	Target 500-yr mean	
WEST COAST	B6	129,130	4285.3	0.3	0.3	0.3	0.4	0.5	0.5	0.4	0.3	0.3	0.5	0.5	0.5	0.3	0.7	0.5	0.7	0.6	0.3	0.5	0.4	1.1	0.8	
	B5	131,132,133	4286.3	0.2	0.3	0.3	0.4	0.3	0.5	0.5	0.4	0.2	0.5	0.4	0.4	0.3	0.9	0.5	0.7	0.7	0.3	0.4	0.4	1.0	0.7	
	B4	134,135	4287.3	0.2	0.3	0.4	0.5	0.5	0.5	0.4	0.3	0.3	0.4	0.4	0.4	0.3	1.0	0.6	0.6	1.0	0.3	0.5	0.6	1.1	0.9	
	B3	136,137	4288.3	0.2	0.4	0.4	0.6	0.5	0.6	0.4	0.3	0.3	0.4	0.5	0.4	0.4	0.9	0.6	0.7	1.2	0.3	0.4	0.5	1.3	0.9	
	B3	1,2,3	4289.3	0.4	0.5	1.0	1.3	1.0	0.9	0.5	0.5	0.5	0.3	0.5	0.6	0.8	0.6	1.3	0.6	0.7	1.2	0.4	1.0	1.2	1.5	1.4
	n/a	4,5	4290.3	0.4	0.5	0.6	1.8	1.1	0.8	0.5	0.6	0.5	0.5	0.8	0.8	0.5	1.0	0.6	0.7	2.7	0.5	0.9	1.3	1.6	1.4	
	B1	6	4291.3	0.4	0.5	0.5	1.1	1.1	1.3	0.5	0.5	0.8	0.5	0.9	0.8	0.8	0.9	0.8	1.2	2.3	0.7	1.2	1.7	1.4	1.7	
EAST COAST	B1	7	4292.3	0.3	0.6	0.4	0.8	0.6	0.8	0.5	0.4	0.4	0.6	0.8	0.7	0.4	0.8	0.5	0.8	2.7	0.5	1.1	1.7	2.4	1.4	
	B1	7	4293.3	0.2	0.6	0.4	0.8	0.6	0.7	0.4	0.3	0.4	0.6	0.8	0.6	0.4	0.7	0.4	0.6	2.3	0.5	1.2	1.7	2.0	1.4	
	B1	7,8	4294.3	0.2	0.5	0.5	0.7	0.5	0.6	0.4	0.4	0.5	0.7	0.9	0.7	0.4	0.7	0.4	0.6	1.4	0.5	0.9	1.7	1.6	1.4	
	B1	9	4295.3	0.2	0.5	0.5	0.6	0.5	0.5	0.4	0.4	0.4	0.7	0.8	0.7	0.4	0.7	0.3	0.3	1.3	0.5	0.8	1.7	0.4	1.1	
	B2	10,11,12	4296.3	0.3	0.5	0.6	0.6	0.7	0.7	0.6	0.5	0.5	0.8	0.9	0.8	0.5	0.8	0.4	0.4	1.2	0.6	0.9	1.9	0.4	1.3	
	B7	13,14	4297.3	0.2	0.5	0.7	1.2	0.8	0.8	0.7	0.6	0.7	0.8	1.0	0.9	0.5	0.7	0.3	0.6	1.2	0.6	1.1	2.3	0.4	1.5	
	B8	15	4298.3	0.3	0.4	0.7	0.9	0.8	0.6	0.8	0.5	0.5	0.6	0.8	1.0	0.9	0.5	0.6	0.4	0.8	1.3	0.6	1.0	2.3	0.5	1.5
	B8	16,17	4299.3	0.3	0.4	0.8	0.8	0.7	0.8	0.9	0.5	0.5	0.7	0.9	1.1	1.0	0.5	0.8	0.4	0.8	1.1	0.6	1.1	2.5	0.5	1.7
	B9	18,19	4300.3	0.5	0.4	1.1	0.8	0.7	0.9	0.9	1.0	0.7	1.0	1.0	1.0	1.1	0.6	0.4	0.9	1.2	0.9	1.0	1.7	0.4	1.8	
	B10	20,21	4301.3	0.4	0.6	1.2	1.1	0.5	0.7	0.6	1.1	0.7	0.9	1.1	1.0	0.9	0.5	0.4	0.6	0.8	0.8	1.3	2.0	0.4	1.8	

Table 4.7 Comparison between modelled tsunami heights at the offshore locations for each source against the 500-year RI value from the Power et al (2021) probabilistic model. East coast locations. The output from sources with the values stricken out in the table below was not used as part of the aggregation step used to determine the overall inundation zone.

#	Name	NP	SA	SA	SA	SA	SA	SA	WP	WP	WP	WP	WP	WP	WP	WP	WP	500-yr 50th	EAST COAST								
		1	2	3	4	5	6	7	1	2	3	4	5	6	1	2	3	4	5	6	7	8	Target H	GNS ZONE			
B1	Far North B																										
C1	Cape Reinga	1.0	1.5	1.3	3.1	2.3	2.3	0.9	1.1	1.4	1.2	2.2	2.2	1.3	4.4	3.6	2.6	7.6	2.7	5.8	5.2	8.3	7.4	6 and 7			
C2	North Cape	0.5	1.0	1.0	1.6	1.4	1.3	0.9	0.6	1.0	1.3	1.8	1.7	0.8	1.7	0.7	1.2	5.1	1.4	4.0	5.5	2.3	4.7	9			
C3	Piwhane Bay	0.7	1.2	1.1	4.1	2.1	2.0	1.0	1.1	1.6	1.2	2.1	2.4	1.5	2.9	2.5	3.0	7.7	2.0	4.1	6.8	18.0	7.4	7 and 8			
C4	Takapakura	0.5	1.3	0.7	4.1	1.7	1.4	0.6	0.6	1.0	1.5	1.7	2.2	1.0	1.9	1.8	1.3	9.3	2.0	5.0	6.6	7.3	6.3	8			
C5	Te Hapua	0.6	2.0	1.4	2.3	1.9	2.2	1.1	0.9	1.2	1.3	2.2	1.9	1.0	1.6	1.1	1.6	3.8	1.8	4.2	5.3	2.9	4.7	9			
B2	Kari Kari B																										
C6	Rarawa	0.9	1.4	1.3	3.0	2.4	2.1	1.4	1.1	1.5	1.4	2.7	2.4	1.4	2.4	0.8	1.8	6.2	1.9	4.5	7.4	2.2	4.1	10			
C7	Hendersons	1.0	1.1	1.3	2.9	2.1	2.1	1.5	1.2	1.3	1.7	2.4	2.2	1.5	2.6	1.1	2.0	4.9	2.0	4.2	7.0	1.8	4.8	11			
C8	Pukenui	1.8	2.0	2.6	3.2	2.7	3.0	2.1	1.6	1.5	2.7	3.6	2.4	2.0	2.8	1.8	3.3	3.9	3.1	3.5	6.8	2.7	4.8	11			
C9	Rangiputa	1.7	2.2	2.6	3.2	2.5	3.1	1.9	2.0	1.4	2.6	3.5	2.5	2.1	3.3	1.7	3.0	3.9	3.1	4.4	5.8	3.0	4.8	12			
C10	Maitai Bay	1.2	1.9	2.2	3.5	2.3	3.1	1.9	1.7	1.7	2.5	3.2	2.5	1.9	2.9	1.4	2.6	5.7	3.9	6.2	8.6	2.7	4.8	12			
C11	Tokerau	1.0	2.3	3.2	4.1	4.5	4.0	2.7	2.0	2.4	3.0	4.8	2.4	2.3	2.4	1.7	3.0	4.4	3.0	3.9	4.8	2.2	4.8	12			
C12	Coopers Beach	0.9	2.2	2.4	2.8	3.4	3.4	2.5	1.5	1.5	2.3	4.0	2.4	1.9	3.0	1.5	2.3	3.6	2.5	3.8	6.3	2.4	4.8	12			
B7	Whangaroa B (100 m)																										
C28	Motuhakahaka	1.1	1.9	1.5	4.8	2.7	2.7	1.7	1.2	3.1	4.1	3.8	3.9	2.1	2.8	1.4	2.4	6.8	6.0	10.1	13.9	1.2	5.8	13			
C29	Taupo Bay	1.0	1.9	1.8	6.0	2.8	3.2	1.6	1.8	3.2	2.9	3.5	2.9	2.8	3.9	1.8	2.7	5.5	4.0	9.2	12.0	2.2	5.8	13			
C30	Whangaroa	0.8	1.5	1.4	4.2	2.1	1.8	1.1	1.3	1.2	1.9	2.1	1.9	1.7	2.4	1.4	1.5	4.7	3.0	4.0	8.2	1.8	5.8	14			
C31	Tauranga Bay	1.1	1.8	1.8	5.4	2.9	2.8	1.6	2.1	1.9	2.4	2.9	2.5	2.0	3.5	1.7	2.1	5.8	4.0	7.9	7.8	1.9	5.8	14			
C32	Te Ngare Bay	0.9	2.8	2.3	4.6	3.5	3.3	1.7	1.7	1.7	2.5	3.6	2.4	1.7	4.5	1.8	3.0	6.0	3.3	4.9	8.2	2.0	5.8	14			
C33	Matauri Bay	1.1	2.6	2.3	3.8	4.1	2.5	1.7	2.0	2.5	3.0	3.8	3.7	2.5	3.3	1.7	3.2	4.8	3.0	4.2	8.6	1.8	5.8	14			
C34	Motukawanui	1.5	2.0	1.8	3.1	3.3	2.1	1.9	1.7	2.2	2.3	3.0	2.8	2.0	2.9	1.7	2.6	4.1	2.7	4.0	6.8	1.9	5.8	14			
B8	Bay of Islands B																										
C35	Takou Bay	0.6	1.8	1.3	2.2	2.5	1.3	1.3	1.7	2.0	2.4	3.1	2.5	1.7	2.2	1.3	1.9	5.0	3.5	6.5	9.8	1.3	5.8	14 and 15			
C36	Te Puna Inlet	0.8	1.4	1.3	2.3	1.7	1.6	1.8	1.4	1.2	1.8	2.1	2.0	1.5	1.6	1.3	1.8	1.9	1.4	2.1	3.9	1.1	5.1	15			
C37	Purerua	0.5	1.1	1.2	2.3	1.6	1.3	1.7	1.0	1.1	1.9	2.2	2.0	1.1	1.4	1.1	2.0	2.7	1.8	5.5	7.7	1.0	5.1	15			
C38	Keri Keri	0.8	1.7	1.9	2.7	2.1	2.3	2.1	1.3	1.3	1.8	2.9	2.6	1.3	1.8	1.6	2.3	2.5	2.0	3.3	6.8	1.3	5.1	15			
C39	Moturoa	0.7	1.6	1.8	1.8	2.1	2.1	2.1	1.2	1.2	1.6	2.6	2.4	1.2	1.6	1.5	2.2	2.2	1.6	2.7	5.5	1.1	5.1	15			
C40	Rawhiti	1.2	2.5	2.8	3.3	2.7	2.8	3.2	2.3	2.1	2.4	3.4	3.3	2.1	2.6	2.2	3.3	3.4	2.6	3.7	6.3	2.0	6.2	16			
C41	Waitangi-Russel	1.0	2.5	2.8	2.9	2.3	2.9	3.3	2.2	2.0	2.3	3.4	3.0	2.1	2.8	2.3	3.0	2.2	2.3	2.8	4.7	1.8	6.2	16			
C42	Elliot Bay	0.8	2.0	1.7	3.5	3.5	2.1	1.6	1.6	3.2	4.7	4.4	3.0	2.5	3.3	1.4	3.4	5.5	4.2	7.1	9.3	1.4	6.2	16			
C43	Whangaruru	0.8	1.5	1.6	3.1	1.9	2.1	2.3	2.3	2.0	2.1	3.1	3.0	2.3	2.2	1.7	1.9	2.3	3.0	3.2	6.6	1.5	6.3	17			
C44	Helena Bay	0.9	2.3	2.0	2.8	2.9	2.6	2.0	2.4	2.3	2.7	4.2	3.6	2.7	2.8	2.1	2.4	3.5	4.1	5.7	9.6	1.8	6.3	17			
B9	Tutukaka B																										
C45	Mimiwhangata	0.8	1.2	1.4	2.1	1.8	1.3	1.5	1.2	1.5	1.7	3.0	2.5	1.9	1.6	0.9	1.3	4.5	2.5	4.3	9.6	1.2	6.2	18			
C46	Whananaki North	0.8	1.3	1.3	2.5	1.9	1.6	1.4	1.2	1.6	1.5	2.7	2.5	1.6	1.5	1.0	1.3	2.7	2.7	4.1	10.7	1.1	6.2	18			
C47	Whananaki South	0.8	1.5	1.8	4.6	3.2	3.0	1.5	1.5	1.9	2.5	3.6	2.8	2.1	2.3	1.2	2.3	5.0	3.3	5.5	10.4	2.3	6.2	18			
C48	Whananaki All	0.8	1.5	1.8	4.5	3.2	3.0	1.5	1.5	1.9	2.5	3.6	2.9	2.1	2.3	1.2	2.3	4.8	3.2	5.3	10.1	2.2	6.2	18			
C49	Matapouri	0.8	1.5	1.8	3.8	2.5	2.6	1.6	1.4	1.9	2.0	3.4	2.8	2.0	2.2	1.1	2.2	4.3	2.9	4.6	10.3	1.9	6.2	18			
C50	Tutukaka Harbour	1.1	1.2	1.5	2.5	1.7	1.8	1.5	1.4	1.6	2.0	2.5	1.9	1.8	1.5	1.0	1.7	3.0	2.3	4.1	7.0	1.3	6.2	18 and 19			
C51	Ngunguru	0.8	1.8	1.9	2.7	1.5	2.1	1.3	1.4	1.8	1.8	3.0	2.5	1.8	2.1	0.9	2.5	3.9	2.6	4.6	5.9	1.4	5.0	19			
C52	Patua	0.9	1.5	1.6	2.2	1.2	1.6	1.3	1.6	1.4	1.7	2.8	2.3	1.8	1.8	0.9	2.3	3.7	3.0	4.3	7.0	1.2	5.0	19			
C53	McGregors Bay	0.8	1.3	1.5	1.9	1.2	1.4	1.3	1.4	1.3	1.6	2.6	2.2	1.7	1.7	0.9	2.2	3.3	2.5	3.5	6.0	1.0	5.0	19			
B10	Whangarei B																										
C54	Whangarei Town	0.4	0.4	0.9	0.7	0.5	0.6	0.5	0.8	0.7	0.9	0.6	0.8	0.7	0.5	0.4	0.4	0.5	0.5	0.6	0.7	0.4	3.5	20			
C55	Marsden Point	1.0	2.0	1.9	3.9	1.9	2.2	2.5	2.1	1.8	2.2	2.0	2.2	2.3	2.1	0.9	1.6	2.8	1.7	2.7	4.7	1.5	3.5	20			
C56	Ocean Beach	0.6	0.8	1.3	1.9	1.1	1.0	1.0	1.5	1.2	1.5	2.3	2.0	1.3	1.5	0.7	2.1	4.1	2.1	2.6	5.3	1.1	3.5	20			
C57	Ruakaka	1.4	2.0	2.4	3.8	2.0	2.5	2.7	2.5	2.3	2.5	2.3	2.3	2.4	1.9	1.1	1.8	2.2	1.7	2.7	4.0	1.6	3.5	20			
C58	Waipu	1.3	1.7	2.2	3.5	1.9	2.2	2.5	2.5	2.3	2.4	2.9	2.6	2.2	2.1	1.0	2.0	2.4	2.1	2.9	4.3	1.3	3.5	20			
C59	Langs Beach	1.3	1.7	2.1	2.7	2.0	2.3	2.7	2.5	2.4	2.4	3.0	2.6	2.3	2.1	1.0	2.1	2.5	2.2	3.5	6.2	1.2	3.5	20			
C60	Mangawhai	0.8	1.3	1.6	2.6	1.6	2.2	2.0	1.6	1.8	1.7	2.3	2.0	1.6	1.2	0.9	1.6	2.3	1.6	3.3	4.1	1.1	3.5	20			

Table 4.8 Comparison between modelled tsunami heights at the offshore locations for each source against the 500-year RI value from the Power et al. (2021) probabilistic model. West coast locations. The output from sources with the values stricken out in the table below was not used as part of the aggregation step used to determine the overall inundation zone.

#	Name	NP	SA	SA	SA	SA	SA	SA	WP	500-yr 50th	WEST COAST													
		1	2	3	4	5	6	7	1	2	3	4	5	6	1	2	3	4	5	6	7	8	Target H	GNS ZONE
B3	Ahipara B																							
C13	Waipapakauri	1.4	2.1	1.7	2.4	3.3	3.7	1.3	1.5	1.2	1.4	2.9	2.1	1.4	3.9	2.0	2.9	6.1	1.9	3.1	3.8	4.1	6.0	1 and 2
C14	Ahipara	1.7	3.3	1.9	6.7	4.7	4.7	1.8	2.1	2.3	2.6	3.5	2.4	1.7	5.3	3.0	5.2	7.9	4.8	6.2	6.4	6.1	6.0	1
C15	Tauroa	1.6	2.4	1.6	5.7	4.2	4.1	1.5	1.8	1.9	2.1	2.8	2.1	1.5	5.0	2.6	4.5	8.1	3.5	5.1	4.1	5.2	6.0	137 and 1
C16	Herekino	0.4	1.1	0.8	2.0	2.0	1.4	0.6	0.8	1.0	1.0	1.3	1.5	0.6	2.4	1.4	1.6	5.9	1.4	3.6	2.9	3.8	3.9	137
B4	Hokianga B																							
C17	Omapere	0.5	1.3	0.7	2.9	1.9	1.1	0.5	0.7	0.8	0.6	1.1	1.3	0.7	2.6	2.2	1.4	3.3	1.6	3.3	2.6	2.8	3.8	135
C18	Opononi	0.6	1.4	0.8	3.4	2.1	1.4	0.5	0.8	1.1	0.8	1.4	1.9	0.7	2.8	2.3	1.2	3.4	1.6	3.6	2.9	2.6	3.8	135
C19	Rawene	0.3	0.5	0.5	1.0	0.7	0.5	0.5	0.4	0.5	0.5	0.6	0.6	0.4	1.0	0.8	0.7	1.1	0.5	0.8	0.9	1.1	3.8	135
B5	Northland West Coast B																							
C20	Omamari	0.3	1.1	0.6	2.3	1.5	1.3	0.7	0.7	0.7	0.9	1.2	1.2	0.8	1.7	1.3	1.8	4.0	1.0	2.6	2.3	2.9	2.6	132
C21	Baylys	0.5	1.0	0.6	2.1	1.6	1.4	0.7	0.6	0.7	0.8	1.3	1.1	0.8	1.9	1.3	1.8	4.5	1.1	1.5	2.1	2.8	2.3	131
C22	Glinks Gully	0.4	0.9	0.6	1.9	1.5	1.5	0.5	0.6	0.6	0.8	1.2	1.2	0.7	1.6	1.0	1.6	2.6	0.9	1.7	1.6	2.3	3.4	131 and 130
B6	Kaipara B																							
C23	Ruawai	0.2	0.2	0.2	0.3	0.2	0.2	0.2	0.3	0.3	0.4	0.3	0.3	0.2	0.3	0.3	0.3	0.2	0.1	0.2	0.2	0.4	3.3	129
C24	Kellys Bay	0.2	0.3	0.3	0.3	0.3	0.2	0.2	0.3	0.4	0.5	0.4	0.4	0.3	0.4	0.3	0.4	0.3	0.2	0.3	0.3	0.6	3.3	129
C25	Pouto	0.3	0.4	0.5	0.7	0.6	0.5	0.3	0.3	0.4	0.5	0.5	0.5	0.4	0.7	0.6	0.8	0.6	0.4	0.7	0.7	1.0	3.3	129
C26	Tinopai	0.2	0.3	0.3	0.3	0.4	0.3	0.2	0.3	0.3	0.4	0.4	0.4	0.3	0.5	0.4	0.5	0.3	0.3	0.4	0.4	0.8	3.3	129
C27	Birds Beach	0.3	0.3	0.4	0.3	0.4	0.3	0.2	0.3	0.4	0.5	0.4	0.4	0.3	0.5	0.4	0.5	0.3	0.2	0.4	0.4	0.7	3.3	129

4.3 Discussion

Below we provide additional discussion around the selection of tsunami sources for defining each inundation hazard zone.

4.3.1 Yellow Zone

For the Yellow Zone, Table 4.2 presents a comparison between offshore maximum modelled tsunami amplitudes from this study against the probabilistically derived tsunami heights at offshore location from Geoscience Australia’s PTHA18 (Davies and Giffen, 2018). As noted above the TK1 source generally overpredicts the target tsunami heights, particularly at the northern and east coast locations. In Table 4.3 and Table 4.4 we then compare the shoreline tsunami heights from our model scenarios against the shoreline tsunami heights predicted from the NTHM 2021 (Power et al, 2022, 2023) probabilistic model. As with the offshore results there is a general overprediction from the TK1 Source against the probabilistic shoreline results, particularly along the most exposed northern and eastern coastline. Moving into the Whangaroa, Bay of Islands and Tutukaka B-grid regions the TK1 source is not as overpowering relative to the probabilistic estimate. However, here we contend that the probabilistic value is likely an overprediction. This is because the method used to derive the probabilistic value is not based on hydrodynamics but rather is an empirical relationship between earthquake magnitude and shoreline tsunami height. These grid regions are characterised by highly complex local topography with numerous offshore islands and a highly irregular coastline. These factors would act reduce tsunami heights at the shoreline though the action of wave breaking and dissipation over reefs and headlands. This is indicated by the hydrodynamic modelling presented here as the model directly and indirectly accounts for these processes. As such, we recommend that for the east coast of Northland, the Yellow Zone be defined through an aggregation of the TK2 through TK6 scenarios.

Along the west coast, the TK sources for the most part capture the 2500-year RI shoreline tsunami heights from NTHM 2022 (Table 4.4). Most of the underprediction can be explained by the fact that the C grids being analysed are inside a harbour (i.e. in Hokianga or Kaipara) while the probabilistically defined value is most appropriately applied to a shoreline point on the open coast. Where we have C grids on an open coast location, as in the Northland West Coast B Grid, the TK sources do a good job of capturing the 50th percentile 2500-year RI shoreline tsunami height although they fall somewhat short of the 84th percentile values.

Close inspection of the comparison between the offshore tsunami heights to the Australian PTHA18 shows a greater degree of underprediction (see Table 4.2) particularly at the four southernmost

offshore points (south of Ahipara to the Kaipara entrance). Looking at the result from the WP sources for the offshore locations, there is a closer match between the WP sources, particularly WP8, and the mean 2500-year RI amplitudes, although an underprediction to the 84th percentile amplitudes is still evident (Table 4.9). Given that the shoreline height values at the open coast sites for the TK sources provide an acceptable fit to the 50th percentile 2500-year RI values and the inclusion of the WP8 sources improves the fit for the offshore locations, we have included the WP8 source to the aggregation for defining the Yellow Zone along the west coast of Northland.

Table 4.9 Comparison of maximum modelled tsunami amplitudes for the WP sources against the offshore values from PTHA18.

POINT	WP1	WP2	WP3	WP4	WP5	WP6	WP7	WP8	2500-yr 84th %ile	2500-yr mean
4285.3	0.7	0.5	0.7	0.6	0.3	0.5	0.4	1.1	1.7	1.5
4286.3	0.9	0.5	0.7	0.7	0.3	0.4	0.4	1.0	1.5	1.3
4287.3	1.0	0.6	0.6	1.0	0.3	0.5	0.6	1.1	1.8	1.6
4288.3	0.9	0.6	0.7	1.2	0.3	0.4	0.5	1.3	2.0	1.7

4.3.2 Orange Zone

For the Orange Zone, the output from the distant source scenarios is compared to the 500-year RI probabilistically defined offshore points from Davies and Griffen (2018) in Table 4.6. Here we see that the target amplitudes are well represented across the various scenarios with some degree of overprediction occurring for the WP4, WP7 and WP8 scenarios (see Figure 4.8) and to a lesser degree with the NP4 scenario. The modelled shoreline heights from the model output are then compared to the probabilistically derived shoreline heights in Table 4.7 and Table 4.8. Again, we see that the overprediction of the modelled output occurs with some of the WP sources but that it is more evident on WP4, WP7 and WP8 and does not occur across all of the C grids.

Thus, for the Orange Zone we propose aggregating a subset of model runs for each C grid region that covers the probabilistically defined value without excessive overprediction of the model. The simulations that are excluded from the aggregation are indicated with a strikethrough in Table 4.7.

Again, we note that the underprediction in the Hokianga and Kaipara B grid zones is due to the fact that the modelled tsunami heights come from grids located inside a harbour while the target tsunami heights from the GNS model are for an open coast location.

4.4 Aggregating the Model Output

The model output was aggregated by selecting the maximum value at each model node across all models run for a particular source region. This process is shown graphically in Figure 4.9 for the North Pacific sources with the lower right plot (highlighted in red) showing the aggregated model output. The aggregated outputs from each of the source regions were then combined in a GIS to produce a raster layer overlay that defined the maximum inundation extents over the entire suite of model runs. This inundation extent layer was then used to define the inundation line after additional post-processing which is described in more detail in Chapter 5.

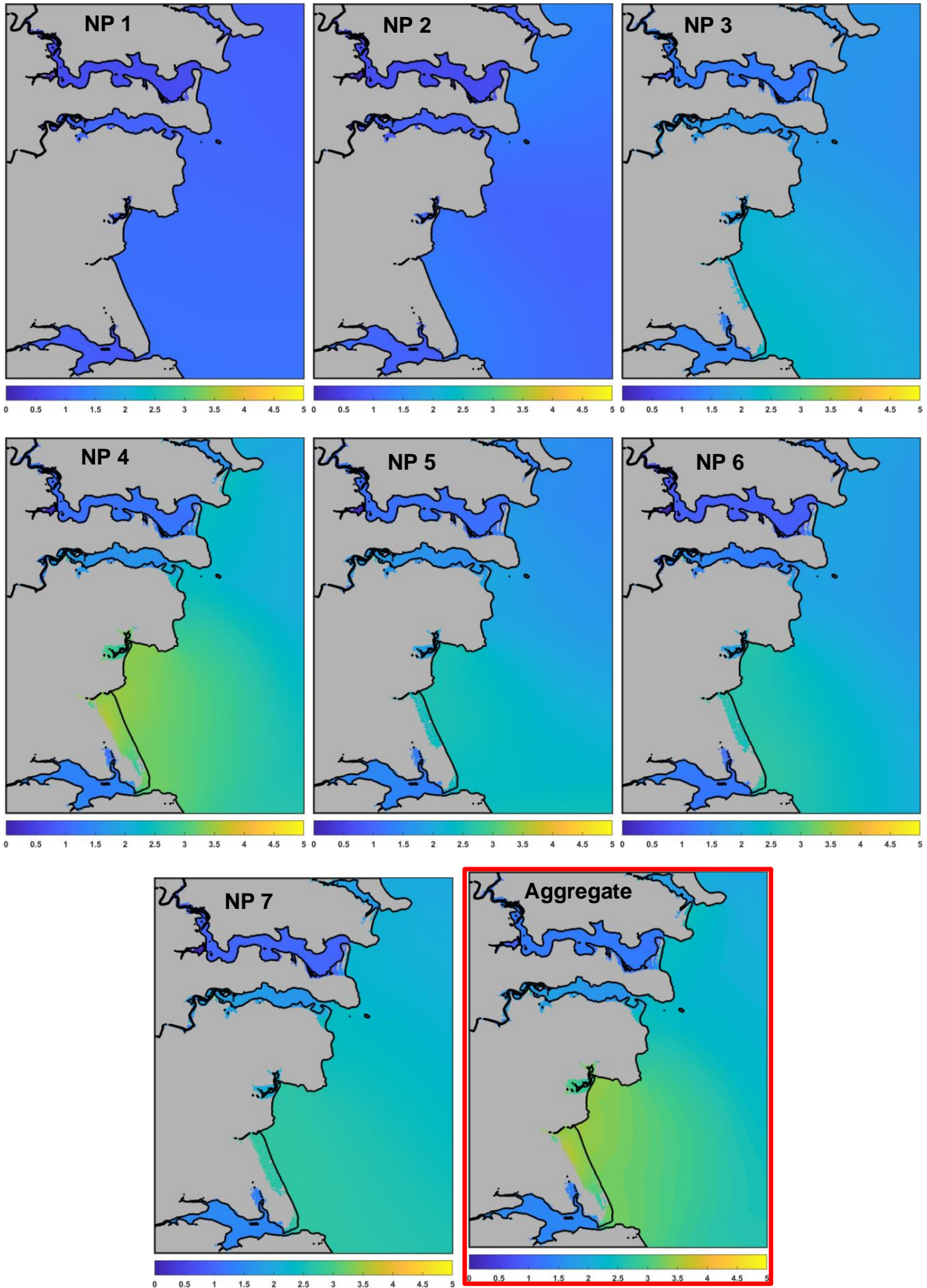


Figure 4.9 Example of aggregating model output for the Orange Zone extents. The maximum tsunami height from each model run at each output node is selected to create the overall maximum value which is contained in the plot with the red outline. This process was repeated for each C grid and each source region.

4.5 Tsunami Travel Times

In Figure 4.10 we present tsunami travel time contours to Northland. These travel times were computed using the 'TTT' software which calculates the speed of propagation of a shallow water wave across variable bathymetry using Huygens' method (Shokin *et al.*, 1987). Rather than determining the travel time from each source to Northland, we plotted the travel times from Northland outward. Plotting the data this way gives a clear indication of the number of hours from any point in the Pacific Ocean to Northland. Note however, that this is a *minimum* arrival time, i.e. this is the fastest possible time that a tsunami could cross from its source location to Northland. Also, observed difference between predicted and actual travel times is due to a combination of factors including inaccuracies in the bathymetry and nonlinear propagation effects. Also, it is important to remember that 'first arrival' is not when the strongest tsunami effects occur. For distant source tsunami in particular, the strongest effects generally occur many hours after first arrival.

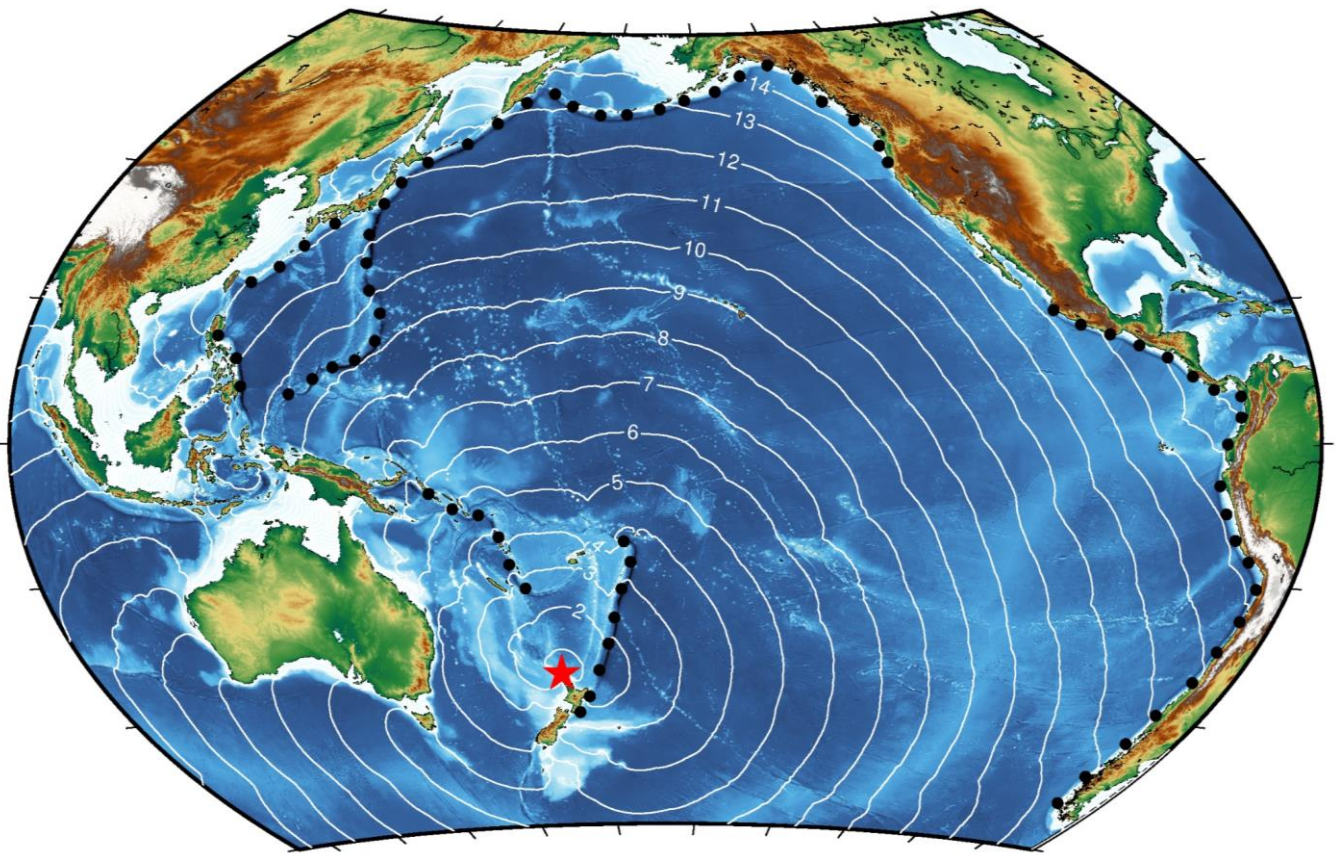


Figure 4.10 Tsunami travel times to Northland (red star). The 72 source locations are shown with black dots while the tsunami travel times are shown as white contours.

5 DEVELOPMENT OF DRAFT INUNDATION ZONES FROM MODEL OUTPUT

This section will describe the method used to convert the inundation model output into evacuation zones as per the DGL (2016). For the Orange and Yellow Zones, the outlines of the inundated areas were developed by first taking the inundation extents from each of the model runs and aggregating them across the relevant model output. That is, the maximum value of the tsunami induced inundation depth at each land pixel was determined by scanning through each output file and keeping the greatest value (see Section 3.3 above).

On the east coast we based the Yellow Zone on the aggregated output from the TK2 through TK 6 sources. This included three sources situated along the southern segment of the Tonga-Kermadec Subduction Zone with 30 m slip and two with 35 m slip (see Figure 4.5). For the west coast, the inundation extents from these sources were augmented with the WP1-8 sources, with the WP4 and WP8 sources contributing to the inundation extents in some cases.

For the Orange Zone we aggregated the relevant model simulation from the distant source scenarios that did not significantly exceed the probabilistically derived values at the 500-year RI level. These are indicated in Table 4.7 and Table 4.8 for each C-grid zone.

Finally, the Red Zone was created using a 100m buffer for rocky and steep coasts, and +2 m MSL elevation contour for all other areas. The final Red Zone was created on the greatest inland extent. This approach is consistent with that used by Auckland Council in their mapping project completed in 2022.

The inundation extents along coastline gaps between modelled C-grid regions (see Figure 3.2) were filled in manually using the inundation heights from the borders of the end-member C-grids and computed shoreline heights from the B-grids output. Where the tsunami inundation model abutted the model tile edges, zones were extended based on the corresponding contour height for the zone. In some cases, an updated C-grid was created with larger extents which did not cause the inundation to be clipped at the grid boundary. These grids were re-run for the dominant inundation source (usually TK 4 on the east coast and WB 4 or WP 8 on the west coast) and those modelled extents were used to revise the inundation zone.

Additionally, all isolated island areas less than 20 m² were removed from both Orange and Yellow Zones and all donut holes within Orange and Yellow Zones were dissolved to form a solid inundation area.

5.1 Differences Between the Old and New Inundation Zones

The tsunami evacuation zones currently in use for the Northland Region were developed by Lukovic and Heron (2016). For their study they used an assumed offshore tsunami height, then doubled it to account for tsunami runup on land. The inundation extents were then determined by applying a GIS-calculated attenuation rules developed for use in open coast, shallow harbour, and river situations.

The assumed offshore tsunami heights were derived from two sources. For the Orange Zone, they used a 3-5 m tsunami height based on the tsunami hazard threat levels defined by NEMA. For the Yellow zone, they used the shoreline tsunami height estimates from Power (2013) – the precursor to the Power (2021) values used in this study.

In the case of the Orange Zone, the assumed runup was 10 m (5 m times 2) plus the height of the water level at high tide which ranged from 1.0 to 1.5 m. For the orange zone, the Power (2013) shoreline heights ranged from ~5 to 23 m, when doubled this yields tsunami runup of ~11 to 46 m. However, the upper end was truncated to a maximum of 35 m, and it was this value that was added to high tide to create the value used to define the inundation zone.

These water levels were then projected inland over their topographic DEM model using different attenuation relationships for the tsunami height depending on whether the coastal zone being analysed was an open coast, shallow harbour or river environment. The specifics of the attenuation relationships can be found in the Lukovic and Heron (2016) report. The end result was a very

conservative estimate of the inundation extents which is much greater than the extents predicted using the numerical modelling approach used in this study (see Figure 5.1).

Based on our assessment of the model output, this large discrepancy come from two primary sources:

- 1) The doubling of the shoreline height used in the GIS rule approach to compensate for runup
- 2) An underprediction of the attenuation of tsunami heights at harbour entrances.

Below we give a specific example of how these two factors are dealt with in the current modelling.

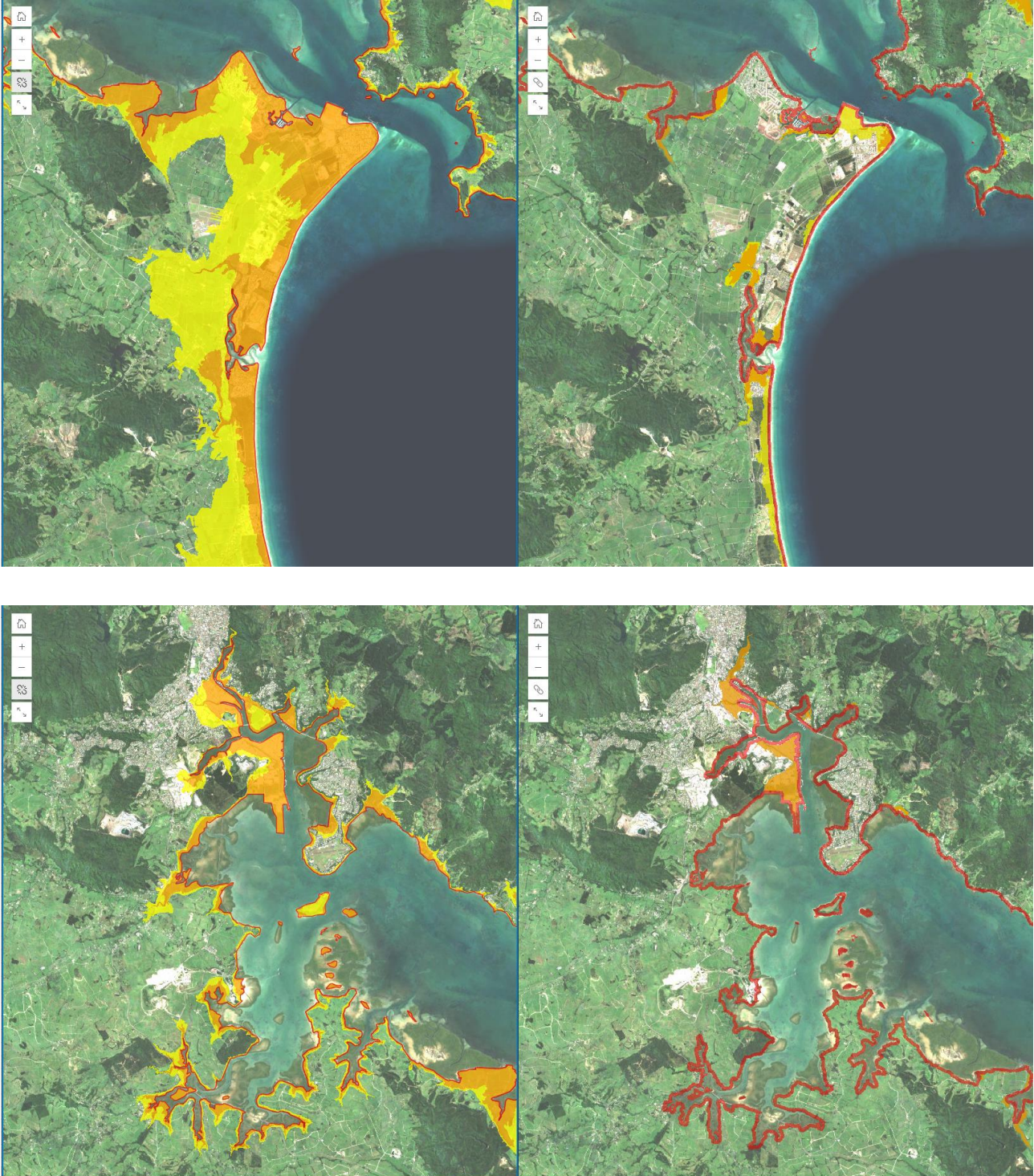


Figure 5.1 Comparison of inundation zones from the GIS attenuation rule (left) vs. hydrodynamic modelling (right) for the entrance to Whangarei Harbour (top) and Whangarei Town area (bottom).

5.1.1 Otaipango (Henderson Bay) and Pukenui

The Stretch of coastline from Otaipango – also known as Henderson Bay to Pukenui, is highly exposed to tsunami generated on the southern Tonga-Kermadec Trench. As such, the 2500-year RI, 84th percentile tsunami height from the Power (2021) study is very large at 17.1 m for this area. Our modelling for the TK4 scenario (30 m slip at the southern end of the Tonga-Kermadec subduction zone) predicts a 95th percentile shoreline tsunami height of 20.7 m in the Otaipango grid and 18.0 m in the Pukenui grid (see Table 4.3). The inundation results shown in Figure 5.2 indicate extensive inundation in some areas. Peak run-up from the model was 32.2 m in the Otaipango grid and 31.9 m in the Pukenui grid. In both cases, these high runup values occurred along steep cliffs as shown in in the plots below. Considering that our modelling was run for a high tide scenario, these values are roughly equivalent to the 33.8 m used in the GIS attenuation study. That value came about by doubling the Power (2013) shoreline tsunami height of 16.4 m (from Power 2013) and adding 1.0 m for high tide.

Despite the peak runup heights being quite similar (~32 m vs ~34 m) the modelled inundation extents are much smaller as compared to those derived from the GIS attenuation rules (Figure 5.3). Close inspection of the model output in Figure 5.2 shows that the tsunami runup is not much greater than the tsunami heights at the shoreline. Along Otaipango beach, shoreline heights of ~17 m yield runup height generally less than 20 m while in the southern embayment where tsunami heights are greater ~20 m or so, the run up heights are 20-23 m along the beach but jump to the peak value on the steep cliffs at the southern end of the beach. In the Pukenui grid, the highest runup occurs on the northern side of the rocky outcrop at the northern end of Houhora Bay with runup heights of >20 m predicted along the steep slopes behind Houhora Bay. However, the beach south of the entrance to Houhora Harbour is affected by significantly lower runup values. Furthermore, the modelling shows the dramatic drop off in tsunami heights at the entrance to Houhora Harbour with very little inundation predicted along the shores of the inner harbour.

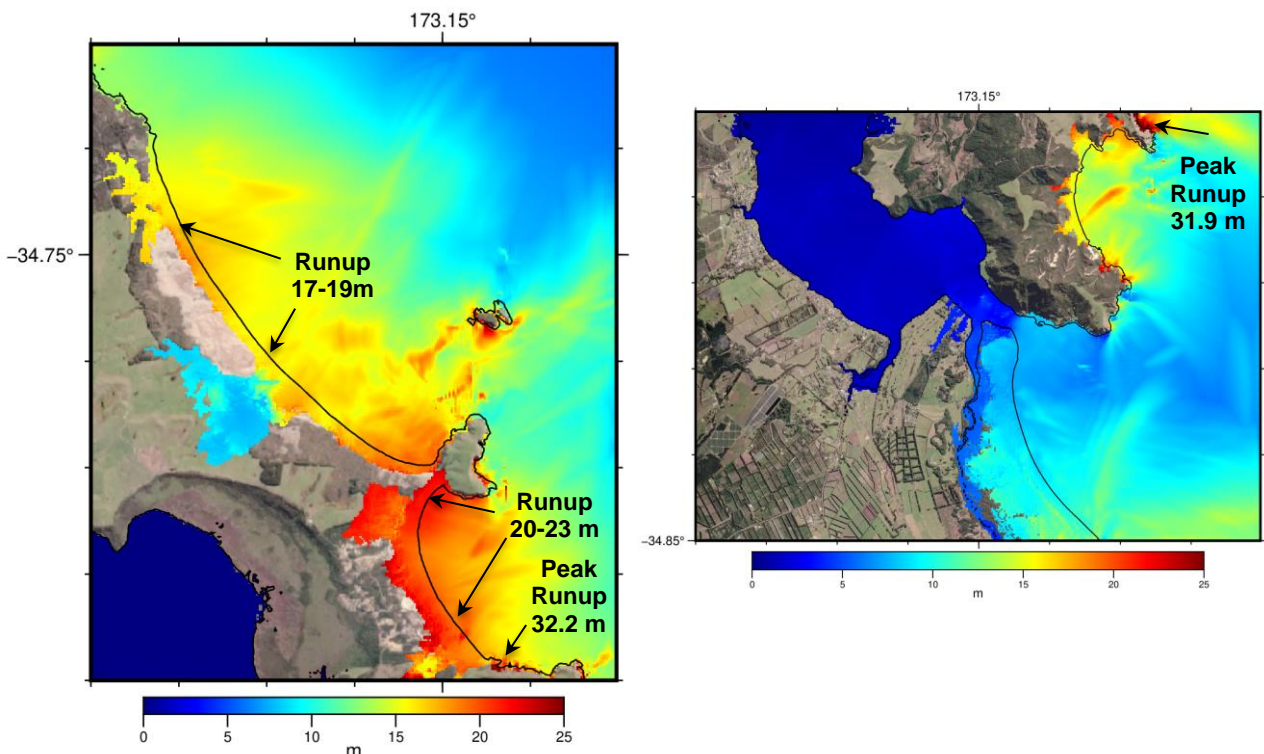


Figure 5.2 Modelled maximum tsunami heights from the TK 4 Source in the Otaipango/Henderson Bay grid (left) and Pukenui grid (right).

Based on these comparisons it is easy to see how applying a uniform value of 33.8 m would result in the inundation extents predicted by the GIS model. This is primarily because the coastal landforms in this area have peak elevations of ~25 m, which are lower than the assumed runup value, leading to predicted inundation. Furthermore, the GIS model does not consider the alongshore variation in tsunami heights that are resolved by the hydrodynamic model, nor does it accurately reproduce the dissipation of tsunami heights at the entrance to the harbour. This is reflected in the large differences in the inundation zones presented in Figure 5.3.

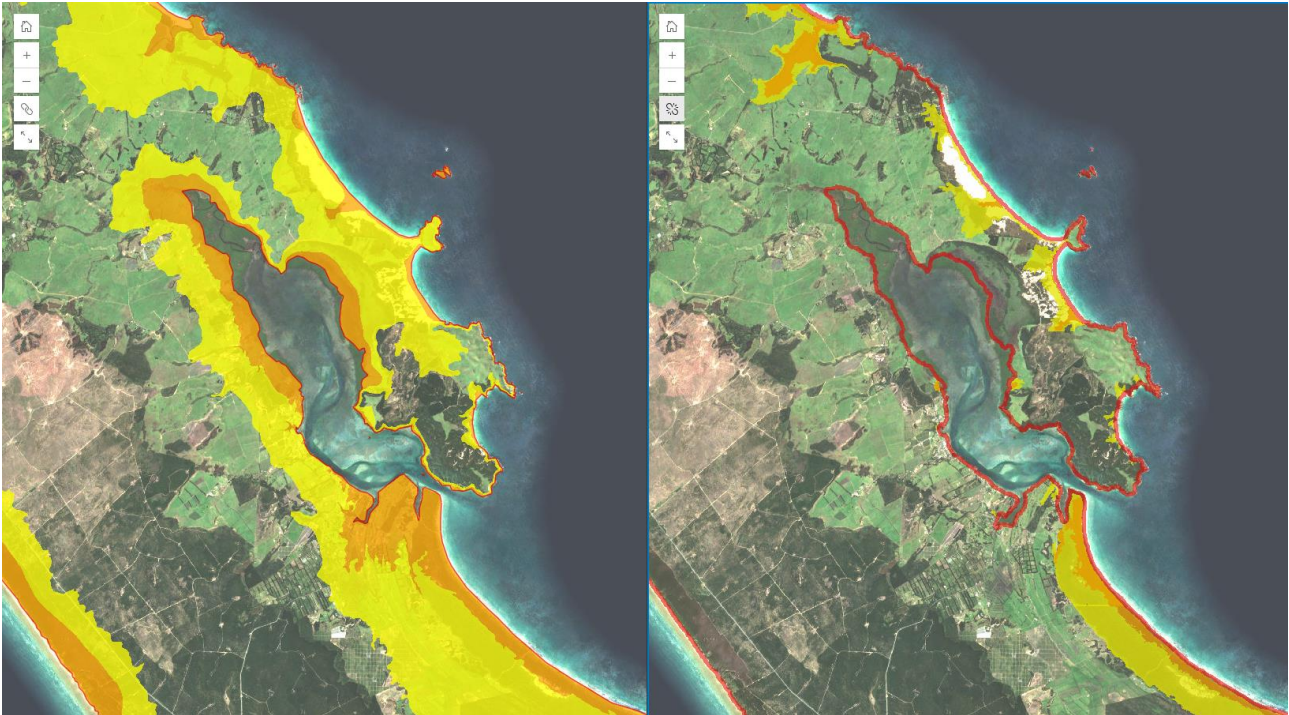


Figure 5.3 Inundation extents for Otaipango/Henderson Bay for the GIS attenuation model (left) and the hydrodynamic modelling (right).

The example discussed above highlights the fundamental differences between the inundation zones defined through hydrodynamic modelling and the use of the GIS based attenuation relationship. As we have shown, the updated modelling approach generally results in a reduction of the inundation zone extents. This result is seen throughout the region and is consistent with modelling done for the Auckland region.

6 SUMMARY AND CONCLUSION

The objective of this study was to produce tsunami inundation and evacuation zones for the Northland region that are compliant with guidelines set forth in the document 'Tsunami Evacuation Zones: Director's Guidelines for Civil Defence Emergency Management Groups' (MCDEM, 2016). This document defines three tsunami evacuation zones: Red, Orange, and Yellow. The Red Zone is the area closest to the coast which would be evacuated in most tsunami warning situations. The Orange Zone is an intermediate zone that considers tsunami hazard from either large tsunami sources located far away or moderate tsunami sources close by (but more than 1 hr travel time away). The Yellow Zone represents the area to be evacuated in the most extreme scenarios of a very large near-source earthquake.

To define these zones, we conducted a numerical modelling study focussed on determining the extents of the tsunami inundation zones for the Northland Region. The study used a Level 3/Level 4 modelling approach (as defined in MCDEM 2016) whereby a physics based numerical model was used to model the evolution of the tsunami from source through to inundation. We used multiple source scenarios based on output from probabilistic tsunami hazard models. Aspects of a Level 4 methodology were also incorporated in that we considered a wide variety of sources, both local and distant, and that the inundation lines were determined based on aggregating the results from multiple sources.

We used the ComMIT tsunami modelling software to simulate the tsunami hydrodynamics from tsunami generation through to inundation on land. The ComMIT model was validated for tsunami effects in the Northland region for several distant and near-source events including the recent Raoul Island earthquake of March 5, 2021. Numerical modelling grids were derived from the best available bathymetry and LiDAR topography. Sixty (60) nearshore modelling grids at 10 m resolution were developed for the simulations and the models were run a mean high-water spring (MHWS) water level with a final model run resolution of 20 m. Twenty-seven (27) source models were run over sixty (60) grids for a total of 1,620 model simulations. Models were batch run on 12 and 16 core desktop modelling computers and were conducted from mid-March to mid-May 2024.

Model output was compared to existing probabilistic tsunami hazard analyses. This includes the work of Power et al. (2021) which provides probabilistic estimates of tsunami heights at the shoreline along 50 km segments of the New Zealand coast. However, these estimates are based on an empirical relationship between earthquake magnitude and tsunami height and do not consider the effects of detailed hydrodynamics, coastal or bathymetric irregularities. Model output was also compared to the probabilistic model of Davies and Griffen (2018). In this model they provided tsunami amplitudes at a range of recurrence intervals (RIs) at deep-water, offshore locations derived from 10's of thousands of hydrodynamic simulations initialised with a wide variety of earthquake sources.

Based on our investigation we determined that the most extreme hazard, the one which governs the Yellow Zone for the east coast, is represented by a large rupture of the southern segments of the Tonga Kermadec Trench. For this scenario we modelled rupture over a 400x100 km fault plane with average slip amount of 30 m. As a matter of comparison, we note that this source is slightly larger in terms of areal extent and average slip than the 2010 Tohoku Japan earthquake and tsunami.

For the Orange Zone, we determined that the hazard was best represented by aggregating the inundation results from a suite of large magnitude, distant and regional source earthquakes. In this case, simulations that produced anomalously large tsunami heights either at the shoreline or at the offshore location were not used in the aggregation. All in all, the final inundation zones correspond best to a tsunami threat level of 3-5 m as defined in the DGL.

Raster files of tsunami inundation flow depth and inundated area were compiled for each of the 60 high resolution model grid regions for the Yellow and Orange Zones. This data was transferred to the GIS Specialist for processing into the continuous inundation zones. As expected, the inundation zones derived from the hydrodynamic model output model were significantly smaller than those produced using GIS-based attenuation rules and an assume uniform value for tsunami height at the shoreline.

7 REFERENCES

- Amanda R. Admire, A., Dengler, L., Crawford, G., Uslu, B., Borrero, J.C., Greer, S. and Wilson, R. (2014) Observed and Modeled Currents from the Tohoku-oki, Japan and other Recent Tsunamis in Northern California, *Pure and Applied Geophysics*, 10.1007/s00024-014-0797-8.
- Arnold, J., Carter, J., Dumas, and Gillebrand, P. (2009) Northland Regional Council Tsunami Modelling Study 3 NIWA Client Report: CHC2009-042 June 2009
- Arnold, J., Gillebrand, P. and Sykes, J. (2011) Numerical modelling of tsunami inundation for Whangarei Harbour and environs NIWA Client Report: CHC2010-133 April 2011.
- Ayca, A. and Lynett, P. (2016) "Effect of Tides and Source Location on Nearshore Tsunami-Induced Currents." *Journal of Geophysical Research: Oceans*, doi: 10.1002/2016JC012435
- Beetham, R. D., McSaveney, M., Dellow, G., N., Rosenberg, M., Johnston, D. & Smith, W., 2004. A review of natural hazards information for Northland Region, Institute of Geological & Nuclear Sciences science report 2004/06 25 p.
- Borrero, J., Bell, R., Csato, C., DeLange, W., Greer, D., Goring, D., Pickett, V. and Power, W. (2012). Observations, Effects and Real Time Assessment of the March 11, 2011 Tohoku-oki Tsunami in New Zealand, *Pure and Applied Geophys.*, 170, 1229-1248, DOI 10.1007/s00024-012-0492-6
- Borrero, J.C. and Greer, S.D. (2012) Comparison of the 2010 Chile and 2010 Japan tsunamis in the Far-field, *Pure and Applied Geophysics*, 170, 1249-1274, DOI 10.1007/s00024-012-0559-4.
- Borrero, J.C., Goring, D.G., Greer, S.D., Power, W.L. and Barberopoulou, A. (2013) Decision Making Tools for the Real-Time Assessment of Far-Field Tsunami Hazards in New Zealand Ports and Harbours Part 1: Background Information and Preliminary Analysis. Prepared for New Zealand Ministry of Business Innovation and Employment, December 20, 2013.
- Borrero, J.C., Goring, D.G., Greer, S.D. and Power, W.L. (2014) Tsunami Hazards in New Zealand Ports, *Pure and Applied Geophysics*, 10.1007/s00024-014-0987-4
- Borrero, J.C., LeVeque, R.J., S. Dougal Greer, Sam O'Neill and Brisa N. Davis (2015a) Observations and Modelling of Tsunami Currents at the Port of Tauranga, New Zealand, *Proceedings of Coasts and Ports Conference*, Auckland, New Zealand, September, 2015.
- Borrero, J.C., Lynett, P.J. and Kalligeris, N. (2015b) Tsunami Currents in Ports, *Philosophical Transactions of the Royal Society A*, 373: 20140372. <http://dx.doi.org/10.1098/rsta.2014.0372>
- Borrero, J. (2017) Assessment of Tsunami Induced Currents in Indian Ocean Ports, *Proceedings of Coasts and Ports Conference*, Cairns, Australia, June, 2017
- Borrero, J.C., and O'Neill, S. (2019) Assessment of Tsunami Hazards in Northland Maritime Facilities. Project for New Zealand Ministry of Civil Defence and Emergency Management and Northland Regional Council, July 2019.
- Chagué-Goff, C. and Goff, J. (2006) Tsunami hazard assessment baseline for the Northland region, NIWA Client Report: CHC2006-069 June 2006
- De Lange, W.P. and Healy, T.R. (1986). New Zealand tsunamis 1840–1982. *New Zealand Journal of Geology and Geophysics*, 29(1), 115–134. doi:10.1080/00288306.1986.10427527
- Downes, G., A. Barberopoulou, U. Cochran, K. Clark, and F. Scheele (2017), The New Zealand Tsunami Database: Historical and Modern Records. *Seismological Research Letters*, 88 (2), 342-353, doi: 10.1785/0220160135.
- Fritz, H., Petroff, C., Catalán, P., Cienfuegos, R., Winckler, P., Kalligeris, N., Weiss, R., Barrientos, S., Meneses, G., Valderas-Bermejo, C., Ebeling, C., Papadopoulos, A., Contreras, M., Almar, R., Dominguez, J., and Synolakis, C. (2011a), Field survey of the 27 February 2010 Chile tsunami, *Pure Appl. Geophys.*, 168, 1989-2010.
- GeoNet (2017), M 7.1 East Cape Fri, Sep 2 2016
<http://www.geonet.org.nz/earthquake/2016p661332> Accessed June 22, 2017.
- Gillebrand, P., Lane, E., Arnold, J., Carter, J., Dumas, J. Enright, M. and Goff, J. and Roulston, H. (2008) Northland Regional Council Tsunami Modelling Study 2 NIWA Client Report: CHC2008-115 August 2008

- Goff, J. Walters, R. and Callaghan, F. (2006) Tsunami source study, NIWA Client Report CHC2006-082, August 2006.
- Goff, J., Pearce, S., Nichol, S. L., Chagué-Goff, C., Horrocks, M., & Strotz, L. (2010a). Multi-proxy records of regionally sourced tsunamis, New Zealand. *Geomorphology*, 118(3-4), 369–382. doi:10.1016/j.geomorph.2010.02.005
- Goff, J., Nichol, S., Chagué-Goff, C., Horrocks, M., McFadgen, B., & Cisternas, M. (2010b). Predecessor to New Zealand's largest historic trans-South Pacific tsunami of 1868AD. *Marine Geology*, 275(1-4), 155–165. doi:10.1016/j.margeo.2010.05.006
- Kalligeris, N., Montoya, L., Ayca, A., and Lynett, P. (2017) "An Approach for Estimating the Largest Expected Tsunami from Far Field Subduction Zone Earthquakes." *Natural Hazards*, v. 89(1), pp. 233-253.
- Kalligeris, N., V. Skanavis, S. Tavakkol, A. Ayca, H. E. Safty, P. Lynett, and C. Synolakis (2016) "Lagrangian flow measurements and observations of the 2015 Chilean tsunami in Ventura, CA." *Geophysical Research Letters*, 43, doi: 10.1002/2016GL068796.
- Keen, A., Lynett, P., Eskijan, M., Ayca, A., and Wilson, R. (2017) "A Monte Carlo Based Approach to Estimate Fragility Curves of Floating Docks for Small Craft Marinas." *Journal of Waterway, Port, Coastal, and Ocean Engineering (ASCE)*, doi: 10.1061/(ASCE)WW.1943-5460.0000385
- Lane, E., Walters, R. Arnold, J. and Roulston, H. (2007) Northland Regional Council Tsunami Modelling Study 1 NIWA Client Report: CHC2007-109 September 2007
- Lynett, P., Borrero, J., Weiss, R., Son, S., Greer, D., Renteria, W. (2012) Observations and Modeling of Tsunami-Induced Currents in Ports and Harbors, *Earth and Planetary Science Letters*, 327-328 (68-74).
- Lynett, P.J., Borrero, J.C., Son, S., Wilson, R.W. and Miller, K. (2014) Assessment of the tsunami-induced current hazard, *Geophysical Research Letters*, DOI: 10.1002/2013GL058680
- Lukovic, B. and Heron, D. (2016) Tsunami evacuation zone boundary mapping: Northland update, GNS Science Consultancy Report 2016/101, July 2016.
- New Zealand Palaeotsunami Database (2017). <https://ptdb.niwa.co.nz>, Accessed October 2018.
- Okal, E.A., H.M. Fritz, R. Raveloson, G. Joelson, P. Pancoskova, and G. Rambolamanana, (2006a) Madagascar field survey after the December 2004 Indian Ocean tsunami, *Earthquake Spectra*, 22, S263-S283.
- Okal, E.A., H.M. Fritz, P.E. Raad, C.E. Synolakis, Y. Al-Shijbi, and M. Al-Saifi, (2006b) Oman field survey after the December 2004 Indian Ocean tsunami, *Earthquake Spectra*, 22, S203-S218.
- Okal, E.A., A. Sladen, and E.A.-S. Okal, Rodrigues, (2006c) Mauritius and Réunion Islands, field survey after the December 2004 Indian Ocean tsunami, *Earthquake Spectra*, 22, S241-S261.
- Percival, D, Denbo, D, Eble, M, Gica, E, Mofjeld, H, Spillane, M, Tang, L, and Titov, V (2010). Extraction of tsunami source coefficients via inversion of DART buoy data, *Nat. Haz.* doi:10.1007/s11069-010-9688-1.
- Popovich, B (2015) Effects of Tsunami Loading on New Zealand Wharf Structures, University of Auckland Ph.D. Thesis
- Power, W and Gale, N. (2010) Tsunami Forecasting and Monitoring in New Zealand *Pure and Applied Geophysics*, DOI 10.1007/s00024-010-0223-9.
- Power, W. Downes, G. and Stirling, M. (2007) Estimation of Tsunami Hazard in New Zealand due to South American Earthquakes, *Pure and Applied Geophysics*, 164 (2007) 547-564 DOI 10.1007/s00024-006-0166-3.
- Power, W. L. (2013). Review of Tsunami Hazard in New Zealand (2013 Update) GNS Science Consultancy Report No. 2013/131, 238 pages.
- Power, W. L. (2014). Tsunami hazard curves and deaggregation plots for 20km coastal sections, derived from the 2013 National Tsunami Hazard Model GNS Science Consultancy Report No. 2013/59, 558 pages.

- Power, W., Borrero, J., Greer, D. and Goring, D. (2015) Developing robust tsunami forecasts for Ports and Harbours, Proceedings of the Australasian Coasts & Ports Conference 2015, 15 - 18 September 2015, Auckland, New Zealand. Available on-line.
- Power WL, Burbidge DR, Gusman AR. (2022) The 2021 update to New Zealand's National Tsunami Hazard Model. Lower Hutt (NZ): GNS Science. 63 p. (GNS Science report; 2022/06). doi:10.21420/X2XQ-HT52.
- Power WL, Burbidge DR, Gusman AR. (2023). Tsunami hazard curves and deaggregation plots for 20 km coastal sections, derived from the 2021 National Tsunami Hazard Model. Lower Hutt (NZ): GNS Science. 545 p. (GNS Science report; 2022/61). doi:10.21420/XPA4-VD47.
- Shokin, *et al.*, 1987, Calculations of tsunami travel time charts in the Pacific Ocean, Science of Tsunami Hazards, vol. 5, p. 85-113.
- Son, S., Lynett, P. J., & Kim, D. H. (2011). Nested and multi-physics modeling of tsunami evolution from generation to inundation. *Ocean Modelling*, 38(1–2), 96–113. <https://doi.org/10.1016/j.ocemod.2011.02.007>
- Todd, E. K., and T. Lay (2013), The 2011 Northern Kermadec earthquake doublet and subduction zone faulting interactions, *J. Geophys. Res.*, 118, doi:10.1029/2012JB009711
- Titov, V. V., & González, Frank, I. (1997). *Implementation and testing of the Method of Splitting Tsunami (MOST) model* (No. ERL PMEL-112) (p. 14). Retrieved from <http://www.pmel.noaa.gov/pubs/PDF/tito1927/tito1927.pdf>
- Titov, V. V., Moore, C. W., Greenslade, D. J. M., Pattiaratchi, C., Badal, R., Synolakis, C. E., & Kânoğlu, U. (2011). A New Tool for Inundation Modeling: Community Modeling Interface for Tsunamis (ComMIT). *Pure and Applied Geophysics*, 168(11), 2121–2131. doi:10.1007/s00024-011-0292-4
- Titov, V.V., and C.E. Synolakis (1995): Modeling of breaking and nonbreaking long wave evolution and runup using VTCS-2. *J. Waterways, Ports, Coastal and Ocean Engineering*, 121(6), 308–316.
- USGS (2016) M 7.0 - 175km NE of Gisborne, New Zealand <https://earthquake.usgs.gov/earthquakes/eventpage/us10006jb>, accessed on June 22, 2017.
- Wei, Y., Chamberlin, C., Titov, V. V., Tang, L., & Bernard, E. N. (2012). Modeling of the 2011 Japan Tsunami: Lessons for Near-Field Forecast. *Pure and Applied Geophysics*, 170(6–8), 1309–1331. <http://doi.org/10.1007/s00024-012-0519-z>
- Wei, Y, Newman, A, Hayes, G, Titov, V, Tang, L (2014). Tsunami Forecast by Joint Inversion of Real-Time Tsunami Waveforms and Seismic or GPS Data: Application to the Tohoku 2011 Tsunami. *Pure Appl. Geophys.* doi:10.1007/s00024-014-0777-z
- Wilson, R., Admire, A., Borrero, J., Dengler, L., Legg, M., Lynett, P., McCrink, T., Miller, K., Ritchie, A., Sterling, K., and Whitmore, P. (2012) Observations and Impacts from the 2010 Chilean and 2011 Japanese Tsunamis in California (USA), *Pure and Applied Geophysics*, DOI 10.1007/s00024-012-0527-z.
- Wilson, R. and Miller, K. (2012) Improving Tsunami Hazard Mitigation and Preparedness Using Real-Time and Post-Tsunami Field Data (abstract) American Geophysical Union, Fall Meeting 2012, abstract id. NH31C-1614.
- Wilson, R., Lynett, P., Eskijian, M., Miller, K., Laduke, Y., Curtis, E., Hornick, M., Keen, A. and Ayca, A. (2017) Tsunami Hazard Analysis and Products for Harbors in California (abstract) GSA Annual Meeting in Seattle, Washington, USA – 2017.

8 APPENDIX 1: VALIDATION OF THE COMMIT MODEL TSUNAMIS AFFECTING NORTHLAND

The ComMIT model has been validated for both distant source and near source events. In the following sections we present results showing the performance.

8.1 Case 1: The February 27, 2010, Maule, Chile Earthquake and Tsunami

For the 2010 Maule Chile event we used the tsunami source model developed by NOAA for use within the ComMIT system. This source is shown in Figure 8.1 below along with the resultant trans-Pacific propagation pattern of the maximum tsunami amplitude. We compared the model output to water levels recorded at Marsden Point as this is the only site in the study area with available tide gauge data from a tsunami event. The model to measured comparison is presented in Figure 8.2 and shows a good fit in terms of arrival time, wave shape and amplitude between the measured and model result.

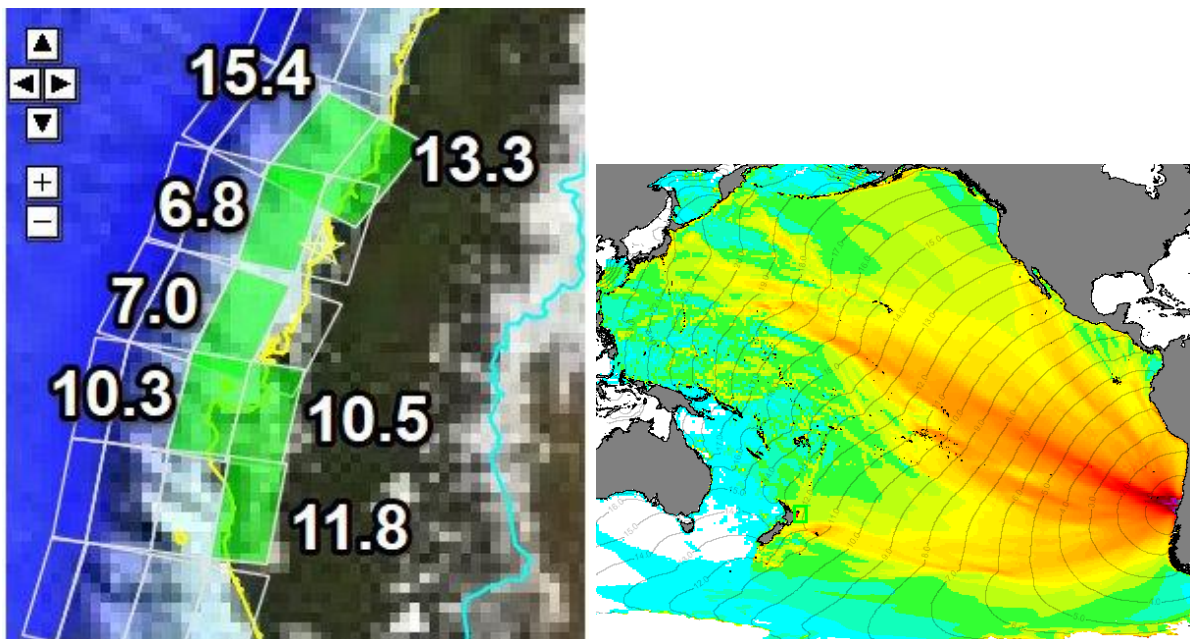


Figure 8.1 Tsunami source model (left) and the trans-Pacific propagation pattern (right) for the 2010 Maule, Chile tsunami. Slip amounts (in meters) for the individual fault segments are indicated in white.

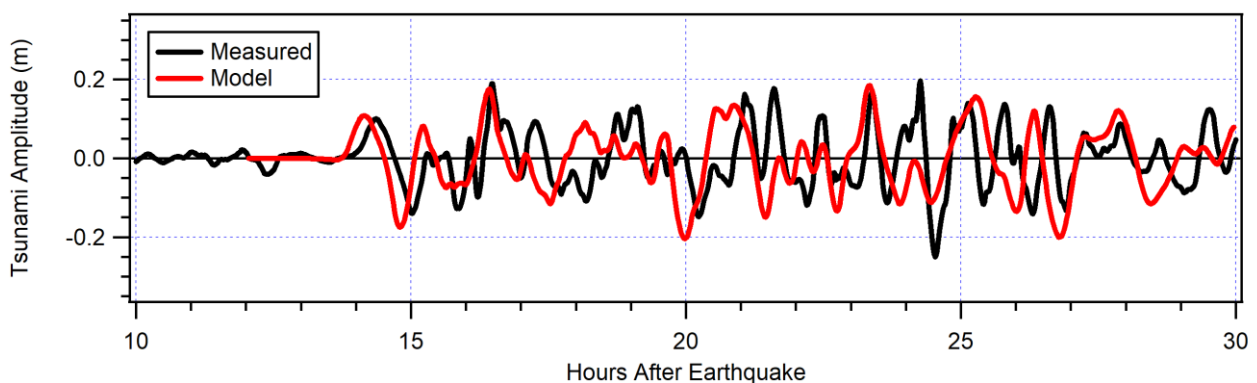


Figure 8.2 Modelled water level time series compared to measured data at the Marsden Point tide gauge for the 2010 Maule, Chile tsunami.

8.2 Case 2: The March 11, 2011, Tohoku Earthquake and Tsunami

The March 11, 2011, Tohoku earthquake and tsunami also presents an excellent case study for the validation of the ComMIT model. The tsunami event was recorded on tide gauges throughout New Zealand with a wealth of data recorded on five water level gauges and one current meter in Tauranga Harbour (Lynett *et al.*, 2012, Borrero *et al.*, 2012, Borrero and Greer 2013) with the effects there modelled in Borrero *et al.*(2015).

As with the 2010 event, here we compare the model results to data recorded on the Marsden Point tide gauge. Also, as with the Chile event, the model was initialised using the tsunami source developed by NOAA for use within the ComMIT modelling system (see Figure 8.3). The model results (Figure 8.4) show a good fit to the measured data in terms of arrival time, wave form and amplitude at Marsden Point.

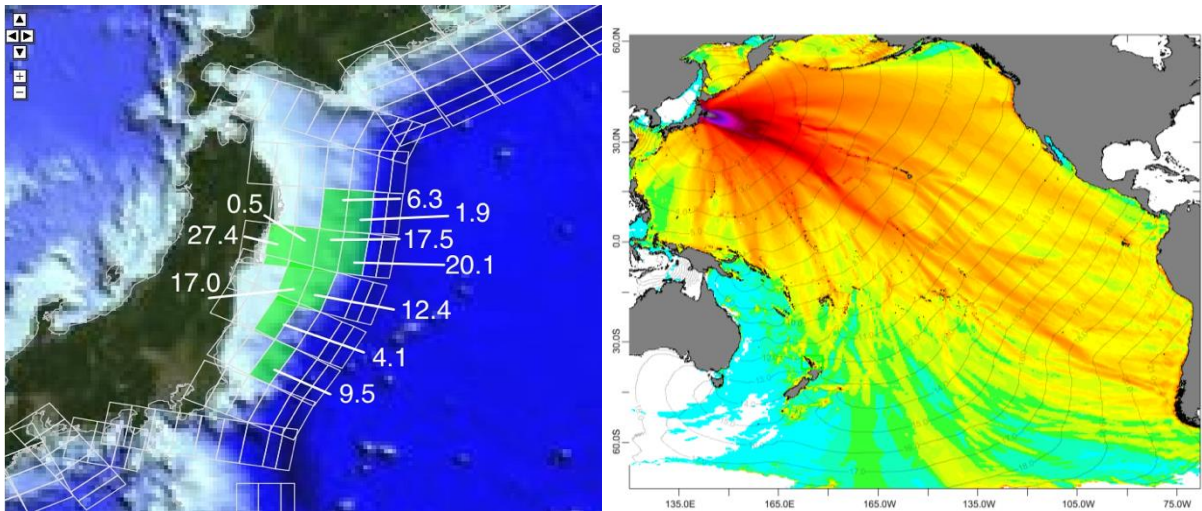


Figure 8.3 Tsunami source model (left) and the trans-pacific propagation pattern (right) for the 2011 Tohoku, Japan tsunami. Slip amounts (in meters) for the individual fault segments are indicated in white.

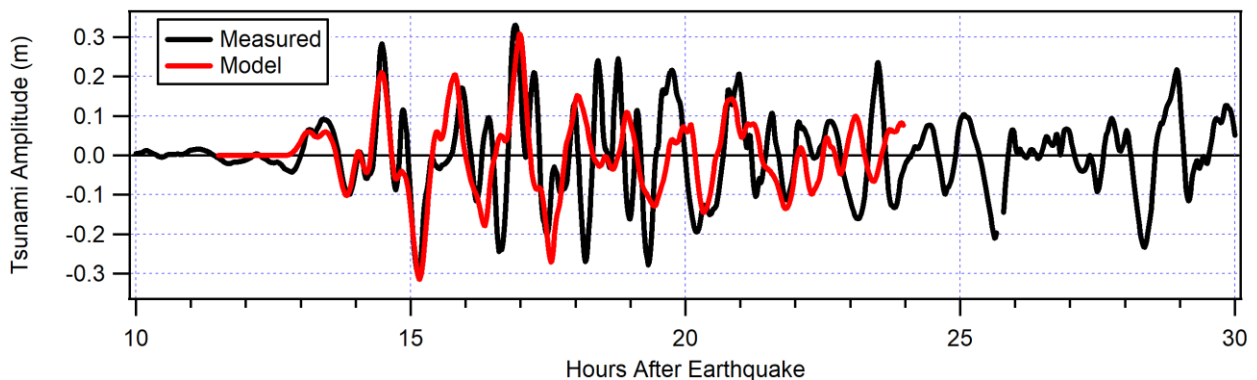


Figure 8.4 Modelled water level time series compared to measured data at Marsden Point for the 2011 Tohoku, Japan tsunami.

8.3 Case 3: The September 2nd, 2016, East Cape Earthquake and Tsunami

On 2nd September 2016 at 4:37 am NZST (1 September 16:37 UTC), a magnitude 7.1 (GeoNet) earthquake struck just north-east of the East Cape of New Zealand (Figure 3.10). The event was felt throughout the North Island. More than 4,000 people filed felt earthquake reports on the GeoNet community reporting system, with reports coming in from as far away as Chatham Island and Christchurch (GeoNet, 2017). The event created a small non-damaging tsunami that was recorded on tide gauges in Gisborne and across the Bay of Plenty.

This event is important in that it was relatively strong and occurred along the Tonga-Kermadec subduction zone, and in an area considered as the 'worst-case' source region for generating tsunamis affecting the East Cape, Bay of Plenty, Coromandel and Northland coasts – this due to its proximity and associated short travel times to these regions.

The source mechanism for this event was not, however, a straightforward subduction zone event. The strike of the fault plane was oblique, and the source region was displaced west of the trench axis, suggesting a seismic rupture within the overriding Australian plate (Figure 8.6, top panel). Additionally, the sense of the rupture was that of a 'normal' fault rather than a thrust or 'reverse' fault commonly associated with ruptures on a subduction zone interface. This means that the seafloor displacement above the source area was downward (i.e. negative) rather than upward (uplift). This is indicated by the direction of the slip vector arrows in the bottom panel of Figure 8.6.

To model this event using the pre-computed sources in the ComMIT database, some assumptions and approximations were necessary. Firstly, it was necessary to use a fault segment located to the east of the actual source region. Next, a negative average displacement was applied to the fault plane to produce a negative initial seafloor displacement. Two slip amounts were trialed, -0.4 m and -0.6 m.

The model results are compared to measured tide gauge data at Lottin Point and Tauranga Harbour in Figure 8.7. The comparison of the waveform at Lottin Point is remarkably good - given the approximations - with the results from the two source models neatly bracketing the measured data. Note that the modelled time series had to be shifted 7 minutes earlier to match the timing of the measured data. This accounts for the fact that the source region used in the model is located further away to the west of the actual source region, thus requiring more time for the wave to reach the tide gauge.

The results for Tauranga are not as good with the model over predicting the measured wave heights and requiring a 14-minute time shift to match the timing of the peaks and troughs. However, this is understandable given the very small size of the tsunami and the degree of attenuation that likely occurred as this small signal passed through the narrow entrance of Tauranga Harbour.

Given the limitations of the ComMIT model, the results are good and show that it can be used to accurately predict tsunami heights along the New Zealand coast from near-field tsunami sources.

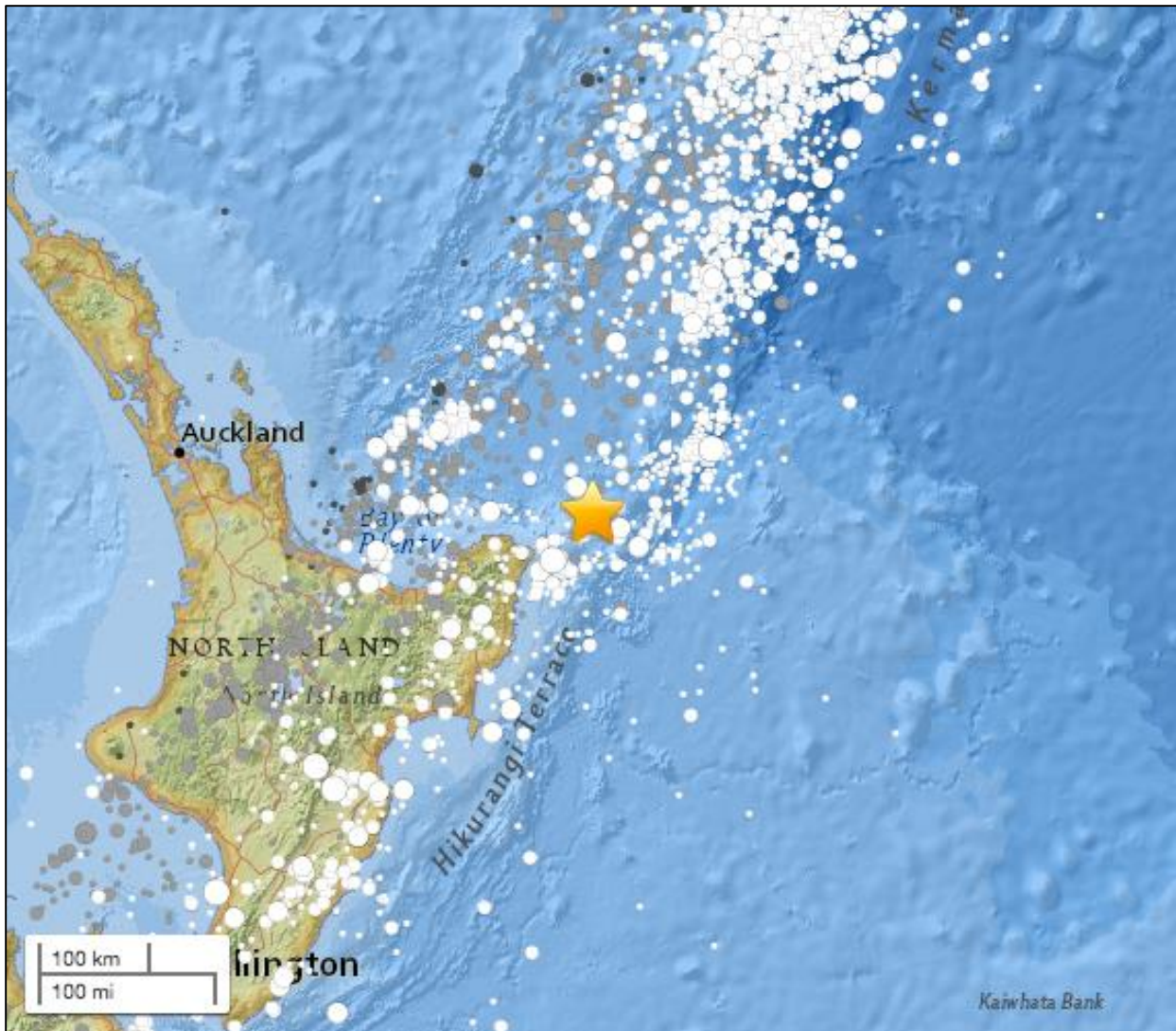
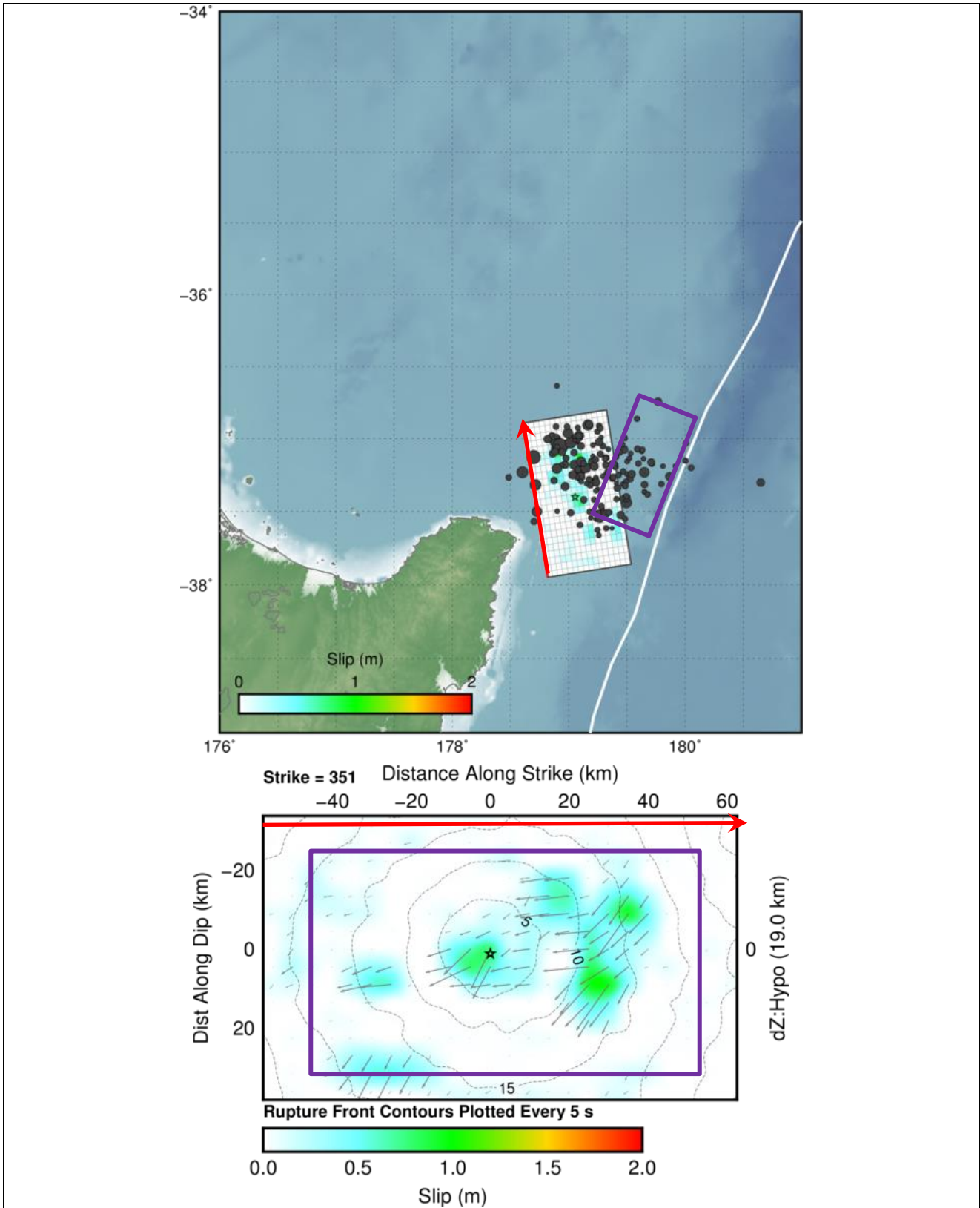


Figure 8.5 Source location of the September 2nd East Cape Earthquake (USGS, 2017).

Figure 8.6 (following page) Top panel: Earthquake source model for the September 2nd, 2016, East Cape earthquake (reproduced from USGS, 2016). The top panel shows the location of the fault plane (white region). Epicentre of the mains shock is indicated by a star with aftershocks indicated by black circles. Coloured patches indicate coseismic slip amounts according to the colour scale. The thin red line is the top of the fault plane. The white line is the axis of the Tonga-Kermadec Trench. The purple rectangle shows the location of a 100x50 km fault plane source available in the ComMIT tsunami modelling database. Bottom panel: A detail of the slip distribution along the fault plane with the amount of slip indicated by the colour scale. The location of the earthquake hypocentre is indicated by the star with the arrows indicating the direction of the rupture displacement. The contour lines are the timing (in seconds) of the rupture. The red arrow at the top of the fault plane corresponds to the red arrow in the upper panel. The purple box shows the dimensions of a 100x50 km fault plane.



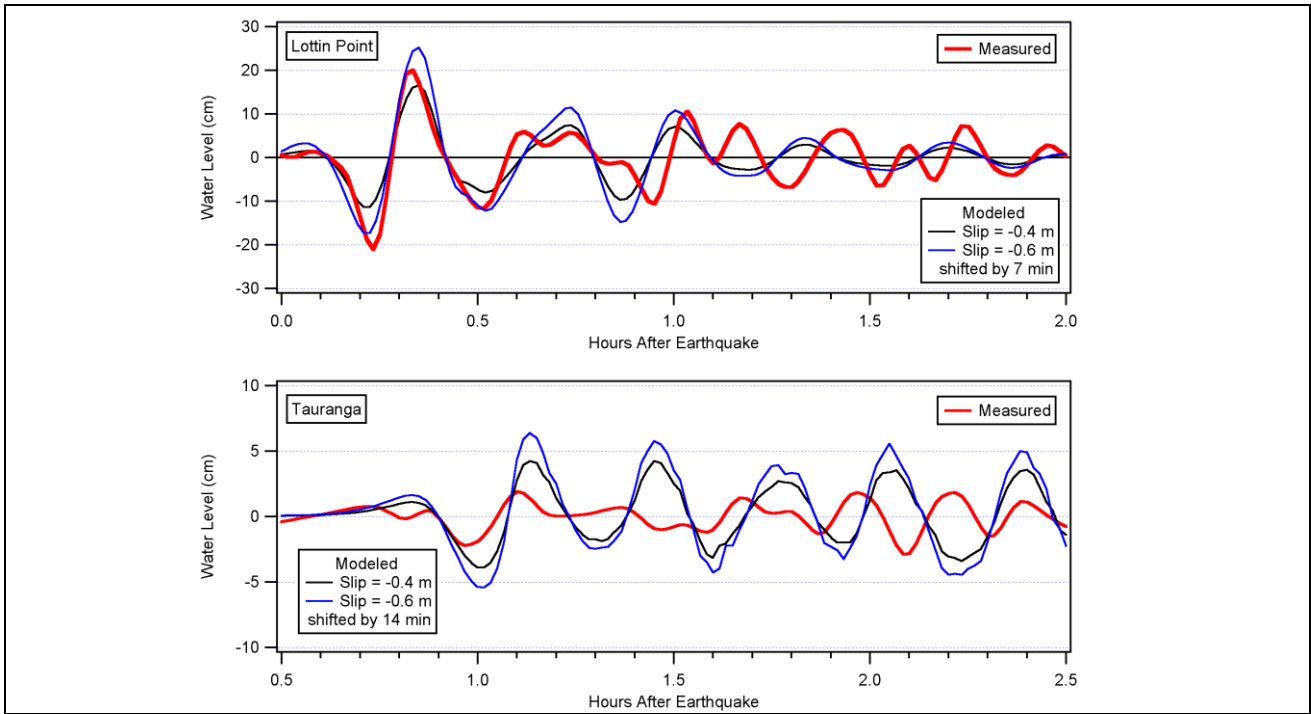


Figure 8.7 Modelled (blue and black traces) versus measured (red trace) water levels at Lottin Point (top) and Tauranga (bottom) for the 2nd September 2016 tsunami.

8.4 Modelling The 1976 Event in Tutukaka

Early in the morning of January 15, 1976, two relatively large earthquakes occurred within one hour of each other along the Tonga-Kermadec Subduction Zone, approximately 1100 km north east of New Zealand's East Cape (Todd and Lay, 2012). The first shock occurred at 4:56 AM NZDT with the second coming at 5:47 AM. The event generated a small tsunami which was recorded through the Pacific Ocean including several sites in New Zealand with noticeably stronger effects in Tutukaka Harbour where the tsunami reached heights of 0.2-0.75 m (newspaper reports are inconsistent) and caused damage to several boats and some port structures such as piles and marker buoys (Downes *et al.*, 2017).

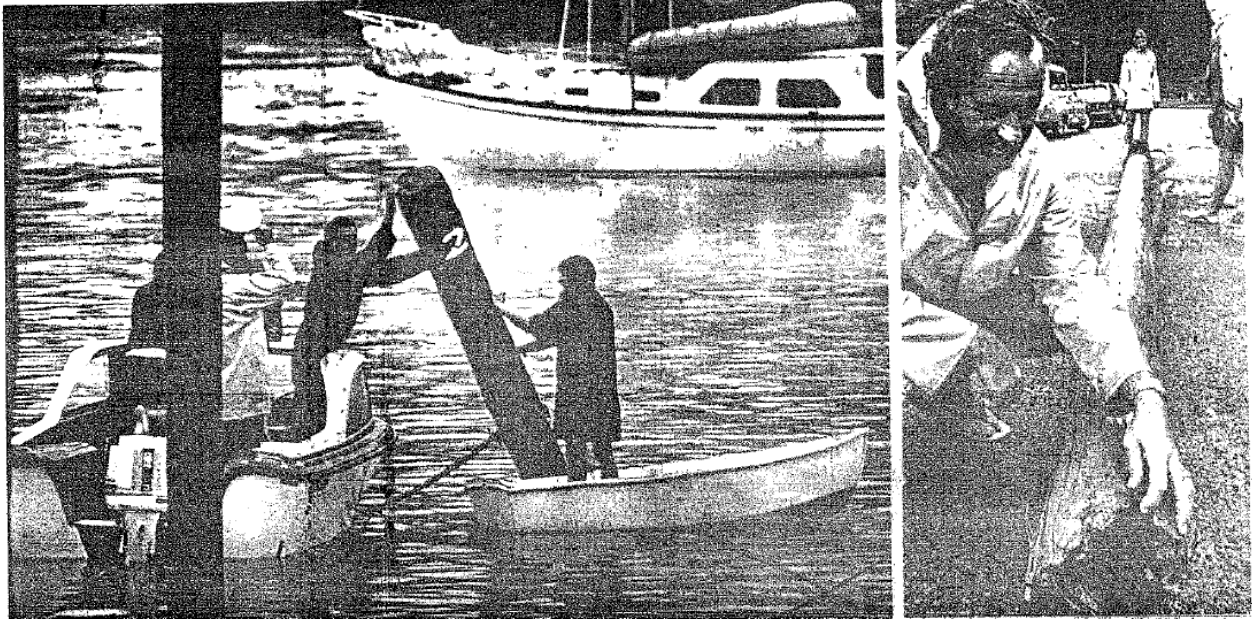


Figure 8.8 Photos from a newspaper account of the 1976 tsunami in Tutukaka. The caption reads “[Left]: A yacht heads out to sea at Tutukaka to escape the tidal wave. In the foreground men steady a pile loosened by surging water. [Right]: Mr D. Cutfield, owner of the launch Willie O inspects a pile snapped off at the base.

Reports suggest that the second earthquake was slightly larger and shallower than the first event and was likely the source for the subsequent tsunami. Among the accounts reported by Downes *et al.* (2017) are descriptions of yacht being torn from their moorings, a surge of 0.75 m, ‘a great big whirlpool’ and current speeds estimated at 8 knots.

To model the event, we used a source model 100 km long by 50 km wide with a uniform slip of 2.8 m occurring along the deeper segments of the TK Trench as indicated in Figure 8.9. The resulting model output is presented in Figure 8.10 and Figure 8.11 and agree well with the eyewitness reports. Our model predicts a maximum tsunami height of 0.81 m while eyewitnesses at the time reported a height of 0.75 m. Additionally the timing of the modelled maximum surge compares well with eyewitness accounts that the strongest effects occurred around 8:45 am on January 15th. In terms of current speeds, the model suggests currents of up to 10 knots, strongest in the entrance to the inner harbour area, while reports from the time estimated current speeds at 8 knots.

Overall, it seems that the modelling is consistent with the available observational data and provides further confidence in the veracity of the modelling methodology used here.

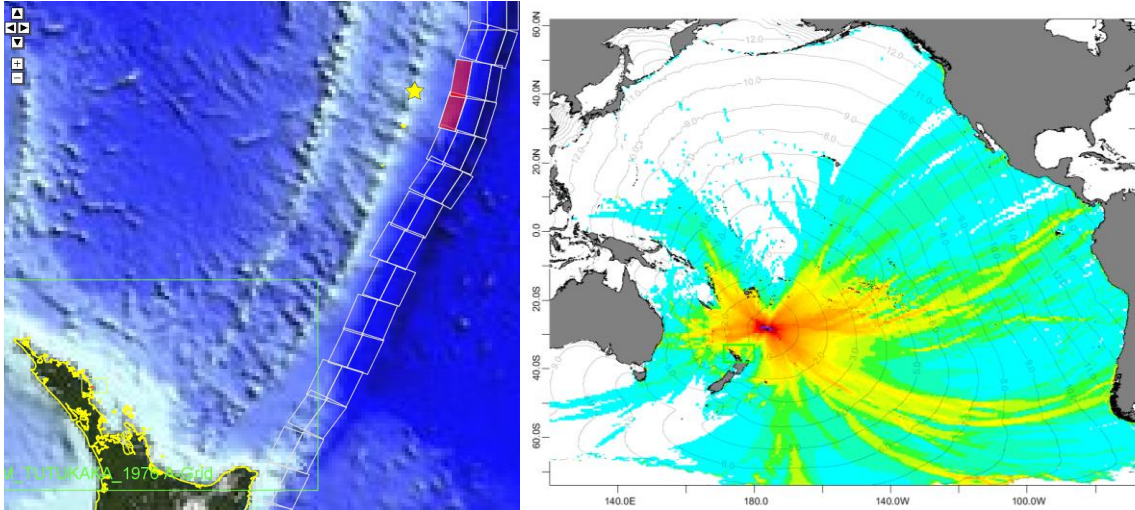


Figure 8.9 The source segments (left) and the trans-Pacific propagation pattern.

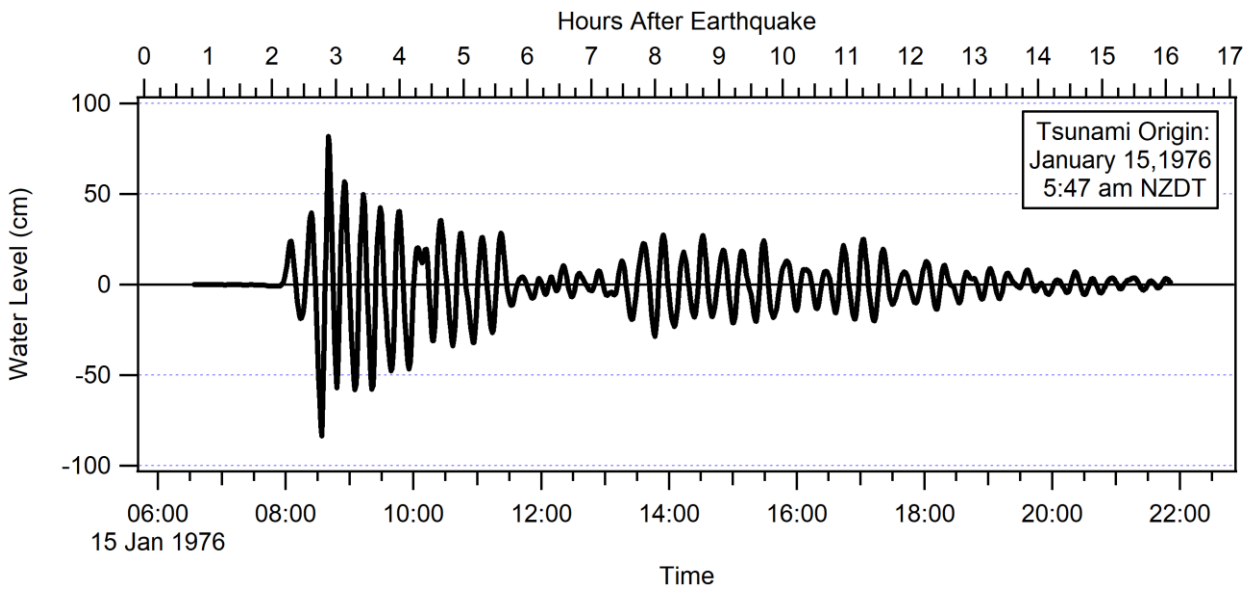


Figure 8.10 Time series of modelled tsunami water level inside Tutukaka Harbour.

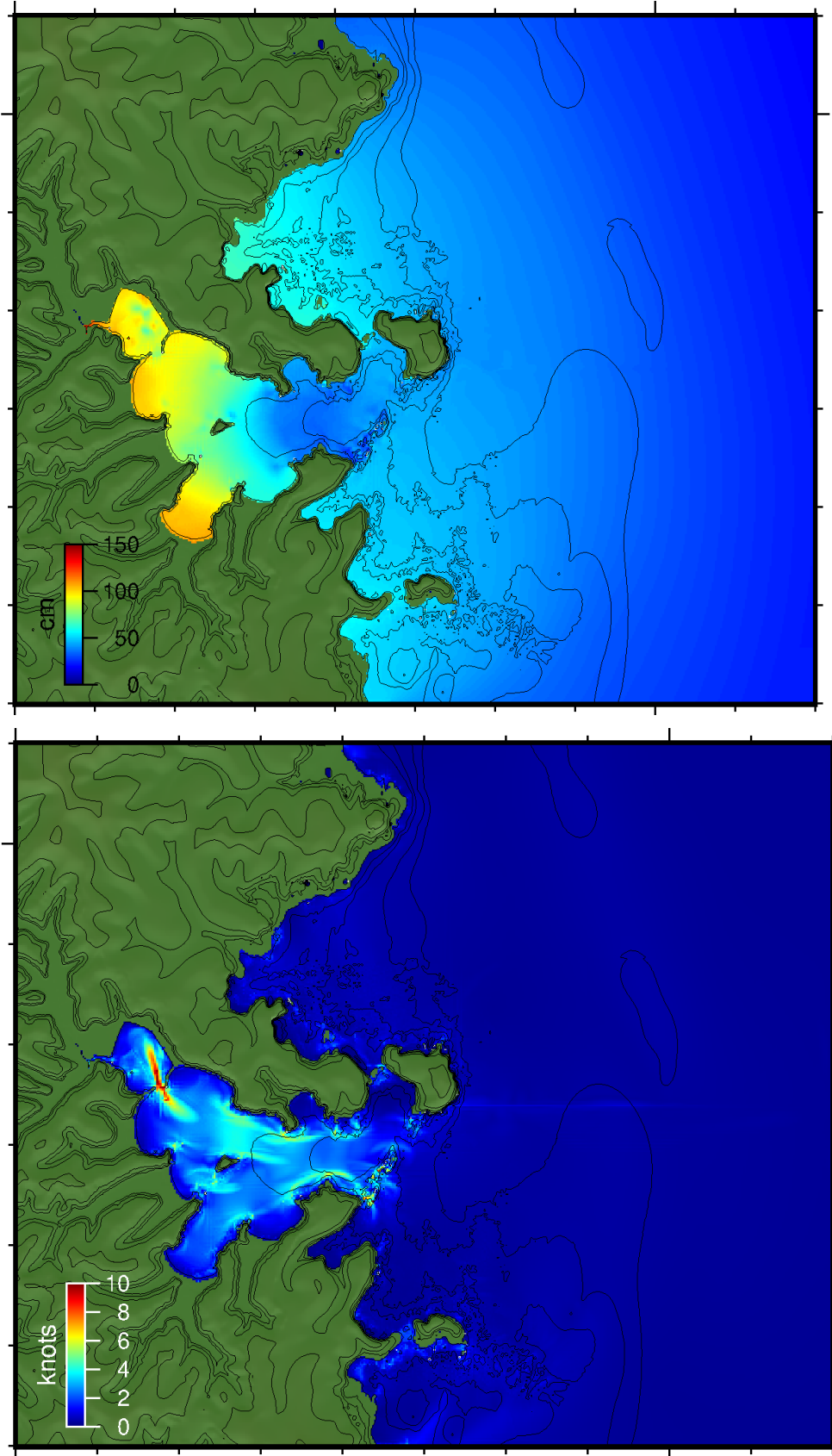


Figure 8.11 Modelled Maximum tsunami amplitude (top) and current speed (bottom).

8.4.1 1976 Source Sensitivity Assessment

Because the details of the 1976 source mechanism are not well defined, we undertook a sensitivity analysis of the tsunami wave forms produced by ComMIT at Tutukaka for a range of different tsunami sources that could be responsible for the 1976 event. To this end we used a 2x2 patch of source segments and varied the distribution of the slip over 13 possible combinations while maintaining a constant earthquake magnitude. This included putting all the slip on each of the four segments, distributing the slip evenly over two segments (either two shallow, two deep or a deep to shallow rupture) as well as spread evenly over the four segments. We also trialled cases where the slip was partitioned nonuniformly between the deep and shallow fault segments. These combinations are laid out in Figure 8.12.

The model results are presented in Figure 8.13 and show that the predicted tsunami heights at Tutukaka are relatively insensitive to the details of the initial condition, particularly in the first 3-4 hours of tsunami activity. However, we note that Source 5 (the source used in the initial assessment described above and shown in black in Figure 8.13) is somewhat smaller than the other cases from 5.5 to 7.5 hours after the earthquake before falling back in with the rest of the simulations after that.

The point of this exercise was to show that Tutukaka Harbour is vulnerable to tsunami generated by relatively small earthquakes located along the Tonga Kermadec Trench. However, based on the output from this sensitivity study, we would be able to generate precomputed predictions of the potential tsunami effects for several different sources that can be used to give guidance for appropriate action within the time between the earthquake and the expected tsunami arrival. Although these detailed, Tutukaka-specific scenarios are out of the scope of this project they should be part of an additional study considering the effect of local or regional earthquakes on maritime facilities.

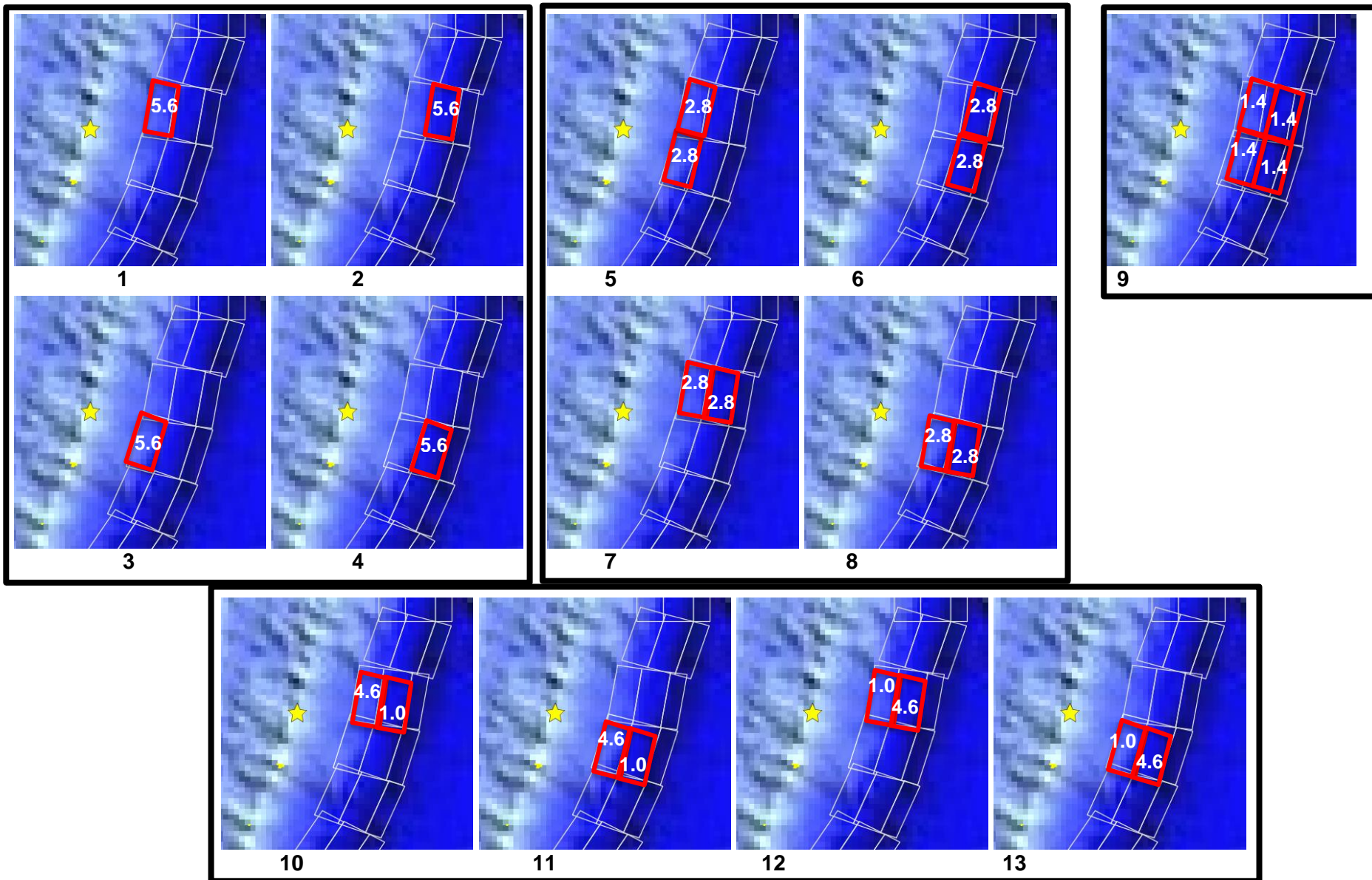


Figure 8.12 Source segments and slip amounts for the January 1976 Kermadec earthquake and tsunami.

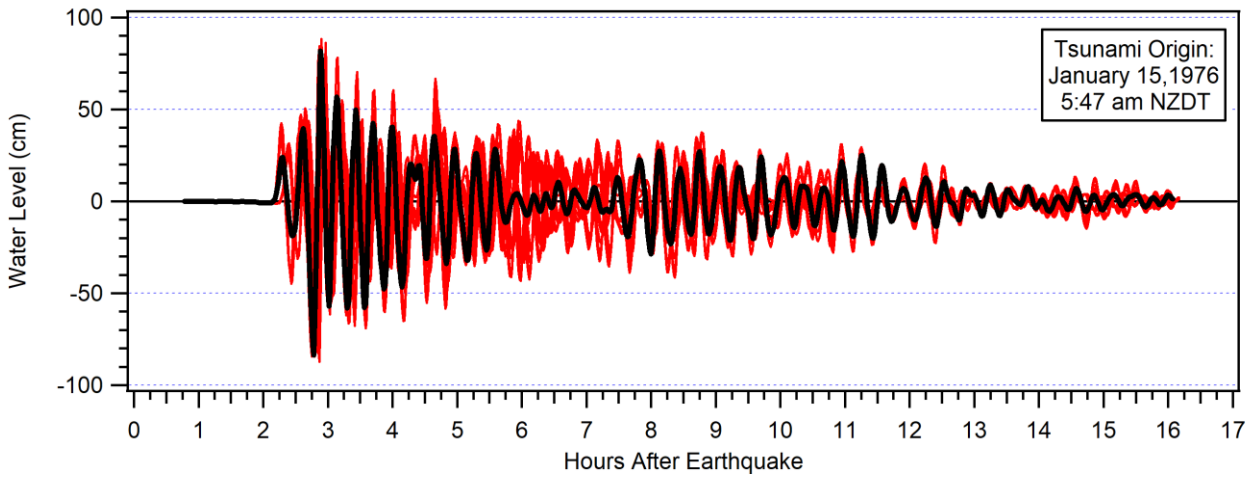


Figure 8.13 Comparison of modelled time series outputs at Tutukaka for the 13 different source scenarios. The black line is Source 5, the one used in the initial modelling shown in Figure 8.9 through Figure 8.11

8.5 Using ComMIT to Model Tsunami Currents

The MOST/ComMIT algorithm and framework has been used numerous times to accurately model tsunami induced wave height and current speeds. Firstly, Lynett *et al.* (2014) showed that the MOST/ComMIT tsunami model accurately reproduced measured tsunami current speeds in Crescent City California caused by the 2011 Tohoku tsunami. Furthermore, they showed that the MOST/ComMIT results were comparable in terms of magnitude and spatial extent to higher order Boussinesq models (Figure 8.14).

This contrasts with the COMCOT model which was shown by Son *et al.* (2011) to be unable to reproduce complex tsunami currents inside the Port of Salalah, Oman during the 2004 Indian Ocean tsunami. They attributed this shortcoming in COMCOT to the numerical truncation error of the upwind differencing in COMCOT which manifests as a diffusion term in COMCOT's governing equations resulting in an overall underprediction of tsunami current speeds. Later, Borrero (2017) showed that the MOST/ComMIT model was able to reproduce the complex current patterns, including the formation of large scale eddies inside the port, observed at Salalah during the 2004 tsunami event (Figure 8.15).

This is an important point since the COMCOT model is used by GNS for tsunami impact studies in New Zealand. While COMCOT is known to behave comparably to MOST/ComMIT (and many other models) for the prediction of water surface elevation and inundation extents, it has also been shown to be deficient in its ability to predict complex, tsunami induced currents.

Additionally, as shown previously in Section 1.1.1 and Figure 1.2, the modelling approach used by NIWA in their studies of tsunami effects in Northland produced current speed predictions that are noticeably deficient in the magnitude and extent of tsunami induced current speeds.

Specific to New Zealand, data of current speeds recorded in Tauranga Harbour during the 2011 Japan tsunami was accurately reproduced by Borrero *et al.* (2015) using the MOST/ComMIT model (Figure 8.16). Careful inspection of Figure 8.16 shows that the deficiencies in the MOST/ComMIT current speed output occur in the portion of the record where the tsunami height is under predicted. Borrero *et al.* (2015) attributes this mismatch to deficiencies in the source model used to initialise the tsunami propagation model and not specifically to any shortcoming in the MOST/ComMIT algorithm itself since the measured current speeds are well reproduced when the modelled tsunami heights match the measured data.

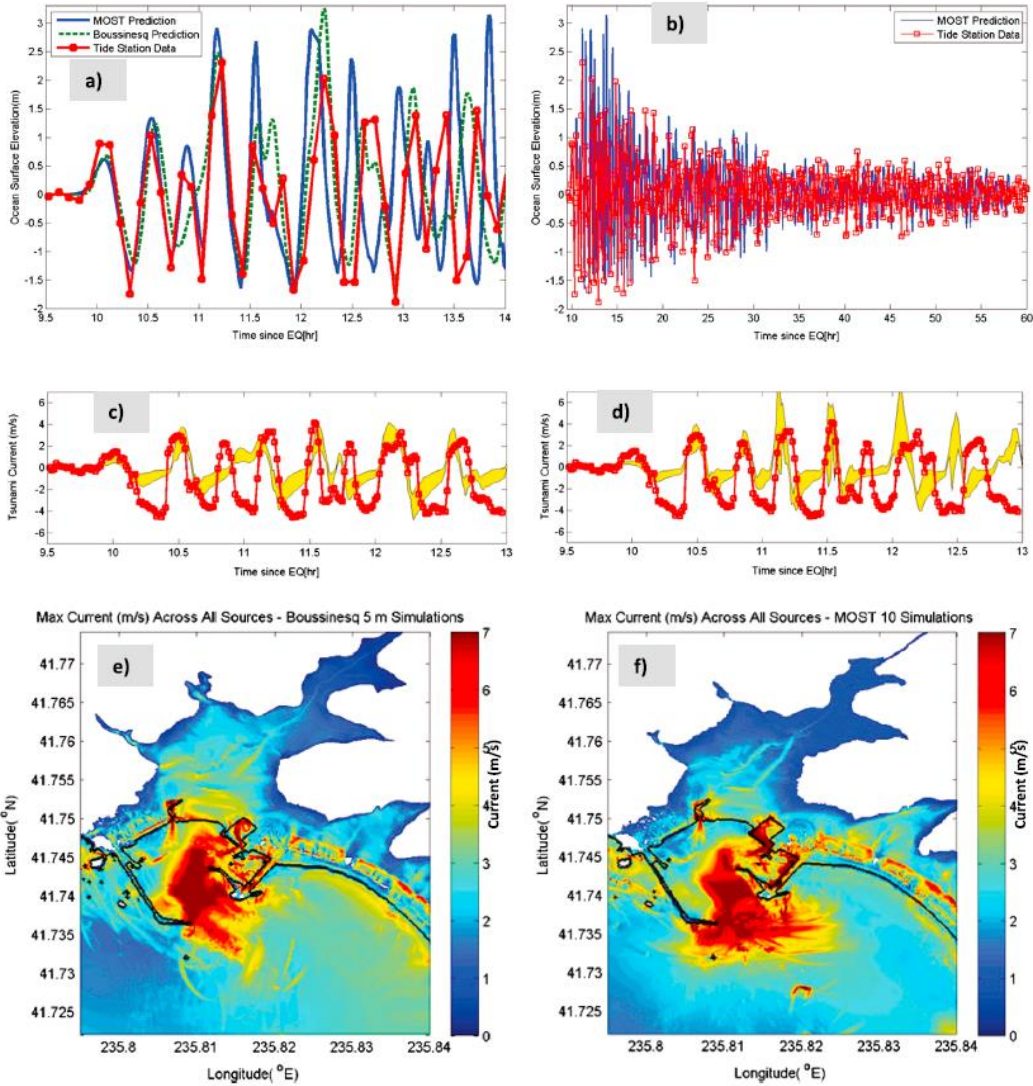


Figure 8.14 Validation and comparison of numerical simulation tools for water surface elevation and currents in Crescent City, CA; (a) comparison of MOST (blue solid), Boussinesq (green dashed), and tide station data (red solid + dots) for the 2011 Tohoku tsunami; (b) comparison of MOST (blue solid) and tide station data (red solid + dots) for 60 h post-EQ; (c) comparison of fluid speed (m/s) at inner boat basin entrance between Boussinesq (yellow) and digitized video data (red solid + dots); (d) comparison of fluid speed (m/s) at inner boat basin entrance between MOST (yellow) and digitized video data (red solid + dots); (e) maximum speed predicted by COULWAVE across a range of different tsunami sources; and (f) maximum speed predicted by MOST across a range of different tsunami sources. (reproduced from Lynett *et al.*, 2014).

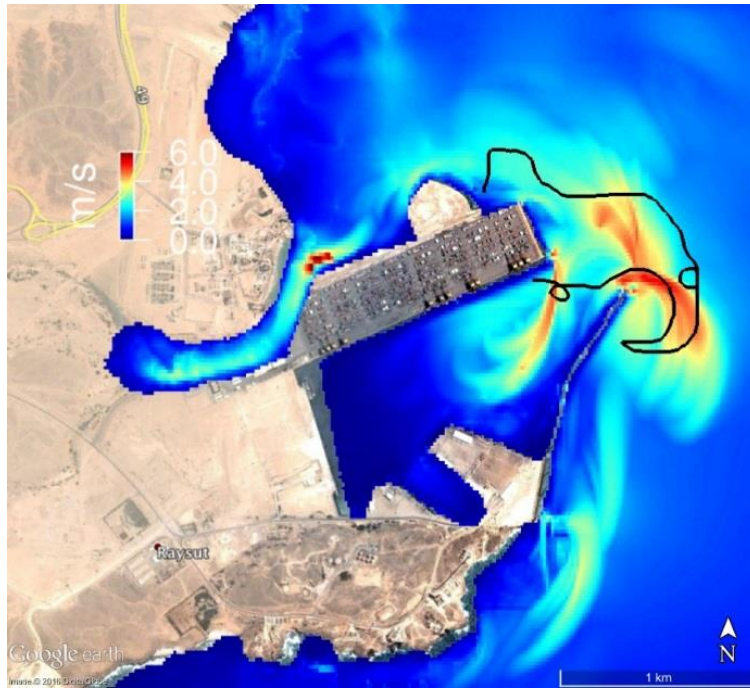


Figure 8.15 Modelled maximum tsunami current speeds at the Port of Salalah during the 2004 Indian Ocean tsunami. Black trace represents the estimated path of the Maersk Mandraki container ship as it drifted through port after it was torn from its mooring by the tsunami currents (see Okal *et al*, 2006b). Figure reproduced from Borrero, 2017.

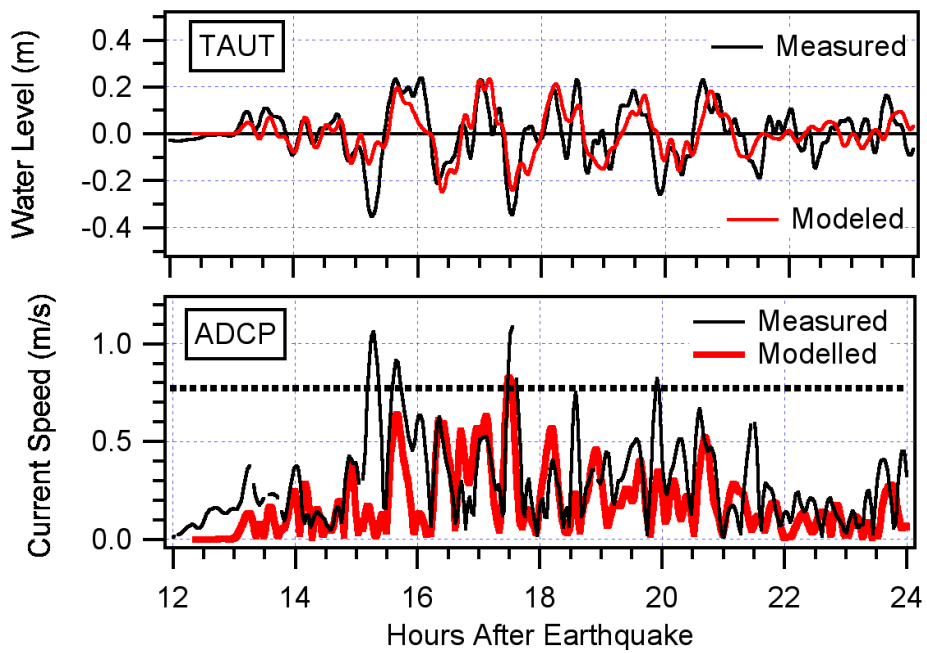
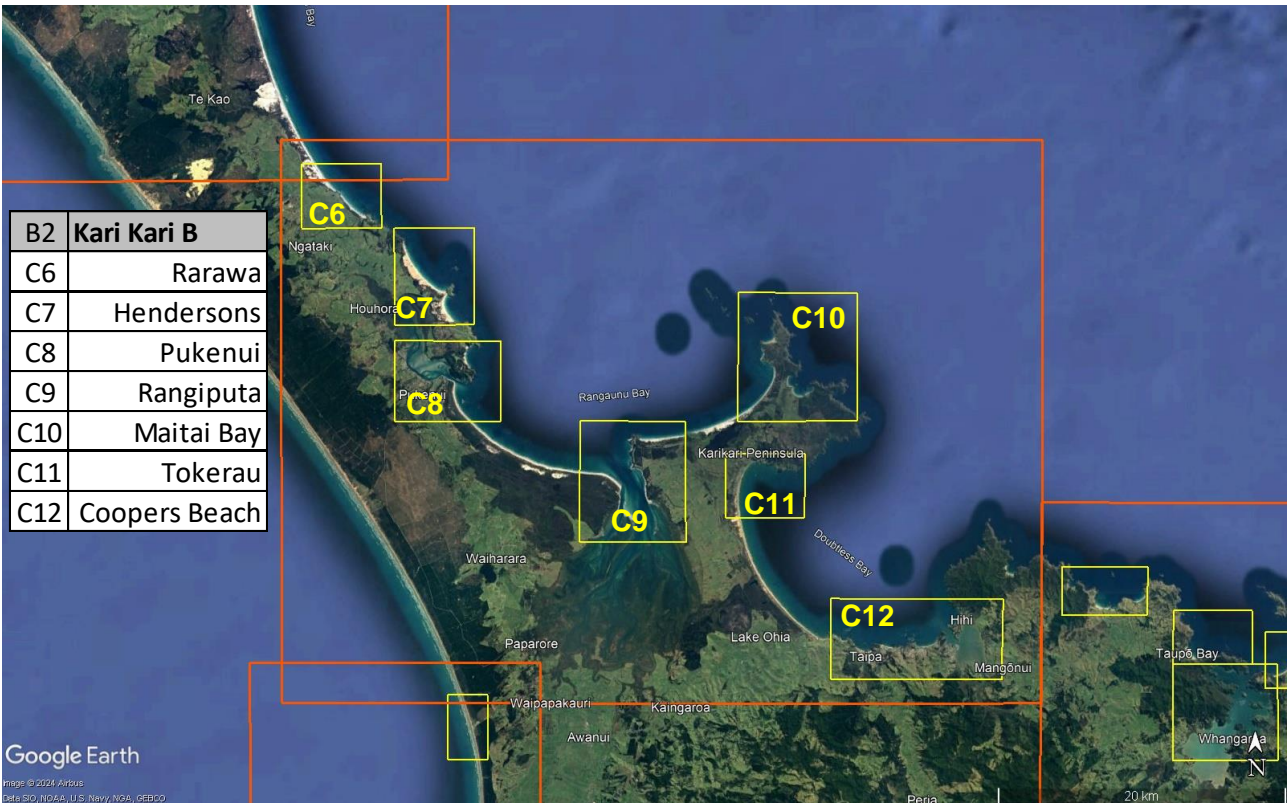
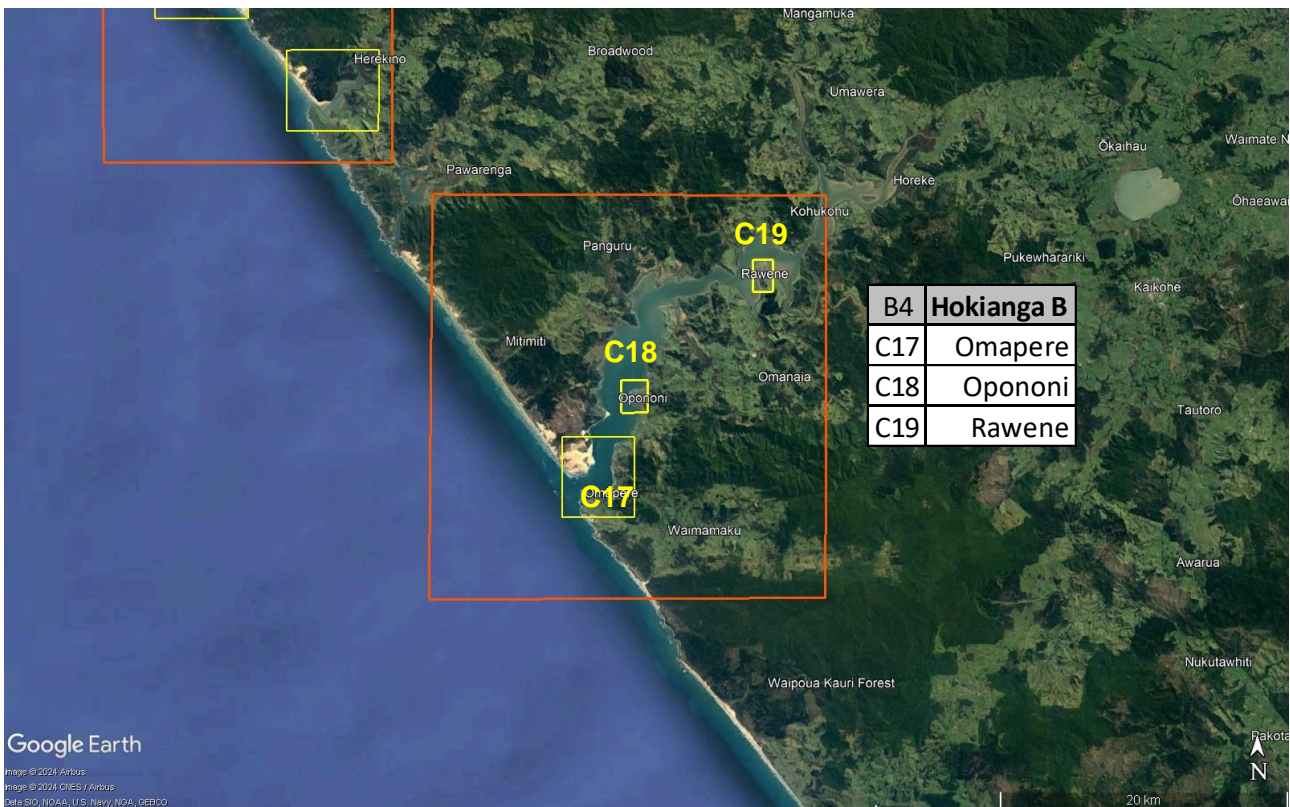
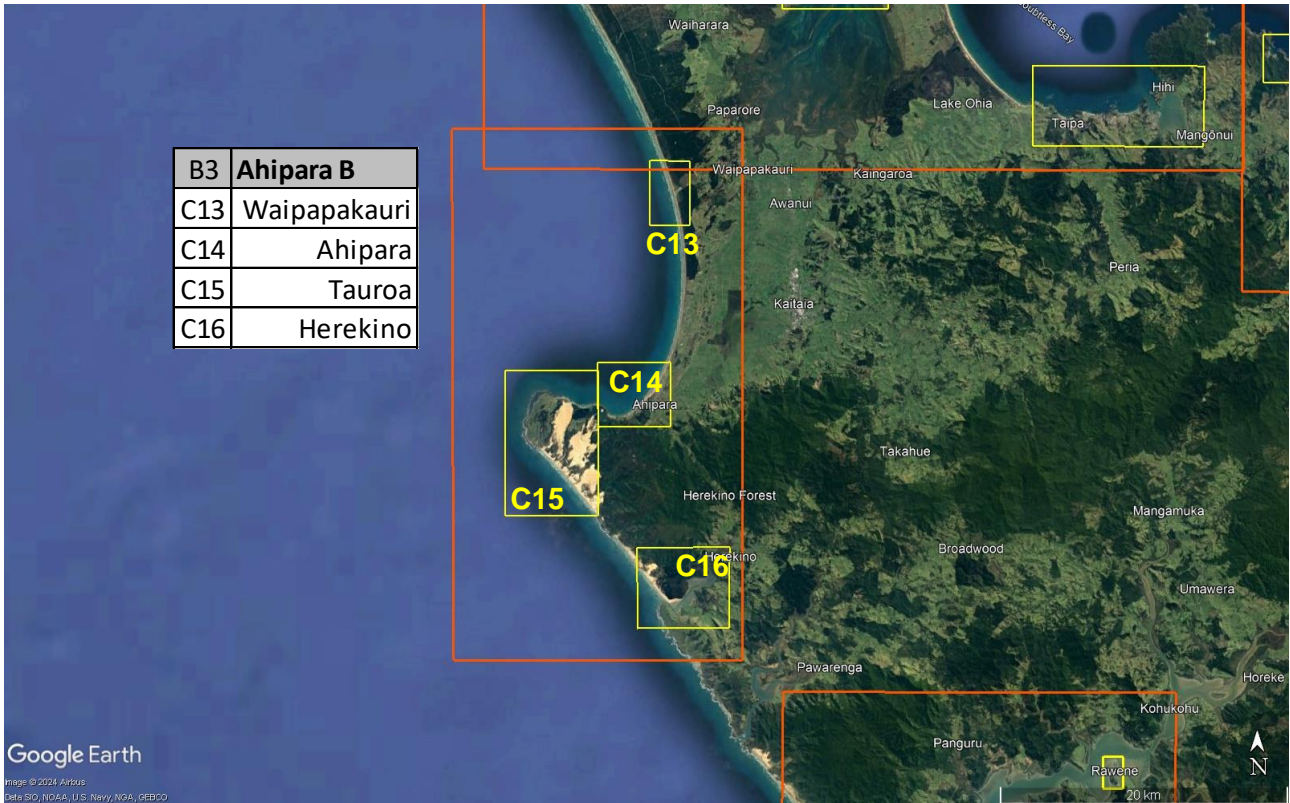
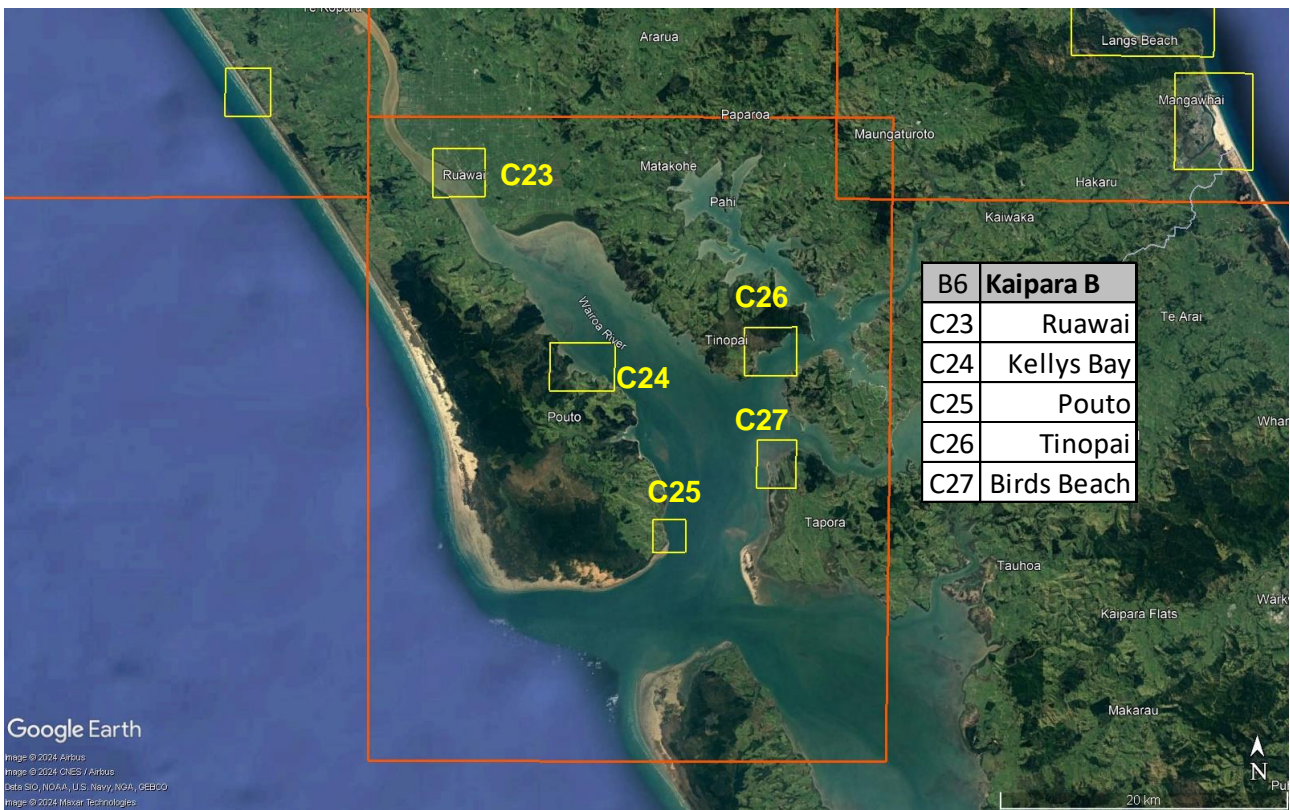


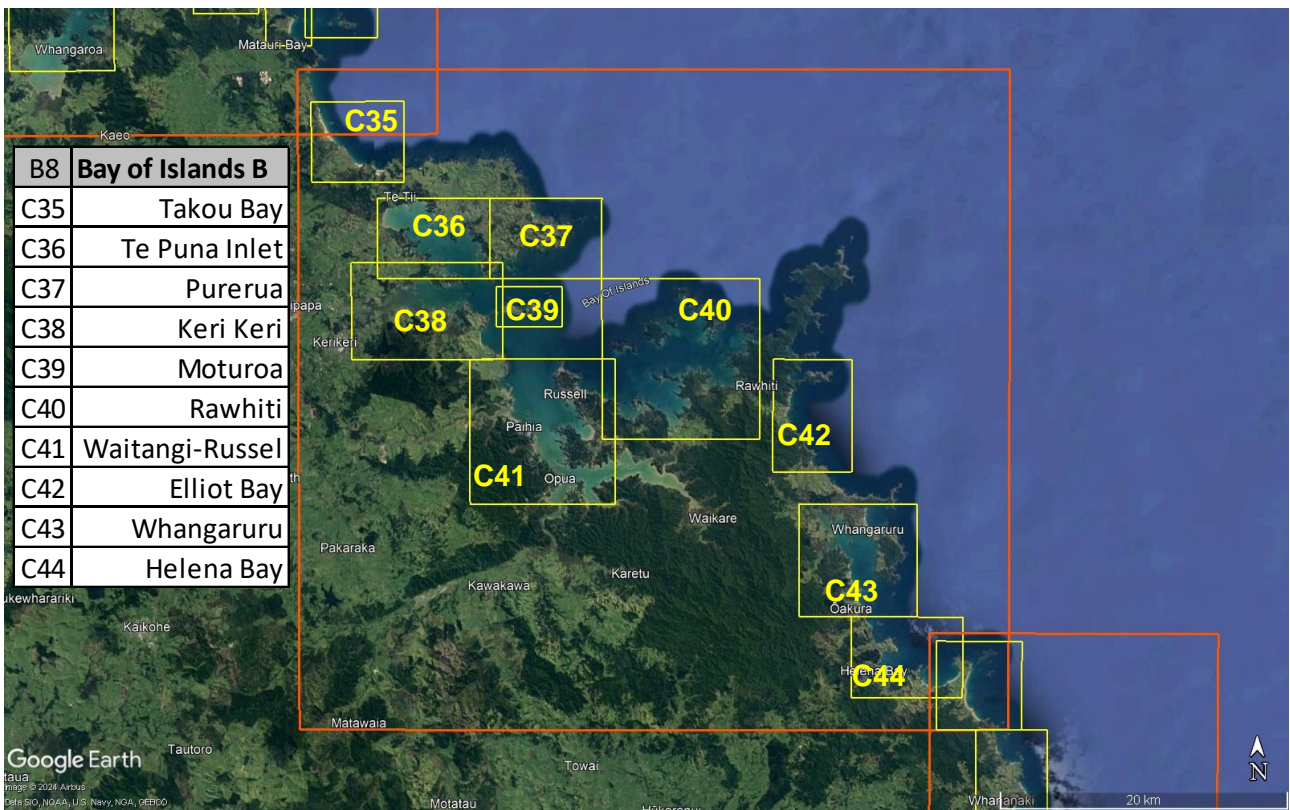
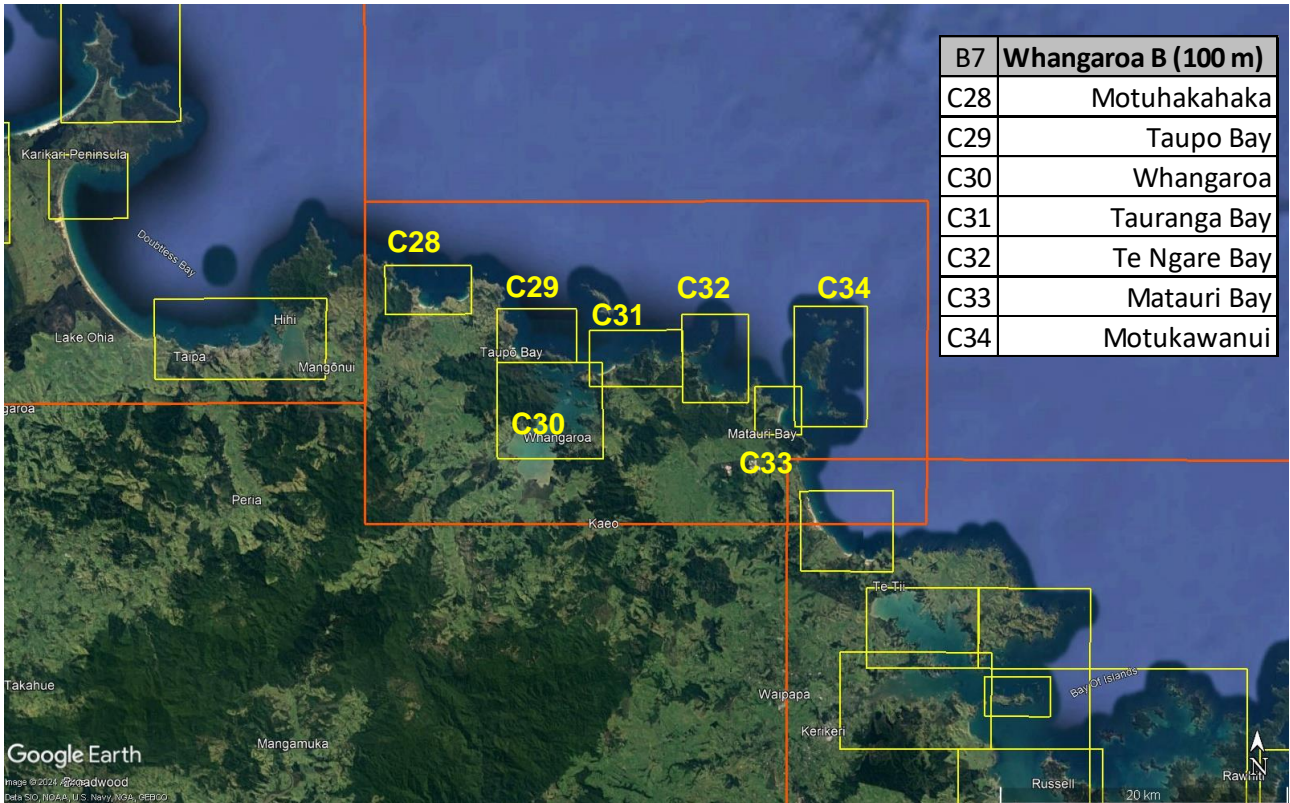
Figure 8.16 Modelled vs. measured tsunami heights (top) and current speeds (bottom) from the 2011 Japan tsunami at the entrance to Tauranga Harbour using the MOST/ComMIT model. Figure reproduced from Borrero *et al*, 2015.

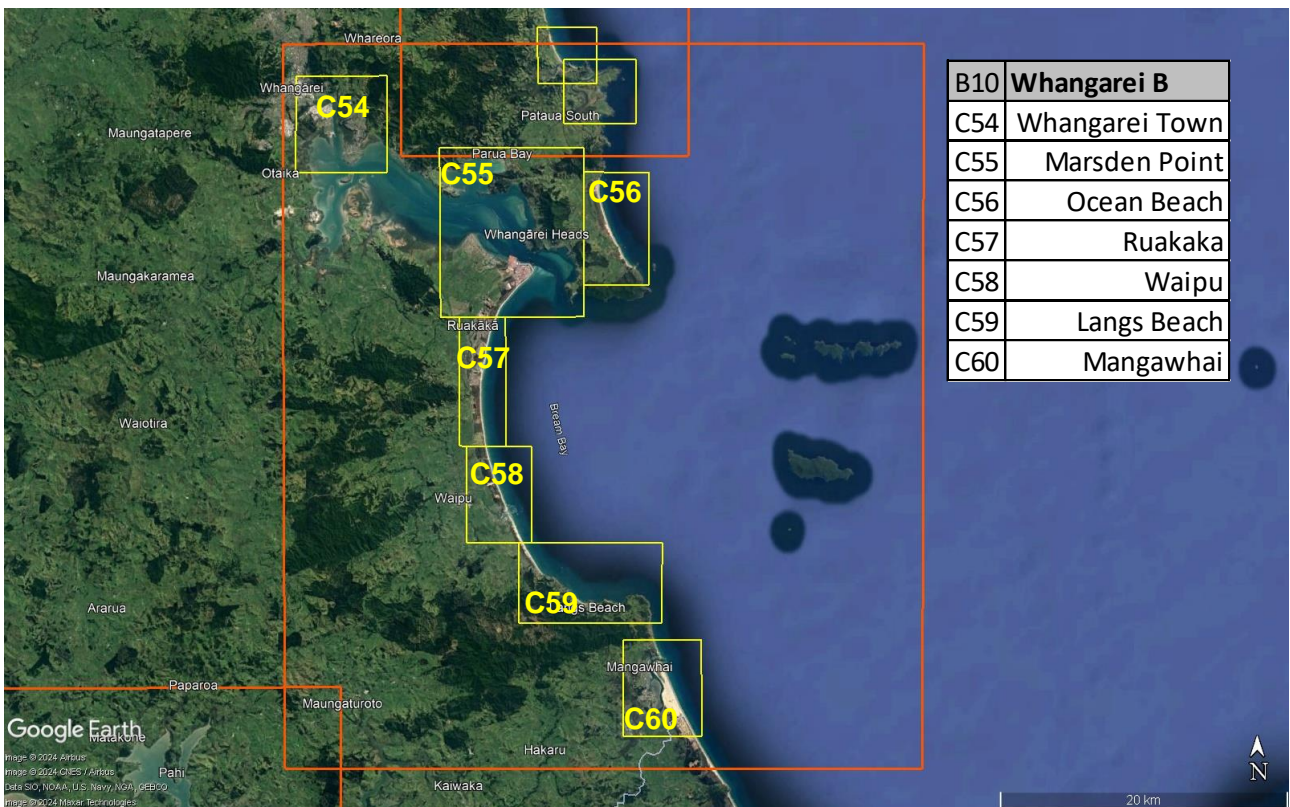
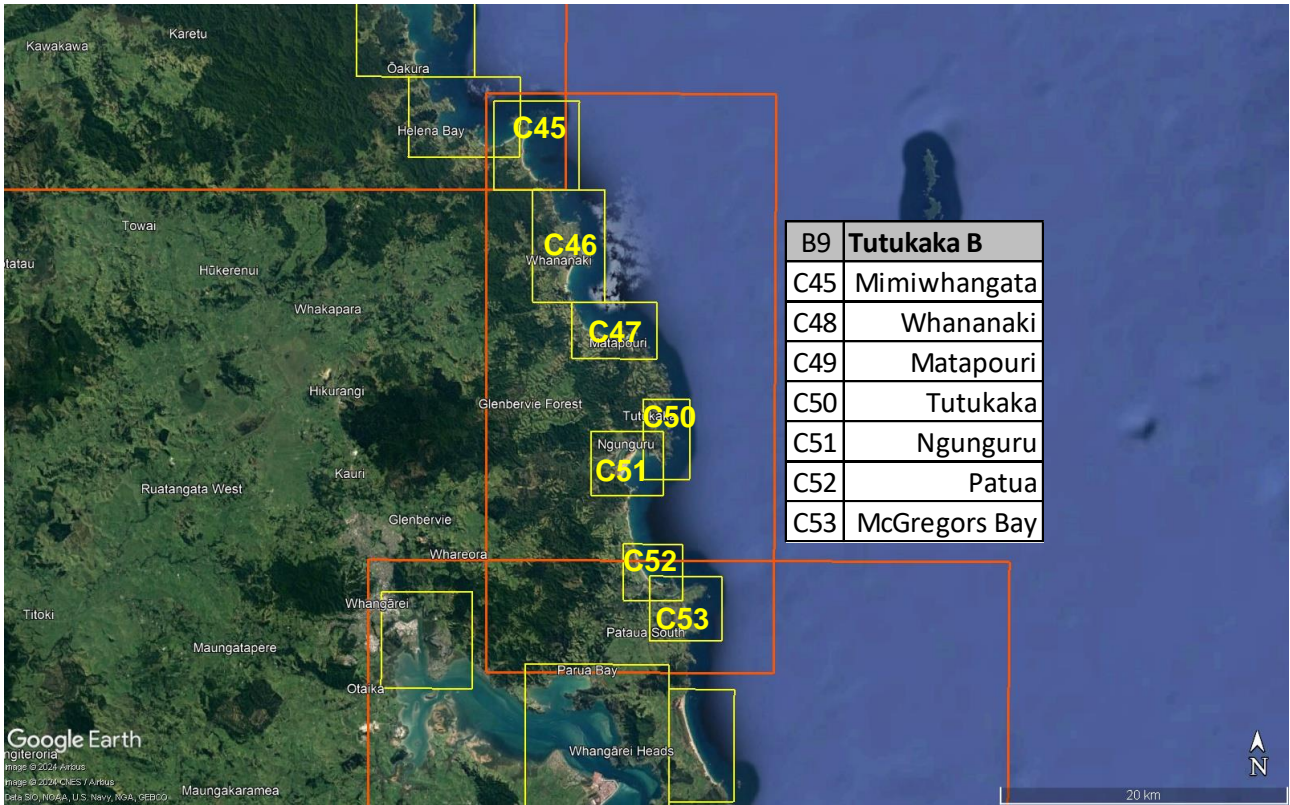
9 APPENDIX 2: GRID REGIONS



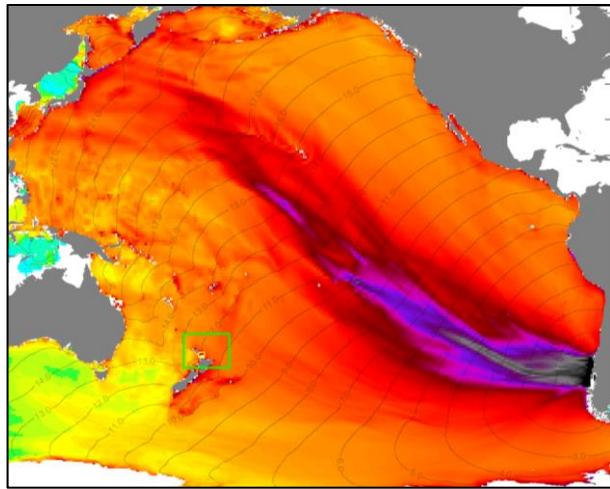




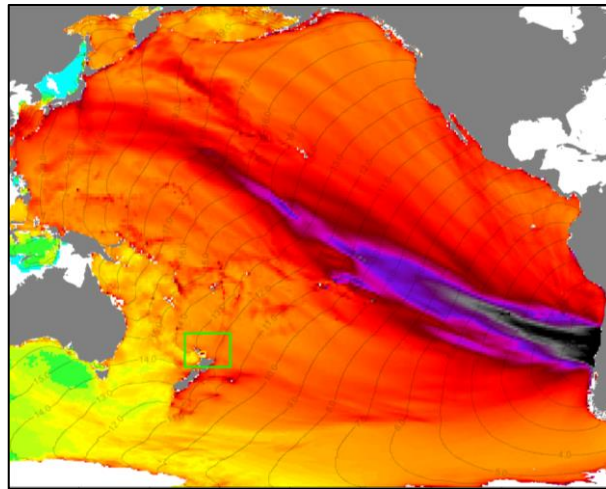




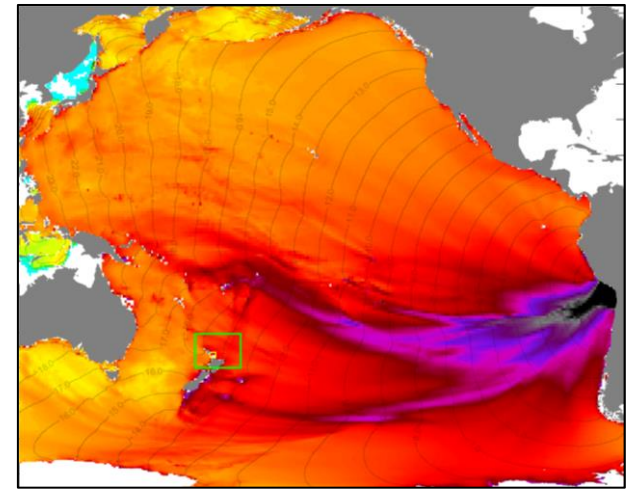
10 APPENDIX 3: TRANS-PACIFIC PROPAGATION PLOTS



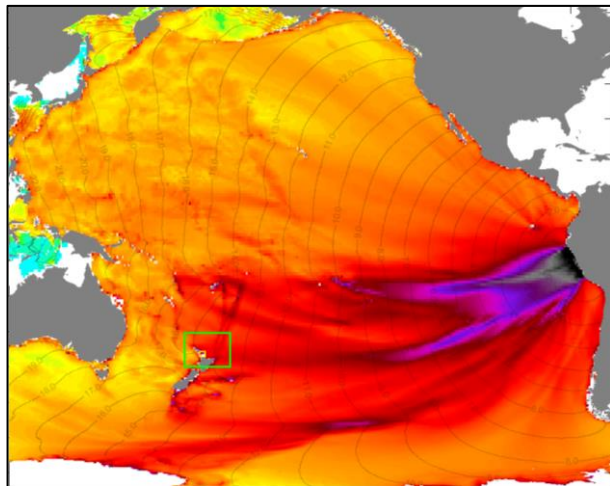
SA 1



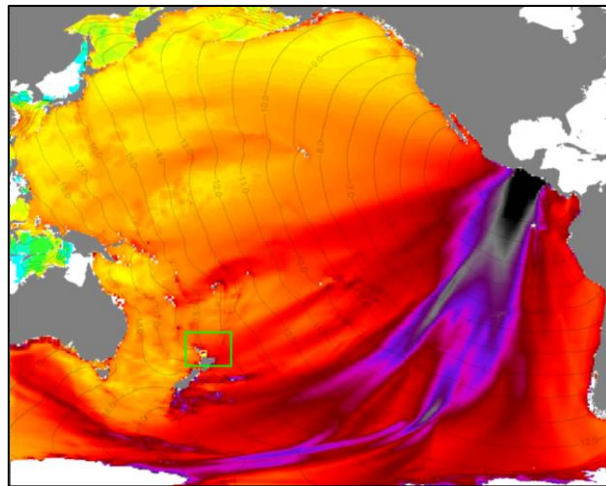
SA 2



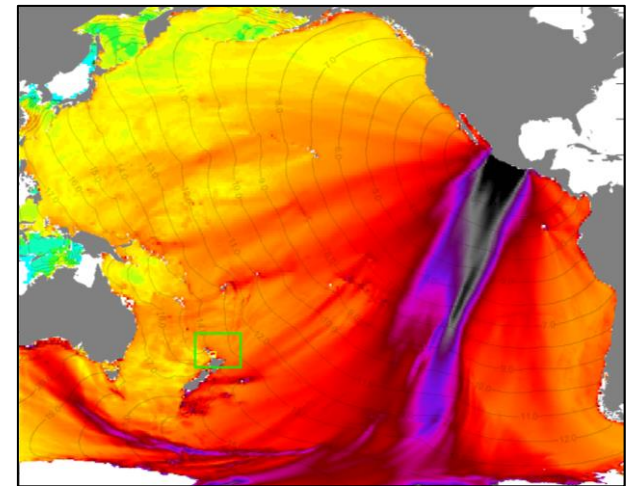
SA 3



SA 4



SA 5



SA 6

